

Microstructure evolution and strengthening mechanism in Ni-based composite coatings

Von der Fakultät für Maschinenbau der
Technischen Universität Chemnitz

Genehmigte Dissertation
zur Erlangung des akademischen Grades

Doktor Ingenieur

(Dr.-Ing.)

Vorgelegt

von

M. Sc. Amir Sadeghi

Geboren am 10.03.1983 in Teheran, Iran

eingereicht am 17.05.2016

Gutachter:

Prof. Dr. ing. habil. Thomas Lampke

Prof. Dr. rer. nat. habil. Andreas Bund

Chemnitz, den 12.10.2016

Acknowledgment

First and foremost, I would like to express my special appreciation and thanks to my advisor Professor Thomas Lampke, he has been a tremendous mentor for me. I would like to thank him for encouraging my research and for allowing me to grow as a research scientist. His advice on both research as well as on my career have been invaluable. I appreciate his contributions of time, ideas, and funding my Ph.D.

The members of the Galvanotechnik group have contributed immensely to my personal and professional time at TU Chemnitz. The group has been a source of friendships as well as good advice and collaboration: Special thanks to Dr. Scharf as my group leader for his novel ideas and his support. I would also like to appreciate my group member Mr. Maximilian Sieber for his support in the part of Impedance investigations.

I am very grateful for the scientific contribution of Dr. Dagmar Dietrich and especially for her professional comments for the part of microscopic characterization.

I would also like to acknowledge honorary contribution of Dr. Hosein Hassannejad, faculty member of Arak University in Iran, whose comments was very helpful for my PhD work.

Furthermore, I would especially like to thank all technical member of materials department and laboratories of TU Chemnitz, especially Mrs. Kaufmann, Mrs. Tauchmann and Mrs. Gläser. All of you have been there to support me during my experiments.

I would like to thank my mother for all her love and encouragement and finally, for the presence of my lovely wife for being with me and supporting me at all times.

Bibliografische Beschreibung

Sadeghi Amir

Topic:

Microstructure evolution and strengthening mechanism in Ni-based composite coatings

Dissertation an der Fakultät für Maschinenbau der Technischen Universität Chemnitz, Institut für Werkstoffwissenschaft und Werkstofftechnik, Chemnitz

Seitenzahl: 128

Anzahl der Abbildungen: 78

Anzahl der Tabellen: 9

Anzahl der Literaturzitate: 177

Schlagworte: Ni-based electrodeposition, layer characterization, electrodeposition mechanism, strengthening mechanism

Summary

Ni electrodeposition is a suitable process for producing thick deposits and thick metallic microstructures, especially for producing relatively deep micromoulds in Microsystems industry.

Ni-P deposits, due to their better properties compared to Ni deposits – particularly high mechanical properties (hardness, wear resistivity), corrosion resistance, magnetic properties, a higher fatigue limit and lower macroscopic deformation – can be a very good alternative for producing Microsystems, especially for MEMS or Microengines. According to few limited literature and our primary investigations, dispersion coating and adding particle into the electrolyte can be considered as an approach in order to decrease the stress and ease the deposition of Ni-P galvanically. Although in the last decades the influence of particles embedment in the matrix by electroplating techniques have attracted the scientific interest, there are still contradictions among the research community concerning the influence of codeposited particles on the microstructure and strengthening properties of Ni-based composites coatings. In many cases, it is believed that the enhanced mechanical performance of the coatings is mainly caused by a change in the microstructure of the metal matrix and not so much by the presence of the particles themselves. In other words, the role of particle characteristics - like their nature, size and concentration - on the layer features and strengthening mechanism of electrodeposited Ni-based composite coating with different matrix is not cleared well.

Furthermore, the incorporation of particles into the deposit is mainly considered as a key factor for determining the composite coatings properties. Despite of existing models of ECD, the mechanism of particle incorporation into the film under influence of different particle characteristics has not been well understood yet.

Therefore, the main aim of this study is to shed light on the effect of particle characteristics (size, concentration, type) on the codeposition process, microstructure and strengthening mechanisms in Ni and Ni-P electrodeposited composite coatings.

Table of Contents

List Abbreviations and symbols

List of figures

List of tables

Summary

1	INTRODUCTION	15
1.1	Motivation	15
1.2	Organization of dissertation	16
2	THEORETICAL BACKGROUND	17
2.1	Nickel Electrodeposition	17
2.2	Application of Ni electrodeposition in microsystems	17
2.3	Ni-P electrodeposited coatings: mechanism, benefits and challenges	18
2.4	Ni-based dispersion coatings	20
2.4.1	Effect of particle features on the electrodeposition behavior	22
2.4.2	Models of electrocodeposition	26
2.4.3	In-situ study of Ni-based coatings by means of EIS	28
2.4.3.1	Applications of EIS	28
2.4.3.2	Concept of EIS method in electrodeposition process	28
2.4.3.3	Evaluation of Ni electrodeposition using EIS	31
2.4.3.4	Interaction of particle-interface in Ni electrodeposition studied by EIS	32
2.5	Strengthening mechanisms in Ni-based composite coatings	36
2.5.1	Dispersion hardening–Orowan	37
2.5.2	Grain size effects: Hall-Petch relation	39
2.5.3	Solid solution strengthening	39
2.6	Summary of theoretical background	41
2.7	Missing points in the recent studies	41
2.8	Research objectives	42
2.9	Work Schedule	43
3	Experimental Methods	44
3.1	Deposition Procedures	44
3.1.1	Electrolyte Composition and Working Conditions	44
3.1.2	Impedance investigation	44
3.2	Layer Characterizations	48

3.2.1 Scanning Electron Microscopy (SEM)/ energy-dispersive X-ray Spectroscopy (EDX)	48
3.2.2 EBSD and TKD	48
3.2.3 Transmission Electron Microscopy (TEM)	49
3.2.4 X-ray Diffraction (XRD)	50
3.2.5 Measuring internal stress by XRD	51
3.2.6 Martens test	51
4 Results and Discussion	52
4.1 Layer Characterization of Ni electrodeposited from Watts electrolyte	52
4.2 Electrodeposition behavior of Ni electrodeposited coatings by means of EIS	56
4.3 Effect of particle properties on the electrodeposition behavior of Ni-Al ₂ O ₃ composite coatings and its layer properties	58
4.3.1 Effect of alumina particle size on the morphology, microstructure and mechanical properties	58
4.3.2 In-situ EIS study of Ni-Al ₂ O ₃ electrodeposition	66
4.3.3 Effect of particle type on the morphology, microstructure and mechanical properties	70
4.3.4 In-situ EIS study of Ni electrodeposited with different particle type	79
4.4 Investigation on electrodeposition behavior of Ni-P and Ni-P composite coatings	81
4.4.1 Layer Characterization of Ni-P electrodeposited coatings	81
4.4.2 Effect of Particles incorporation in Ni-P galvanic coatings	88
4.4.2.1 Effect of particle size on the layer characteristics and electrodeposition behavior of Ni-P electrodeposited coatings	88
4.4.2.2 Effect of particle type on the layer characteristics and electrodeposition behavior of Ni-P electrodeposited coatings	97
4.4.2.3 EIS study of Ni-P composite coatings	105
5 Conclusions and Suggested Future Work	108
5.1 Conclusions	108
5.1.1 The Electrodeposition of Nickel from Watts electrolyte	108
5.1.2 The effect of particle size on electrodeposition behavior and features of Ni layer	109
5.1.3 The effect of particle type on electrodeposition behavior and features of Ni layer	110
5.1.4 The electrodeposition behavior of Ni-P electrodeposited from Watts electrolyte containing phosphorous source	111
5.1.5 The effect of particle size on electrodeposition behavior and features of Ni-P layer	111

5.1.6 The effect of particle type on electrodeposition behavior and features of Ni-P layer	112
5.2 Achievements	113
5.3 Suggested future works	115
References	116
Publications	128

List of abbreviations and symbols

Electrochemical Impedance Spectroscopy	EIS
Lithographie, Galvanoformung und Abformung	LIGA
Micro Engine Motors	MEMS
Electro-Co-Deposition	ECD
Sodium Dodecyl Sulphate	SDS
Constant Phase Element	CPE
Cyclic Voltammetry	CV
Chronoamperometry	CA
Charge transfer resistance	R_p
Double layer capacity	C_{dl}
Scanning Electron Microscopy	SEM
Energy dispersive X-ray	EDX
Electron Backscattered Diffraction	EBSD
Transmission Kikuchi Diffraction	TKD
Transmission Electron Microscopy	TEM
X-ray Diffraction	XRD
Direct Current	DC
Alternating Current	AC
Dark field	DF
Bright field	BF

List of Figures

Figure 2.1 Ni electrodeposited Microresonator by LIGA process

Figure 2.2 Schematic of electrodeposition process

Figure 2.3 Typical surface profile of composite coatings: a) containing conducting particles; b) containing non- conducting particles

Figure 2.4 Electric equivalent circuit for the nickel electrocrystallization process from a Watts bath containing SiC

Figure 2.5 Guglielmi's ECD Model

Figure 2.6 AC voltage signal imposed on an electrochemical system and the resulting AC current and impedance

Figure 2.7 Complex plane impedance spectrum for Ni electrolyte containing 150 g/l NiSO₄, $i = 20$ mA/cm², pH 2.5, T 60°C, no stirring, Pt anode, EW-Ni substrate

Figure 2.8 Schematic models of the double-layer structure

Figure 2.9 Impedance diagrams performed at cathodic potential of 2750 mV Ag/AgCl: codeposition of nano- SiC with nickel 50 g/L SiC in the electrolyte and pure nickel electrodeposition. Disk rotation rate 100 rpm

Figure 2.10 SEM surface morphology of pure Ni electroplating (a) Ni-SiC nanostructured composite coating. Current density 4 A/dm², 50 g/l SiC in the plating bath, disk cathode (b)

Figure 2.11 Experimental data (points) and simulated plots (solid line) for Ni-TiO₂ composite system (a) and pure Ni system (b) at various potentials

Figure 2.12 Various strengthening against dislocation motion

Figure 2.13 Onset of plastic flow controlled by particles in the metal matrix

Figure 2.14 Illustration of dislocation mechanism in slip distance model: dislocation-free slip distance is decreased in smaller grain sizes

Figure 2.15 Dependences of microhardness of the as-deposited Ni-P films on P content and micro-structure

Figure 2.16 Schematic of project

Figure 3.1 Set up of electrodeposition and EIS investigation

Figure 3.2 Schematic of EBSD and TKD (t-EBSD) analysis

Figure 3.3 The procedure of forming BF and DF in TEM

Figure 4.1 XRD results of Ni electrodeposited from Watts Bath in different current density: (a) 1, (b) 2 and (c) 4 A/dm²

Figure 4.2 Effect of current density on texture of Ni electrodeposits

Figure 4.3 Effect of current density on grain size of Ni electrodeposited in different current density of 1, 2 and 4 A/dm²

Figure 4.4 Effect of current density on Martens hardening of Ni electrodeposited in different current density of 1, 2 and 4 A/dm²

Figure 4.5 SEM morphology images of Ni in different current density: (a) 1, (b) 2 and (c) 4 A/dm²

Figure 4.6 Galvanostatic polarization (a) and Nyquist spectrums (b) of Ni deposition in current densities of 1, 2 and 4 A/dm² vs Ag/Ag/Cl

Figure 4.7 Simple circuit model for the Ni electrodeposition from Watts's electrolyte

Figure 4.8 Charge transfer vs current density for electrodeposition of Ni from Watts's electrolyte

Figure 4.9 SEM images of the surface morphology: (a) Ni-sm Al₂O₃ 20 g/l (b) Ni-n Al₂O₃ 20 g/l electrodeposited at $i = 4$ A/dm² for 40 min

Figure 4.10 SEM images of cross-section: (a) Ni, (b) Ni-sm Al₂O₃ 20 g/l (c) Ni-n Al₂O₃ 20 g/l electrodeposited at $i = 4$ A/dm² for 40 min

Figure 4.11 Effect of particle size and concentration on the incorporation value of particles achieved from EDX mapping analysis from the thickness of the deposits

Figure 4.12 Volume percentages of alumina particles estimated by image analyzer software: (a) Ni-n Al₂O₃ 20 g/l (b) Ni-sm Al₂O₃ 20 g/l electrodeposited under the same working conditions

Figure 4.13 Effect of particle size and concentration on the Ni grain size

Figure 4.14 EBSD texture of Ni-nano Al₂O₃ and Ni-sm Al₂O₃ with 20 g/l under other same working Parameters

Figure 4.15 Effect of particle size and concentration on the thickness value of the deposits electrodeposited under the same conditions

Figure 4.16 Texture values in (a) Ni-Al₂O₃ 13 nm (b) Ni-Al₂O₃ 200 nm electrodeposited at $i = 4$ A/dm² with 20 g/l particle concentration into Watts's electrolyte

Figure 4.17 Concentrations including the effect of grain size and particle content

Figure 4.18 Effect of particle size and concentration on the Nyquist spectrums: (a) Ni-n Al₂O₃ (b) Ni-sm Al₂O₃ (c) comparison at the concentration of 20 g/l

Figure 4.19 Circuit model used for impedance measurements for the frequency range of 10 kHz-10 Hz

Figure 4.20 Results of C_{dl} (a) and R_{dl} (b) calculated by fitting the impedance results with the suggested circuit model by means of Matlab

Figure 4.21 Schematic of the particle incorporation mechanism based on particle size and concentration
(a) at lower concentrations (b) at higher concentrations

Figure 4.22 SEM images from the surface morphology of Ni coatings with different type of particles deposited under the same working conditions : (a) Ni, (b) Ni-Al₂O₃, (c) Ni-TiO₂, (d) Ni-SiC

Figure 4.23 SEM images from cross-section of Ni coatings with different type of particles electrodeposited under the same working conditions

Figure 4.24 Thickness results of Ni coatings with different type of particles electrodeposited under the same working conditions

Figure 4.25 Particle content vs. particle concentration/type for Ni electrodeposited composite coatings

Figure 4.26 Grain size results for $i = 4 \text{ A/dm}^2$, from XRD

Figure 4.27 Texture values in Ni electrodeposited coatings with different particle type

Figure 4.28 Internal stress in Ni electrodeposited composite coatings with different particle types measured with XRD technique

Figure 4.29 EBSD images of Ni composite coatings with different particle type electrodeposited under same working conditions

Figure 4.30 TKD images of Ni composite coatings with different particle type electrodeposited under same working conditions

Figure 4.31 Comparison between TEM and TKD images for Ni composite coatings with different particle type electrodeposited under same working conditions

Figure 4.32 Hardness vs. particle concentration/particle type

Figure 4.33 EIS results from the effect of particle type on the electrodeposition behavior of Ni

Figure 4.34 Correlation of phosphorous content in Ni-P deposit with current density and NaP₂H₂O₂ as phosphorous source in Watts Ni bath

Figure 4.35 Effect of phosphorous source concentration on the crystallinity of Ni deposit indicated by XRD. Coatings electrodeposited at $i = 4 \text{ A/dm}^2$ and under same working conditions

Figure 4.36 Morphology of Ni deposit with and without phosphorous source in Watts Ni

Figure 4.37 Effect of NaP₂H₂O₂ concentrations on the impedance behavior of Ni-P deposit

Figure 4.38 Effect of current density on the impedance behavior of Ni-P electrodeposited under the same NaP₂H₂O₂ concentration: P content 8.25, 7.5, 5.75

Figure 4.39 Effect of Lamellar layers in Ni-P on the potential during deposition

Figure 4.40 Effect of phosphorous content on the microstructure of Ni-P electroplated coating

Figure 4.41 Elemental EDX shows phosphorus distributions in the cross-section of Ni-P galvanic coating

Figure 4.42 Photos from samples (a) Ni-P and (b) Ni-P-Al₂O₃ 13 nm, (c) 200 nm electrodeposited under same working conditions

Figure 4.43 Morphology of (a) Ni-P, (b) Ni-P-Al₂O₃ 13 nm, (c) 200 nm electrodeposited under same working conditions

Figure 4.44 Cross section SEM images of (a) Ni-P, (b) Ni-P-Al₂O₃ 13 nm, (c) 200 nm electrodeposited under same working conditions

Figure 4.45 EDX results from P content and particle incorporation in Ni-P composite coatings electrodeposited with nano and submicron particles

Figure 4.46 Thickness results of Ni-P and Ni-P-Al₂O₃ with nano and submicron particles electrodeposited under same working conditions

Figure 4.47 Internal stress of Ni-P and Ni-P-Al₂O₃ with nano and submicron particles measured with XRD

Figure 4.48 EBSD images of Ni-P-n Al₂O₃ and Ni-sm Al₂O₃ composite coatings

Figure 4.49 Martens results of Ni-P, Ni-P-n Al₂O₃ and Ni-P-sm Al₂O₃ composite coatings as-deposited and after annealing at 400°C, 1 hr.

Figure 4.50 Morphology SEM images of Ni-P deposit and Ni-P composite coatings electrodeposited with different particle types under same working conditions

Figure 4.51 SEM images from cross-section of Ni-P deposit and Ni-P composite coatings electrodeposited with different particle types under same working conditions

Figure 4.52 EDX results of Ni-P deposit and Ni-P composite coatings electrodeposited with different particle types under same working conditions: (a) particle content (b) phosphorous content

Figure 4.53 Thickness of Ni-P deposit and Ni-P composite coatings electrodeposited with different particle types under same working conditions at current density of 4 A/dm²

Figure 4.54 Effect of different particle type on the residual stress of Ni-P electrodeposited coating, measured with XRD technique after annealing

Figure 4.55 EBSD images of Ni-P deposit and Ni-P composite coatings electrodeposited with different particle types under same working conditions

Figure 4.56 Martens test results of Ni-P deposit and Ni-P composite coatings electrodeposited with different particle types under same working conditions

Figure 4.57 Ni/Ni-P grain size after annealing for Ni-P and Ni-P composite coating electrodeposited with different particle types

Figure 4.58 Particle size effect on the EIS results of Ni-P electrodeposition

Figure 4.59 Particle type effect on the EIS results of Ni-P electrodeposition

List of Tables

Table 2.1 Codeposition of Al_2O_3 particle, 120 g/l at 20 mA/cm^2 and using a rotating cylinder electrode at 1000 rpm

Table 2.2 Size of particles used by Stankovic and Gojo in their investigations

Table 2.3 Applications of impedance studies

Table 2.4 Past EIS studies on the process on Ni composite electrodeposition

Table 2.5 Various strengthening method

Table 3.1 Electrolyte composition and working condition

Table 3.2 Table of Experiments

Table 4.1 Effect of $\text{NaP}_2\text{H}_2\text{O}_2$ and current density on the phosphorous content of Ni-P electrodeposits measured by EDX and GODES

Table 4.2 Crystalline phase fractions and grain sizes of the composites after heat-treatment

1 INTRODUCTION

Ni-P deposits, due to their better properties compared to Ni deposits – especially high mechanical properties (hardness, wear resistivity), corrosion resistance, magnetic properties, a higher fatigue limit and lower macroscopic deformation – can be a very good alternative for producing Microsystems, particularly for MEMS or Microengines. Moreover, strengthening properties of Ni-P after annealing is comparable with chromium deposits which can make this deposit a very good alternative for substitution of traditional hard chromium coatings because of the environmental problems chromium coatings cause. There are generally two methods of fabrication for Ni-P deposition: electroless and galvanic. Galvanic Ni-P is - especially due to its higher deposition rate, higher stability of electrolyte, lower working temperature and generally lower expenses - suggested to be the more effective process for fabrication of microcomponents. In the last decades some researchers have investigated on galvanic Ni-P depositions and explored the effect of different working parameters on phosphorous content and layer properties. Meanwhile, there are still some challenges existing in the Ni-P galvanic process. The main challenge here lies with large residual stresses which lead to cracking and spallation of deposits, specifically in moderately high current densities. This prevents galvanic Ni-P from being successfully used in manufacturing high-strength and high-aspect ratio in micro- nanostructures.

1.1 Motivation

For many years dispersion coatings have been clearly accepted as an approach for improving the properties of deposits, particularly mechanical properties. According to few limited literature and our primary investigations, adding particle into the electrolyte can be considered as an approach in order to decrease the stress and ease the deposition of Ni-P galvanically. Although the influence of particles embedment in the matrix by electroplating techniques has attracted the scientific interest in Ni-P matrix composites, there are still contradictions among the research community concerning the influence of codeposited particles on the microstructure and strengthening properties of Ni-P composites coatings. In many cases it is believed that the enhanced mechanical performance of the coatings is mainly caused by a change in the microstructure of the metal matrix and not so much by the characteristic of the particles themselves. In other words, the role of particle characteristics - like their nature, size and concentration- on the layer features and strengthening mechanism of electrodeposited Ni-P is not cleared and no systematic investigation of these factors has been reported yet on electrodeposited Ni-P composite coatings.

Furthermore, the incorporation of particles into the deposit is mainly considered as key factor for determining the composite coatings properties. Despite of several existing explanations for the mechanisms of codeposition processes proposed by some researchers like Guglielmi, Celis, Fransaer and others [1-3], the mechanism of particle incorporation into the film under influence of different particle characteristics and also different Matrix (Ni and Ni-P) has not been well understood yet.

Therefore in this study, it is intended to shed more light on the effect of particle characteristics (size, concentration, type) on the codeposition process, microstructure and strengthening mechanisms in Ni and Ni-P electrodeposited coatings.

1.2 Organization of dissertation

Chapter 2 provides fundamental information on Ni-based electrodeposited composite coatings and state of the art. The subsequent sections include information about the most important models of electrodeposition processes and certain process parameters affecting the particle incorporation. The following section is dedicated to fundamentals of in-situ EIS study of electrodeposition. The next section contains information about the strengthening performance with special regards to strengthening mechanisms in Ni-based composite coatings. In the last section, the objectives of this project have been mentioned and illustrated with a schematic view.

Chapter 3 focuses on the experimental procedure, materials and chemicals which were used in this work, and the following section contains a brief description about the characterization and analyzing tools which were used in this project.

Chapter 4 contains both achieved results and discussion. The first section regards the results and the discussion about Ni and Ni composite coatings. The influence of particle size, concentration and particle type on the layer characterization, electrodeposition behavior and strengthening of deposits will be discussed in this section. The next section covers the same procedure for the Ni-P and its composite coatings.

Finally, the conclusion, further works and references are given respectively.

2 THEORETICAL BACKGROUND

2.1 Nickel Electrodeposition

The electrodeposition of nickel was first described in 1837. Bird electrolyzed solutions of nickel chloride or Sulfate for some hours and obtained a crust of metallic nickel on a platinum electrode. In 1840, the first patent for commercial nickel plating was granted to J. Shore of England who specified a solution of nickel nitrate.

Nickel plating is similar to other electroplating processes that employ soluble metal anodes. It requires the passage of current between two electrodes that are immersed in a conductive, aqueous solution of nickel salts. The flow of current causes one of the electrodes (the anode) to dissolve and the other electrode (the cathode) to become covered with nickel. The nickel in solution is present in the form of divalent positively charged ions (Ni^{2+}). When the current flows, the positive ions react with two electrons and are converted to metallic nickel at the cathode surface. The reverse occurs in the anode, where metallic nickel is dissolved to form divalent positively charged ions which enter the solution. The nickel ions discharged at the cathode are replenished by those formed at the anode.

Most commercial nickel plating solutions are based on the Watts bath, including nickel sulfate as the main source of nickel ions, nickel chloride which provides anode corrosion and increases the diffusion coefficient of nickel ions, thus permitting a higher limiting current density and finally boric acid as pH buffer [4-6].

2.2 Application of Ni electrodeposition in microsystems

Electrodeposition is a suitable process for producing thick metallic microstructures, especially for producing relatively deep micromoulds in Microsystems industry. A renowned technique in this field is LIGA, pioneered in Germany in the early 1980s [9]. Since then, LIGA fabricated Ni microcomponents have been largely applied in micro sensors and actuators (Figure 2.1).

However, applications in harsh service conditions - such as high temperature, high pressure, constant corrosion and friction - put forward a requirement of better material properties on LIGA Ni. Numerous studies in characterizing LIGA fabricated samples have shown the insufficient mechanical and tribological properties of pure Ni. For example, Ni has been found to have a high friction coefficient during the wear testing of LIGA fabricated microrotors [10]. It implies that Ni lifetime was well below the required level. The high friction coefficient of Ni leads to problems in obtaining dimensionally accurate microcomponents with high aspect ratio during the plastic moulding process [11]. The stress-life experiments have shown that LIGA Ni structures have endurance limits that scale with tensile strength [12]. Electroformed alloys and metal matrix composites (MMC) are promising alternatives to pure metals, which is proposed in literature for improving properties of LIGA Ni or replace Ni for microsystem applications. The former introduces alloy elements into Ni during the electroforming process. For example, nanocrystalline nickel-

Tungsten (Ni-W) alloys are being considered as an attractive alternative to electroformed Ni for applications such as mould inserts and micro motors [13]. So far, only a few numbers of binary alloys, i.e. Ni-Cu, Ni-Fe, Ni-Co and Ni-P, have been investigated for the purpose of microsystems fabrication [7-15]. Among them, Ni-P has, due to its better properties compared to Ni and even Ni composite coatings, especially high mechanical properties (hardness, wear resistivity) and higher corrosion resistance [15-19]. Magnetic properties of Ni-P - particularly in low phosphorous content - can also play a determining role in applications of MEMS devices, because electromagnetically actuated MEMS are more stable for high force and large actuation gap applications [20, 21]. Recently, Kobayashi and his colleagues [22] showed that nanocrystalline Ni-P has a higher fatigue limit, more than two times, than electrodeposited microcrystalline Ni polycrystal.

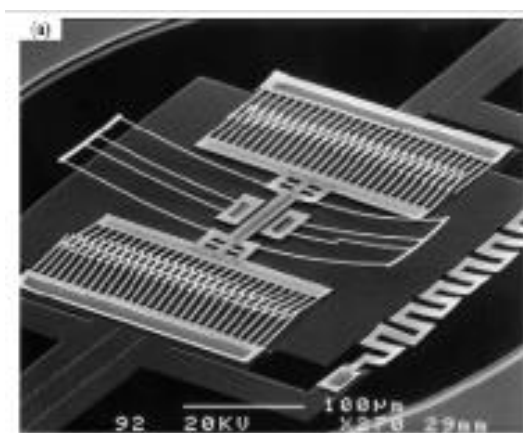


Figure 2.1 Ni electrodeposited Microresonator by LIGA process [23]

2.3 Ni-P electrodeposited coatings: mechanism, benefits and challenges

Among the various transition metal-metalloid alloys, nickel-phosphorous (Ni-P) alloys have received considerable interest as a result of their interesting functional properties. Ni-P coatings exhibit good corrosion [24-28] and wear resistance [29-30]. The high hardness and excellent machinability of this material makes it suitable for diamond turning applications, such as fabrication of large optics and other high precision parts [30]. Furthermore, Ni-P is a promising material as a diffusion barrier and as an undercoat for goldplated components, which enables a drastic decrease in the gold layer thickness. Additional technological applications of Ni-P coatings involve their use as catalytic coatings for hydrogen evolution reactions [31-32], as thin film resistors and underlayers of thin film magnetic discs [33-34], in microgalvanics applications [166] and for decorative applications in automotive industries. [35-36]

Phosphorous cannot be electrodeposited as a pure phase, but can be readily codeposited with iron group metals such as nickel, from solutions containing both Ni and P ions [37]. It is believed that strong atomic interactions between Ni and P make the induced codeposition of Ni-P alloy with stoichiometric composition possible. Electrolytic formation of nickel takes place in the face centered cubic (FCC) system and the codeposition of phosphorous occurs in the octahedral interstitial sites. It is generally accept-

ed that the crystallographic structure of Ni-P alloys is influenced by the amount of P present in the alloy and undergoes transitions from crystalline to nanocrystalline, and eventually becomes amorphous with increasing P content. In the codeposition process, the reduction of $[\text{Ni}^{2+}]$ ions at an active center on the cathode surface is followed by the surface diffusion of the Ni adsorbed atom to a suitable crystal lattice site. Reduction and codeposition of phosphorous inhibits this surface diffusion of the Ni atoms and hence, growth of crystal nuclei.

With increasing P content in the deposit, the rate of fresh nucleus formation becomes higher than the rate of growth of existing crystal nuclei, thus refining the deposit grain size. Finally, when a critical P content is achieved, nucleus growth effectively ceases and results in an amorphous structure having short range order over a few atomic distances [38]. There exists a considerable inconsistency in the available literature about the phosphorous content of the deposit at which crystalline to amorphous transition occurs. Researchers have come to the conclusion that the transition from crystalline to amorphous structure takes place over a range of concentration of P rather than in an abrupt way at a certain composition [39-41].

There are generally two methods of electroless and galvanic plating for fabrication of Ni-P deposits. Galvanic Ni-P, however, is suggested to be the more effective process in the fabrication of microcomponents. Especially, if higher thickness is needed in microsystems, usually between 50 to hundreds of micron, using electroless with its low deposition rate is limited [42, 43]. In galvanic processes, the deposition rate is determined easily by the current density. Besides, the relatively low working temperature in galvanic techniques provides milder operation conditions, and also makes the process less energy intensive. Also, the absence of additives - such as complexing agents and stabilizers - in electroplating solutions make the electrodeposition of Ni-P more attractive for applications in microsystem technology. Up to now, several researchers have performed investigations on the deposition of Ni-P via electroplating and studied the effect of various working parameters like current density, temperature, pH, agitation rate, etc. on phosphorous content and properties of these deposits [45-53].

Since MEMS devices typically contain several deposited and bonded layers of dissimilar materials, residual stresses can play an important role in determining the reliability of the processes and the fabricated devices [54]. Therefore, one main challenge with electroplated Ni-P is higher internal stress and higher concentration of dislocations. Particularly in low and medium phosphorous content this problem occurs which appears as dendrites and cracks on the deposit which would be deteriorating, especially for high-strength and high-aspect ratio in micro-nano structures [15, 17, 18, 41, 55]. The problem of high internal stress can also arise for Ni electrodeposits under certain conditions – like high current densities or low temperature – which mainly leads to deformation and swelling of deposit (Figure 1) [15]. The action of internal stresses during depositing of coatings results in oriented resultant strain in the final product [15, 16]. Prevailing of tensile stresses increases abrasion resistance, while predominance of compression stresses rises strength and hardness of the coating. High internal stresses increase brittleness.

According to literature [17, 57], the magnitude of stresses during electrodeposition processes can be influenced by some parameters like temperature or additives. One alternative to decrease the stress is using stress-reducing agents in order to induce compressive stress. Compressive stresses are advantageous in mechanical structures under load, since they tend to inhibit crack formation and growth. The anode material in nickel plating is usually metallic nickel. Chloride or halogen ions are required to activate the anode and enable its dissolution. Chloride additions in MEMS applications, however, are particularly harmful since they tend to increase the tensile stresses [18]. The stresses can also be decreased by increasing plating temperature [18], but this is not a particularly attractive option in MEMS application since higher temperatures can induce swelling of the resist and induce uncontrolled dimensional variations in the finished part. Another alternative is the use of sulfur-containing compounds such as saccharin in small amounts [17, 22]. These additives act as grain refiners and stress relievers, rapidly inducing compressive stresses. Grain refinement through addition of saccharin in the solution, though, results in the incorporation and accumulation of sulfur at the grain boundaries, which increases the susceptibility of the nickel part to corrosion [18]. According to few investigations, it was seen that adding particles into the electrolyte – except for their strengthening role - could also decline internal stress in the Ni deposit [15, 56]. Therefore, the focus of the following sections is on the role of particles from different aspects on the layer characterization of Ni-based coatings.

2.4 Ni-based dispersion coatings

Codeposition is a coating protective technique which consists on introducing homogeneously inert particles of a different material in the metal matrix (Figure 2.2). This two-phase coating improves corrosion and mechanical resistance. The improvement of these properties depends on the combination of both particles and metal matrix. As with conventional electrolytic deposition, the matrix of electrodeposited composite coatings can be in the form of a pure metal or an alloy. A wide range of composites can be obtained by selecting different types of inert particles like metal oxides, metal carbides or organic compounds. The second phase can be in the form of a powder or a fiber (either oriented or of random orientation) and conducting or non-conducting, depending upon the intended application. It is important that the second phase material is insoluble in the electrolyte to be used, and that it can be wetted.

In particular, nickel composite deposits prepared by electrodeposition are characterized by their high density, minimum porosity, excellent corrosion resistance and good wear resistance [62], as well as the reduction in the grain size of Ni deposit leading to increased strength and strain hardening rate [63]. For nickel matrix electrodeposits, a great variety of particles have been used such as oxides (i.e. TiO_2 , SiO_2 , Al_2O_3 , CeO_2 , ZrO_2 , SnO_2 and Cr_2O_3 [64-69]), carbides (i.e. WC [70], TiC [61] and SiC [60, 71-76]), nitrides (i.e. Si_3N_4 , BN [77-78]), carbon nanotubes [79], etc.

Nowadays, the ability to produce new composite materials with good properties by using micro- and nanoparticles is leading technological interests. This improvement depends on the particle characteristics,

mainly the size and the percentage of the particles codeposition, as well as the distribution of these particles in the metallic matrix [80].

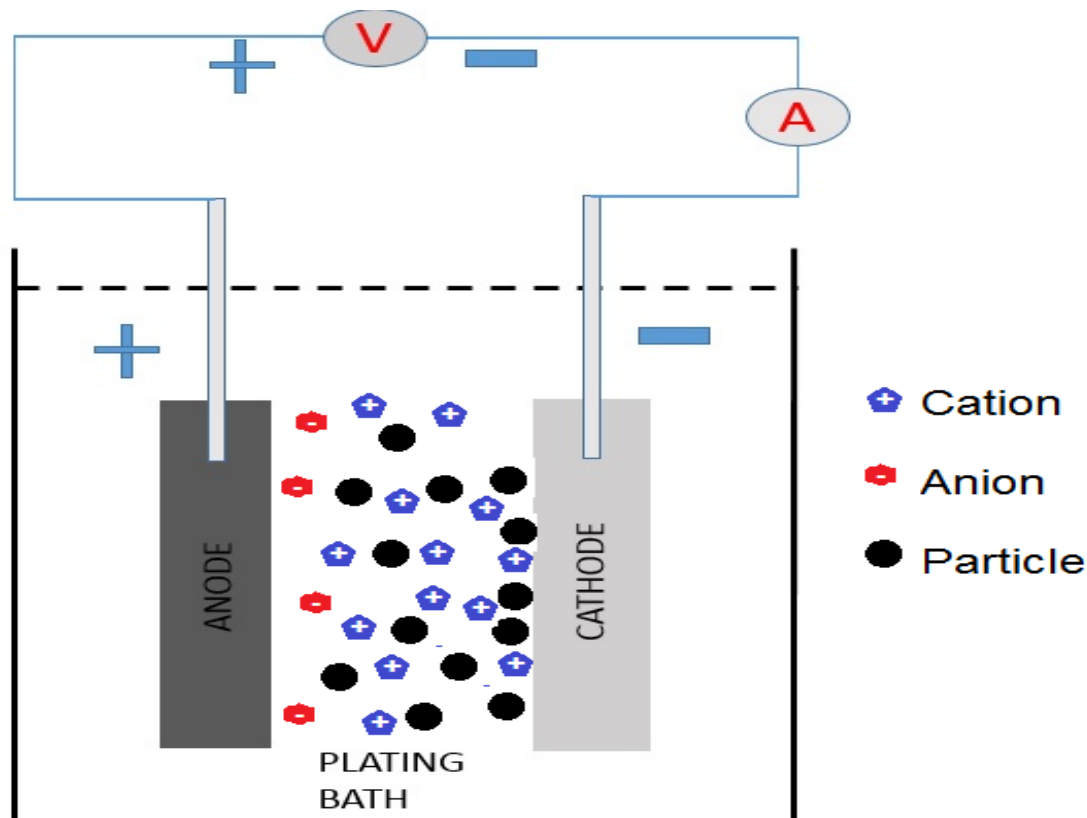


Figure 2.2 Schematic of electrodeposition process [108]

Furthermore, the influence of particles embedment in the matrix by either electroless or electroplating techniques has attracted the scientific interest in Ni-P matrix composites [17, 19, 81-94]. However, there are still contradictions among the research community concerning the influence of codeposited particles on the mechanical properties of Ni-P composites coatings.

For example, Berkh [84] believes that wear resistance, internal stress, and ductility of Ni-P-SiC composites were appreciably improved by electrodeposition in the presence of fine SiC powders. On the other hand, some researchers like Aslanyan [87] reported that SiC showed negative effect on mechanical behavior of Ni-P deposits. However, some researchers [95] studied the effect of P content on possible strengthening mechanisms occurring in Ni-P electroplated deposits without particles. It can be concluded that the role of particles on strengthening mechanism of electrodeposited Ni-P is not well-understood yet. Some researchers believe that there could be an interaction between the addition of particles in the bath and the phosphorus content in the deposit [84]. According to limited available data [17, 84], the level of P in the Ni-P matrix can affect particle incorporation, and conversely the particles can considerably influence the process of Ni-P alloy deposition. In fact, an extremely important role in codeposition is played by characteristics of the particles like their nature, size and concentration. Still, no systematic investigation of these factors has been reported yet on electrodeposited Ni-P composite coatings.

2.4.1 Effect of particle features on the electrodeposition behavior

Based on recent research on the process of electrodeposition, the important parameters that influence the composition of the deposit have been identified as electrode orientation, hydrodynamics, particle characteristics – such as size, shape, and type – current density and current modulation, composition, temperature and pH of the electrolyte, and the particle loading of the electrolyte [3, 71, 72, 111, 112, 114]. The influence of a particular variable on the electrodeposition process is typically assessed by the change in the amount of particle incorporation obtained when that parameter is varied. It has to be emphasized that the effects of certain process parameters, which are often interrelated, may vary for different particle-metal combinations [3, 111]. The following section describes the effects of selected process parameters including particle characteristics on the electrodeposition process.

Generally, increasing the particle content of an electrolyte increases the volume percentage of particles found in the deposit until a maximum is reached. Still, the percentage of embedded particles depends partly upon the electrolyte composition and partly on the type of particles added. An example can be found in the work by Greco and Baldauf [96], who noted that three times as much TiO_2 than Al_2O_3 could be deposited with nickel in the same conditions. Also for conducting particles, relatively large amounts of entrapment can be obtained, while for non-conductive particles it is more difficult [97].

In their work on nickel/chromium composite electroplating, Bazzard and Boden [98] found that codeposition of conductive particles can be problematic because of the dendritic growth on their deposits, caused by the fact that an incorporated particle acted as a conductive "high spot" in the coating for the deposition.

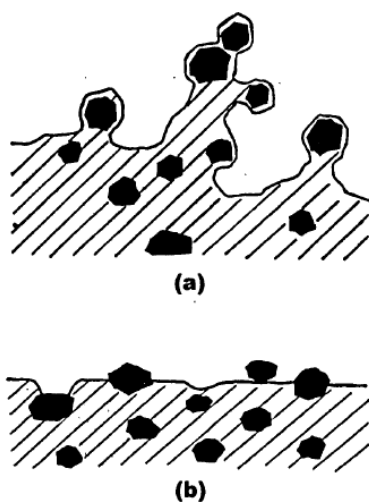


Figure 2.3 Typical surface profile of composite coatings: a) containing conducting particles; b) containing non-conducting particles [99]

Similar findings have been reported by others [99-101] who stated that semi-conductive and conductive particles (e. g. chromium carbide, zirconium diboride, graphite) tended to form surface nodules, whereas non-conductive particles (e. g. silicon carbide, Alumina) did not (Figure 2.3). Stankovic [101], in particular, noted that particle type and current density have greater influence over coating morphology than particle size.

However, Sova [102] did not find any of the nodulation previously mentioned in his trials on the codeposition of zirconium particles with a nickel-cobalt alloy. The reason was that the zirconium particles were covered with a very thin stable layer of oxide, so that they behave more like inert non-conductors.

Chen et al. [103], studying the codeposition of copper with Alumina, stated that particle structure plays an important role. The hexagonal structured α -Alumina can be readily codeposited, while spinel cubic structured γ -Alumina was reported to show no codeposition (γ -Alumina can be partially or totally converted to α -Alumina after heating at 1125°C). Roos et al. [2], on the other hand, disagreed with these results, stating that γ -Alumina can be deposited as well as α -Alumina, but in much smaller amounts. This was found to be because of the different amounts of ions adsorbed on the particle surfaces. The ionic cloud around the particle plays two different roles on the codeposition rate. On one hand, it could help the attraction towards the cathode, if a positive charge is present at the particle surface (and giving time for the particle to be engulfed by the growing metal layer). But on the other hand, it can interfere with the diffusion layer. Chen et al. [103] also noted that titania behaves in a similar way to Alumina, with rutile being the most favored deposited form, while Anatase did not codeposit at all.

Stojack and Talbot [104] studied the influence of suspended sub-micrometer diameter Alumina particles on polarization during electrocodeposition with copper at a rotating cylinder electrode. The authors stated that particle incorporation behavior, as a function of increasing current density, can be divided into several general regions: initially a region where incorporation increases sharply reaching a maximum value, followed by a sharp decrease in incorporation, then a region where incorporation is relatively constant, and lastly, another decrease as mass-transport-limited conditions are approached. The regions wherein the amounts of incorporation sharply increase or decrease with current density are more sensitive to particle size, crystallographic phase and even to the particle manufacturing process. When the incorporation increases the rate-determining step for codeposition appears to be the reduction of metallic ions adsorbed onto the Alumina particles. The peak in particle incorporation was found to coincide with the point of zero charge (PZC) of copper in an acid copper plating solution. The results are shown in table 2.1. Essentially, Verelest et al. [110] reached the same conclusion for Ag/Al₂O₃ composite coatings. Recently, Nowak et al. [72] used the electrochemical impedance spectroscopy (EIS) technique for an in situ investigation of the electrolytic codeposition of Ni-SiO₂ and Ni-SiC composite coatings. They tried to clarify why silica particles hardly codeposited in comparison to silicon carbide particles. They stated that the presence of SiO₂ and SiC particles influences the metal deposition process in different ways. SiC particles are embedded in the growing layer because of an apparent decrease in the electrode surface

area, probably due to blocking the part of the surface by partly engulfed particles. Meanwhile, in the case of SiO_2 particles no blocking has been observed.

Particle identification	Current density / mA/cm^2	Particle incorporation / wt %
$0.3 \mu\text{m } \alpha\text{-Al}_2\text{O}_3$	20	0.7
$0.3 \mu\text{m } \alpha\text{-Al}_2\text{O}_3$	24.5	0.9
$0.3 \mu\text{m } \alpha\text{-Al}_2\text{O}_3$	35	0.5
$1 \mu\text{m } \alpha\text{-Al}_2\text{O}_3$	20	0.7

Table 2.1 Codeposition of Al_2O_3 -a 20 mA/cm^2 , 120 g/l particle and using a rotating cylinder electrode at 1000 rpm [110]

EIS has also been used by Benea et al. [106] to study the influence of silicon carbide nanoparticles on nickel electroplating. Particles affected the nickel reduction as outlined by the displacement of the polarization curve to a lower reduction potential and by the presence of a lower charge-transfer resistance. They also stated that the surface morphology of nanostructured composite layers is different compared to a pure nickel coating. The effect of SiC particles is to increase the number of nucleation sites with a reduction in crystal growth, resulting in smaller grain size of the nickel matrix.

Masalki et al. [107] determined the equivalent circuit for the nickel electrocrystallization process from a Watts bath containing SiC as shown in Figure 2.4.

The authors added a surfactant (sodium dodecyl sulphate) and a brightening agent (2- butyne-1,4-diol and saccharine) to the electrolyte. In the equivalent circuit proposed, R1 amounts relate to the electrolyte resistance, R3 is related to the charge transfer resistance, R4 is the desorption resistance, C2 is the double layer capacitance, and finally, C5 is the pseudo-capacitance of adsorbed intermediates.

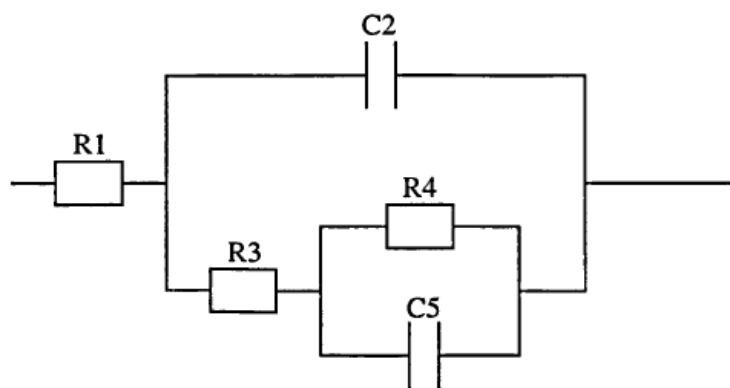


Figure 2.4 Electric equivalent circuits for the nickel electrocrystallization process from a Watts bath containing SiC [107]

Kondo et al. [149] proposed two different ways for the deposition of SiO_2 into a (0 0 1) oriented zinc electrodeposit: (a) by particles lining up along the laterally growing macrosteps on the (0 0 1) and (b) by randomly dispersed particles on the (0 0 1). They proposed that the sidewalls of particles are incorporated into the macrosteps at the edge of (0 0 1), whilst the bottom of randomly dispersed particles is incorporated into the (0 0 1) probably by atomic steps.

Bozzini et al. [150] found that when B_4C micrometer-sized particles are added to an electrodeposition bath containing $\text{KAu}(\text{CN})_2$ and citrates, a decrease or increase of the cathode overvoltage is observed depending on the deposition current density (overvoltage decreases for low current density range and the opposite for high current density range). They relate this phenomenon to the morphology of the deposit (surface roughness) and to the hydrodynamic conditions prevailing at the cathode surface. They stated the hydrodynamic effects were minor. The observed overvoltage variations were dominated, according to the authors, by the competition of two morphological effects. These were in addition to the usual polarization increase with current density increase and were a reduction of the overvoltage due to the increase of the effective cathode area because of the formation of "humps" and enhancing the reduction of effective cathode area because of the screening effect of ceramic particles.

In 2001, Surveliene et al. [151] studied the influence of the presence of oxides (MoO_2 and TiO_2) on the electrodeposition of chromium. They found a lower rate for the formation of composite Cr- MoO_2 and Cr- TiO_2 compared with that of a Cr coating. They suggested this is related to the adsorptive capacity of MoO_2 and TiO_2 and desorption of their hydrides from the electrode surface. They showed that highly dispersed particles of MoO_2 might be used to reduce hydrogenation of the substrate, since MoO_2 acts as an inhibitor of hydrogen adsorption in the substrate, and its efficiency increases with increase in MoO_2 concentration. Moreover, both oxides have an effect on coating properties such as hardness, ductility, internal stresses and high temperature resistance. Despite the large range of sizes employed, the authors found out that particle type (in terms of "chemical" nature) and current density had a greater influence on coating morphology than particle size.

Support for the importance of the particle nature rather than particle sizes comes from Chen et al. [103]. They stated that the codeposition of Alumina with copper is easier if $\alpha\text{-Al}_2\text{O}_3$ is codeposited rather than $\text{g-Al}_2\text{O}_3$. This was found to be more important than the particle sizes.

There are few studies regarding the effect of particle shape on codeposition. Of course particle shape would affect adsorption onto the cathode, adsorption of ions onto the particle themselves and suspension stability. Greco [108], in a review, noted those composites containing discontinuous fibers are far more difficult to produce than particulate composites. Different results have been reported for the influence of particle size. Chen et al. [103] found that they could increase the codeposition rate of chromium in a nickel matrix by increasing the particle size. Suzuki and Asai [109], however, found that the opposite occurs with $\text{Ag/Al}_2\text{O}_3$, while Verelest et al. [110] have stated that the effect of particle size on codeposition is very small. Recently, Garcia et al. [152] examined Ni-SiC composites. They codeposited SiC particles of three different sizes (namely 5, 0.7 and 0.3 μm) with nickel from a Watts' bath. They found that

for a specific density of particles in the plating solution, the number of particles in the coating increases with increasing particle size.

Stankovic and Gojo [101] performed a similar investigation, but they also tested the influence of different particle types, rather than just different particle dimensions.

Table 2.2 shows the particles analyzed by these authors together with their main dimensions.

Kind of particle	Main diameter (μm)
$\alpha\text{-Al}_2\text{O}_3$	0.3
SiC	2.3
MoS ₂	6.1
Graphite	5.4

Table 2.2 Size of particles used by Stankovic and Gojo in their investigations [101]

While refined models have been developed during the years, the ECD process is still not understood completely.

2.4.2 Models of electrocodeposition

The purpose of this chapter is to give a short summary on the main theories which have been developed to describe the ECD process. In general, there are three main steps that must occur during ECD:

(I) Transport of particles from the bulk electrolyte to the electrode surface by means of various mechanisms, e.g. convection, diffusion and electrophoresis.

(II) Particle adsorption at the electrode surface.

(III) Irreversible entrapment of the particles in the growing metal layer.

In general, the following discussed models differ in the description of these three stages of the ECD process. A more detailed description of all the models developed for the ECD process can be found in several review papers which describe models, mechanisms, effects of process parameters, and possible applications [2, 3, 111-115].

The first model that accounts for the electrodeposition of metal reinforced with particles was proposed by Guglielmi [1].

According to this mechanism the electrocodeposition process proceeds via two steps (Figure 2.5). Firstly, particles are weakly adsorbed on the cathode surface by van der Waals forces with high degree of surface coverage which can be presented by Langmuir adsorption isotherm. Secondly, particles are strongly adsorbed on the surface by Coulomb forces under the effect of applied electric field and incor-

porated in the growing metal matrix. According to this model the volume fraction of the incorporated particles, α , can be expressed as:

$$\frac{\alpha}{1-\alpha} = \frac{z F \rho_m V_0}{M_m i_0} \cdot e^{(B-A)\eta} \cdot \frac{k c_{p,b}}{1+k c_{p,b}}$$

Where M_m and ρ_m are the atomic weight and the density of the deposited metal, respectively, i_0 is the exchange current density, z is the valence of the electrodeposited metal, F is Faraday constant, V_0 is the electrode overpotential, c_p , is the bulk concentration of particles and k is the Langmuir adsorption constant. The main drawback of this model is that it neglects the particle size and hydrodynamics i.e. mass transfer of particles.

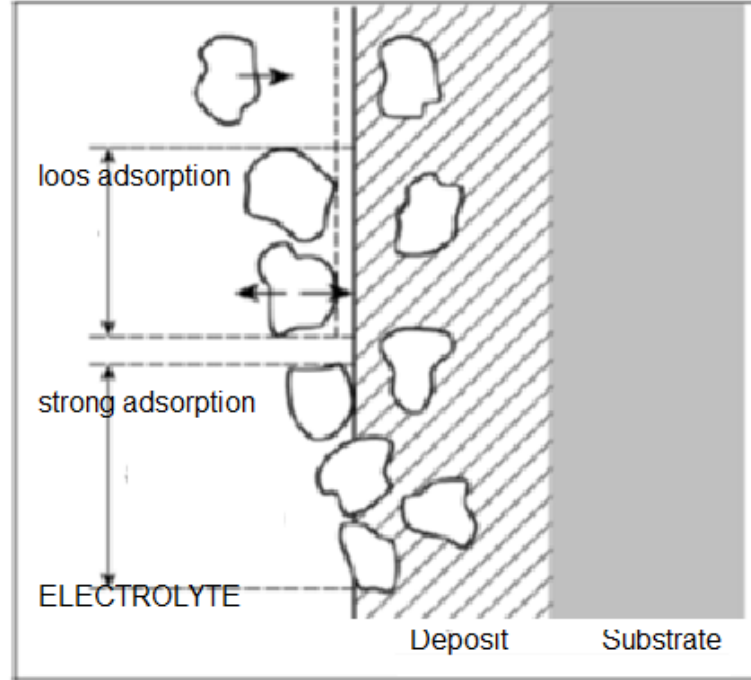


Figure 2.5 Guglielmi's ECD Model [1]

Celis [2] proposed a five-step mechanism to account for the electrocodeposition process: (1) formation of ionic cloud around the particles, (2) mass transfer of particles by convection to the hydrodynamic boundary layer, (3) mass transfer of particles to the cathode surface by diffusion, (4) adsorption of free ions and electroactive ions adsorbed on the particles on the cathode, and (5) electroreduction of adsorbed ions accompanied with incorporation of particles into the growing metal matrix.

According to Kurozaki's study [116], dispersed particles are transferred to the Helmholtz's double layer by mechanical agitation in the first step. Secondly, particles which are charged in the high potential gradient are transferred to the cathode by electrophoresis. In the third step, particles are adsorbed on the cathode surface by Coulomb attraction between them and adsorbed anions on the cathode, and hence,

are incorporated into the growing metal layer. Other models were also suggested by other authors [27, 28]. Meanwhile, more investigation is still needed that accounts more with the particle characteristics (composition, size, and crystallinity) and the operating electrodeposition parameters. In this work, we did a survey on the behavior of electrodeposition affected by different particle characteristics.

2.4.3 In-situ study of Ni-based coatings by means of EIS

2.4.3.1 Applications of EIS

Electrochemical impedance spectroscopy (EIS) can provide accurate, error-free kinetic and mechanistic information using a variety of techniques and output formats. EIS techniques use very small excitation amplitudes, often in the range of 5 to 10 mV peak-to-peak. Excitation waveforms of this amplitude cause only minimal perturbation of the electrochemical test system, reducing errors caused by the measurement technique.

Moreover, EIS techniques can provide valuable mechanistic information. Measurement accuracy is another benefit coming with EIS. In fact, because the method does not involve a potential scan, measurements can be made in low conductivity solutions where DC techniques are subject to serious potential-control errors. In fact, you can use EIS to determine the uncompensated resistance of an electrochemical cell. For this reason, EIS is becoming a powerful tool in the study of corrosion, semiconductors, batteries, electroplating, and electro-organic synthesis. Table 2.3 summarizes some of the electrochemical phenomena that have been studied using EIS [117].

2.4.3.2 Concept of EIS method in electrodeposition process

EIS is a steady-state technique capable of observing phenomena in electrochemical systems whose relaxation times vary over many orders in magnitude [118]. The EIS technique applies a small-amplitude sinusoidal voltage to a working electrode at a number of discrete frequencies, ω , ranging from 0.01 to 62,500 Hz as shown in Figure 2.6. At each of these frequencies, the resulting current exhibits a sinusoidal response, $I(\omega)$ that is out-of-phase with the applied sinusoidal voltage signal. The electrochemical impedance, termed $Z(\omega)$, is the frequency-dependent proportionality factor between the voltage signal and current response [127]:

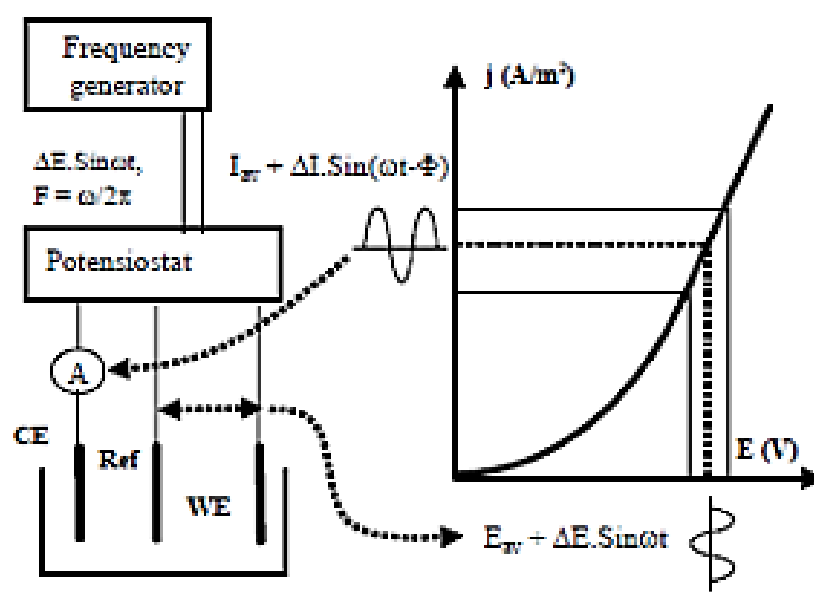
$$Z(\omega) = V(\omega) / I(\omega)$$

$Z(\omega)$ is a complex-valued vector quantity with real and imaginary components, whose values are frequency-dependent:

$$Z(\omega) = Z_{\text{Real}}(\omega) + j Z_{\text{Imag}}(\omega)$$

Research Area	Application
Corrosion	<ul style="list-style-type: none"> • Rate Determinations • Inhibitor and Coatings • Passive Layer Investigations
Coatings Evaluation	<ul style="list-style-type: none"> • Dielectric Measurements • Corrosion Protection
Batteries	<ul style="list-style-type: none"> • State-of-charge • Materials Selection • Electrode Design
Electrodeposition	<ul style="list-style-type: none"> • Bath Formulation • Surface Pretreatment • Deposition Mechanism • Deposit Characterization
Electro-Organic Synthesis	<ul style="list-style-type: none"> • Adsorption/Desorption • Reaction Mechanism
Semiconductors	<ul style="list-style-type: none"> • Photovoltaic work • Dopant Distributions

Table 2.3 Applications of impedance studies [117]



$$\text{For each frequency : } Z(F) = \frac{\Delta E}{\Delta I} = |Z|e^{j\theta}.$$

Figure 2.6 AC voltage signal imposed on an electrochemical system and the resulting AC current and impedance [119]

The real and imaginary impedance components can be plotted against each other to generate a Nyquist plot. Figure 2.7 shows a typical example of Nyquist plot for Ni electrodeposition.

Each point on the plot is the impedance at one frequency, and each semicircle is a characteristic of a single time constant. The ohmic or electrolyte solution resistance is determined at the high frequency intercept on the real (horizontal) axis. The semicircle diameter (Loop 1) gives the charge transfer resistance, which is related to the rate of the electrochemical reaction. The inductive loop (2) is related to ion-additive complexation, adsorption mechanisms, or additive degradation processes.

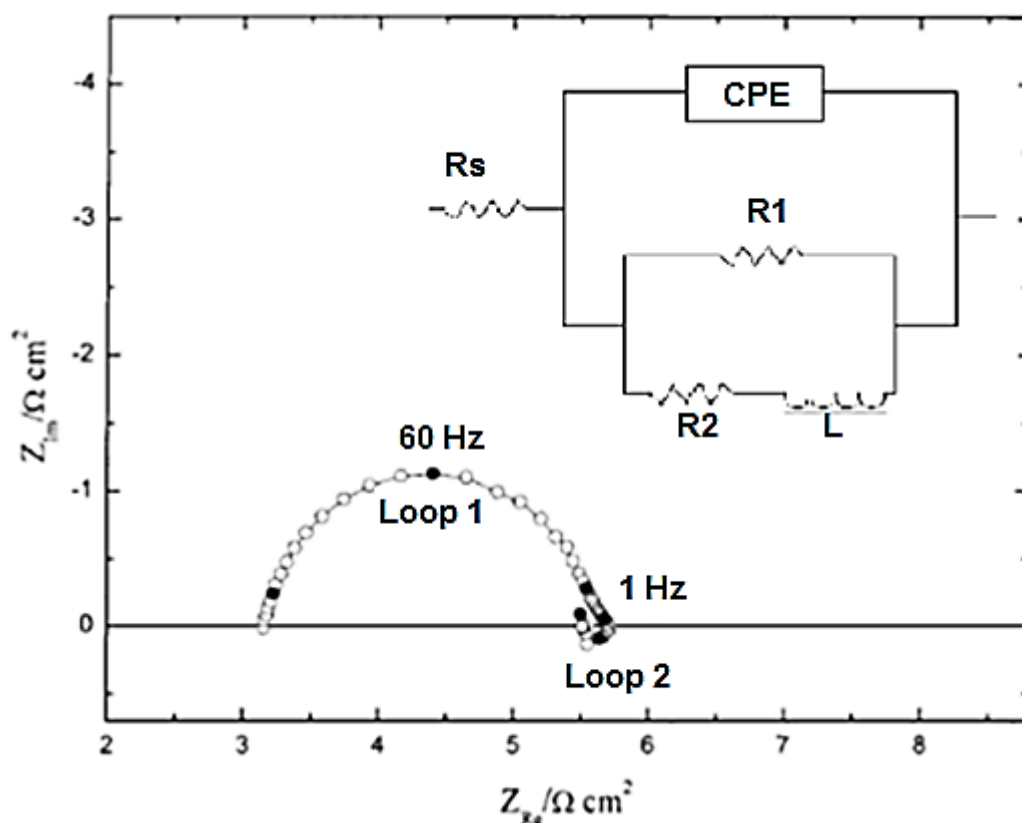


Figure 2.7 Complex plane impedance spectrum for Ni electrolyte containing 150 g/l NiSO₄, i 20mA/cm², pH 2.5, T 60°C, no stirring, Pt anode, EW-Ni substrate [34]

To better understand the double layer capacitance, it is helpful to review the double layer that forms at all electrode interfaces immersed in electrolyte solutions. The model of the double layer originated from the work of Helmholtz (1853) on the interfaces of colloidal suspensions and was subsequently modified by Gouy, Chapman and Stern, and later Grahame [119]. Under the influence of applied potential, rearrangement of ions near the electrode surface results in an electrical double layer called the Helmholtz double layer, followed by the formation of a diffusion layer as shown in Figure 2.8. These two layers are referred as the Gouy-Chapman layer. The process is as follows:

- *Migration*: The hydrated metal ions in the solution migrate towards the cathode under the influence of impressed current as well as by diffusion and convection.
- *Electron transfer*: At the cathode surface, a hydrated metal ion enters the diffused double layer where the water molecules of the hydrated ion are aligned. Then the metal ion enters the Helmholtz double layer where it is deprived of its hydrate envelope.
- The dehydrated ion is neutralized and adsorbed on the cathode surface.
- The adsorbed atom then migrates or diffuses to the growth point on the cathode surface.

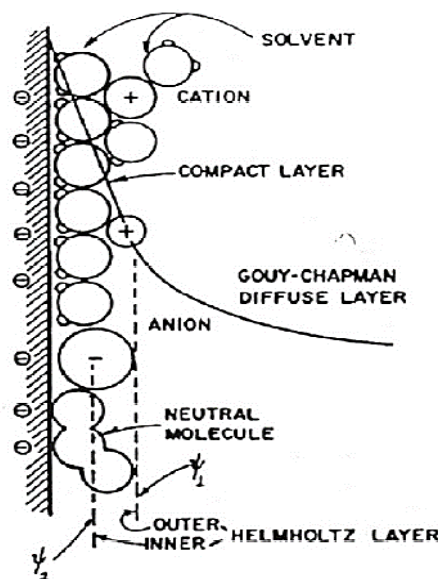
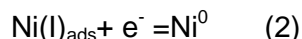
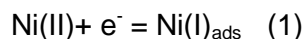


Figure 2.8 Schematic models of the double-layer structure [120]

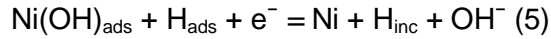
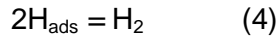
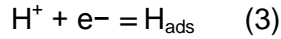
2.4.3.3 Evaluation of Ni electrodeposition using EIS

The mechanism of Ni^{2+} reduction from acid sulfate solutions has been extensively studied by Epelboin et al.; using Watt's electrolytes and many investigations related to mechanism of Ni electrodeposition have been cited to his results [121-124]. It is generally acknowledged that the electrocrystallization of the Ni^{2+} ion occurs in two steps. In the first step, Ni ion is converted to elemental nickel by the one electron step:



In the second step, the intermediate acts as a catalyst for the reduction of Ni (II) by a two-electron step, although, its occurrence has not been confirmed by others. Based on the considerations proposed by Epelboin et al. [123, 124], they provided further support that nickel deposition occurs exclusively by Reactions 1 and 2 above. Because hydrogen evolution reaction (HER) occurs simultaneously during nickel deposition, it must also be included in the mechanism. This reaction has been assumed to proceed via a single two-electron step by some researchers [123, 124], but has been considered by others to proceed by more complex mechanisms involving the formation of an adsorbed intermediate H_{ads} [124- 127]. In the

latter cases, HER was considered to occur by a one-electron step (Reaction 3) followed by the chemical combination (Reaction 4) of adjacent H_{ads} adatoms. Hydrogen incorporation in the coating (Reaction 5) was also included in one study [20].



In another study [126], the analysis of a model for nickel deposition involving reactions 3 and 4 indicated that H_{ads} adsorbs on the electrode and blocks active sites at the expense of the iron-group metal intermediates, e.g. $Ni(I)_{ads}$ and $Fe(I)_{ads}$. Regardless of the specific mechanism, the HER raises the pH in the boundary layer and can even passivate the electrode at high enough overpotentials through the formation of $Ni(OH)_2$ [125].

Up to now, EIS has been employed by several researchers in order to investigate deposition of Ni under the influence of various working parameters including electrolyte type, ion concentration, additive, pH, temperature, agitation and applied potential and additives [118-125]. The early studies of EIS involved mainly simulations of spectra with no comparison to experimental data [123-125] while there are few investigations [125, 128] which have also compared simulations of a physicochemical model for nickel deposition to experimental EIS spectrum.

2.4.3.4 Interaction of particle-interface in Ni electrodeposition studied by EIS

According to recent literature, Electrochemical Impedance Spectroscopy (EIS) can also be a reliable tool which can provide a better understanding on electrocodeposition processes by considering adding particles into the electrolyte. The present paper summarizes (Table 2.4) the works regarded EIS study during electrodeposition of Ni based composite coatings. The majority of these investigations have been presented by the research community in the last decade.

Deposit type	Studied parameters	Effects on impedance behavior	Correlated layer properties	Reference
Ni-SiC	<ul style="list-style-type: none"> Comparison between SiC and Cr particles Potential effect agitation effect 	Catalyzing H^+	<ul style="list-style-type: none"> Current efficiency Hydrogen inclusion 	138 (1993)
Ni-SiC	<ul style="list-style-type: none"> Different size Different concentration 	Charge transfer and inductive loop	<ul style="list-style-type: none"> Morphology 	139 (2012)

Deposit type	Studied parameters	Effects on impedance behavior	Correlated layer properties	Reference
Ni-SiC	<ul style="list-style-type: none"> • SiC 100 nm • Potential effect • triangular current 	No contribution in charge transfer for direct current but for triangular current.	<ul style="list-style-type: none"> • Morphology • Hardness 	140 (2005)
Ni-SiC	<ul style="list-style-type: none"> • magnetic field 	Improve mass transfer and accelerating charge transfer	<ul style="list-style-type: none"> • Morphology and microstructure • orientation 	141 (2007)
Ni-SiC	<ul style="list-style-type: none"> • SiC nano (20 nm) • Potential • Rotation 	Charge transfer	<ul style="list-style-type: none"> • Morphology • texture 	142 (2001) 143 (2002)
Ni-SiC and Ni-SiO ₂	<ul style="list-style-type: none"> • Effect of particle hydrophobicity 	effect of double layer capacity	<ul style="list-style-type: none"> • texture orientation • grain size • Morphology 	144 (2004)
Ni-SiC	<ul style="list-style-type: none"> • Pulse current (duty cycle) 	Charge transfer reveals duty cycle influences on peak current	<ul style="list-style-type: none"> • Grain size • Volume fraction • Morphology 	145 (2008)
Ni-TiO ₂	<ul style="list-style-type: none"> • 1 µm TiO₂ • Potential 	Change in charge transfer in low potential	<ul style="list-style-type: none"> • Morphology 	145 (2010)
Ni-ZrO ₂	<ul style="list-style-type: none"> • 10 µm ZrO₂ 	Not change electrocrystallization mechanism but increase deposition rate	<ul style="list-style-type: none"> • Microstructure and morphology • tribocorrosion 	146 (2009)
Ni-Al ₂ O ₃	<ul style="list-style-type: none"> • Nano Alumina • Potential 	Changes in impedance dependent on potential range	<ul style="list-style-type: none"> • Ni crystallization mechanism 	147 (2004)
Ni-Co-Al ₂ O ₃	<ul style="list-style-type: none"> • Ni concentration • Co concentration 	Increase in charge transfer for Ni-rich but decrease for Co-rich	<ul style="list-style-type: none"> • zeta potential 	148 (2010)

Table 2.4 Past EIS studies on the process of Ni composite electrodeposition

One of the first EIS studies on Ni electrodeposition with particles was done by Watson [130]. In this study the effect of Cr and SiC particles as respectively conductive and semi-conductive particles on the occlusion process of Ni electrodeposition was investigated [130]. According to impedance results, the capacitance loop with SiC addition was much larger compared to the one with Cr particles and even with no particles. Watson believed that the effect of SiC particles on nickel electrodeposition was to catalyze H_{ads} and Ni_{ads} intermediates. As proof of this theory, hydrogen amounts of deposits correlated with impedance results.

Meanwhile, in Watson's research [130], the low frequency part was very poorly defined and she considered that the addition of micrometric SiC particles preferentially catalyzes a H_{ads} intermediate and not a Ni_{ads} . While Benea et al. [38, 39] showed that by decreasing the charge-transfer resistance, as seen in Figure 2.9, the nanosized SiC particles can activate the nickel reduction. The same mechanism was found by Jousselein et al. [122]. They consider that the preferentially catalyzing intermediate is Ni_{ads} . It is well known that the electrodeposition process is a competition between nucleation and crystal growth. The SiC nanoparticles act mainly as nucleation sites and as a detriment to crystal growth. The corresponding nickel matrix has a smaller crystal size according to this mechanism. In subsequent SEM surface morphology investigations, they observed changes of the composite coatings compared with a pure nickel coating with smaller grain sizes being seen in the nanocomposite (Figure 2.10). Furthermore, XRD of the same composite layer showed a low texture of nickel matrix with orientation (1 1 0), in agreement with electro-chemical measurements which showed a disturbance of free growth of the nickel crystals in the presence of nanoparticles.

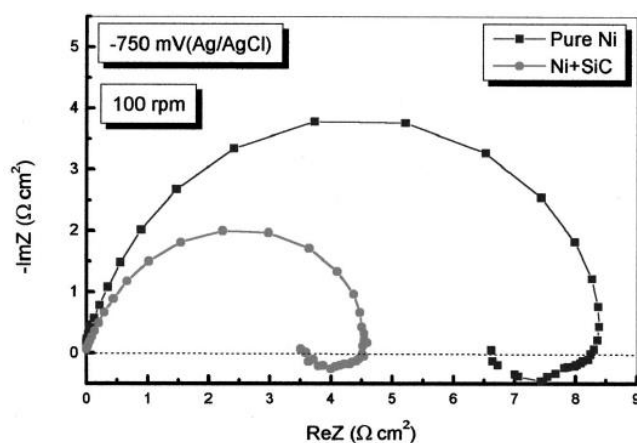


Figure 2.9 Impedance diagrams performed at cathodic potential of 2750 mV; Ag/AgCl: codeposition of nano-SiC with nickel 50 g/L SiC in the electrolyte and pure nickel electrodeposition. Disk rotation rate 100 rpm. [106]

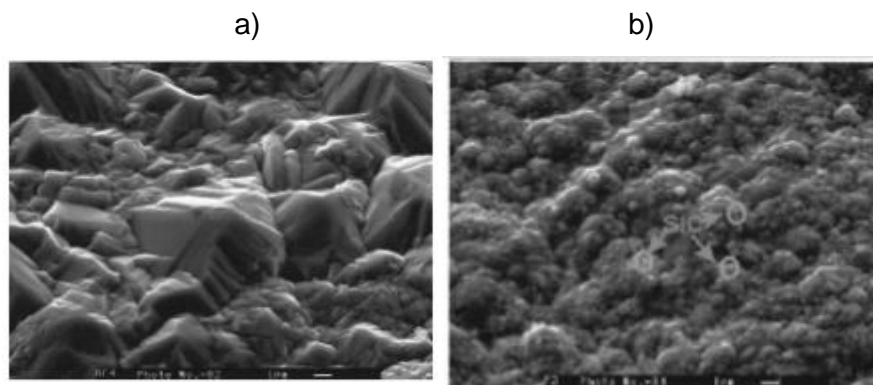


Figure 2.10 SEM surface morphology of pure Ni electroplating (a) Ni-SiC nanostructured composite coating. Current density 4 A dm^{-2} , 50 g/l SiC in the plating bath, disk cathode (b) [106]

The initial stage of Ni-TiO₂ composite system electrodeposition on glassy carbon electrode from an acidic solution of nickel sulfate has been investigated a few years ago by Wi and his colleagues [47]. In this investigation a combination of cyclic voltammetry (CV), chronoamperometry (CA) and electrochemical impedance spectroscopy (EIS) were used for analyzing the results. Figure 2.11 shows Nyquist plots and simulated plots for pure Ni and Ni-TiO₂ composite systems at different negative potentials (from -730 to -850 mV). To confirm the diffusion process of Ni reduction and the influence of TiO₂ particles, EIS measurements were performed at different applied potentials.

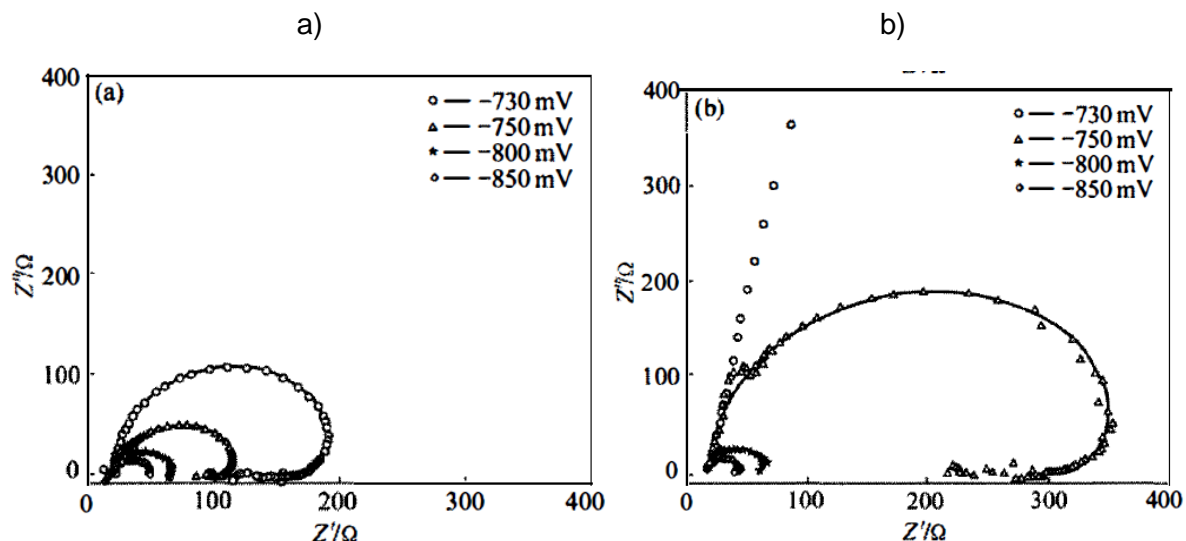


Figure 2.11 Experimental data (points) and simulated plots (solid line) for Ni-TiO₂ composite system (a) and pure Ni system (b) at various potentials [136].

The plots exhibit two regions of distinct electrochemical response: (1) at high frequencies a semicircular arc is obtained, characterized by a solution resistance, a double layer capacitance and a charge transfer

resistance (R_1). R_1 is estimated from the diameter of this first high frequency capacitive loop; (2) at low frequencies, the capacitive loop registered at more anodic potentials (< -730 mV) having the characteristics of diffusion impedance, is transformed at more cathodic potential (-730 mV) into a inductive loop in the Ni-TiO₂ system (Figure 2.11 (a)). While in the pure Ni system, at more cathodic potential (-750 mV) the inductive loop as seen in Figure 2.11 (b) is obtained.

The inductive loop was also observed by other researchers. It was believed that the inductive loop represented the presence of the intermediate. Some researchers characterized the inductive loops as the surface coverage of the adsorbed intermediate [140], whereas other researchers considered that the loop was related to the adsorption/desorption process of intermediates on/from the cathode surface [27]. Epelboin et al. [130] proposed a model using a chemical impedance procedure. In this work, it is considered that the reaction mechanism involving an intermediate species plays an important role in the rate determining step. Under the experimental conditions, Ni-TiO₂ and pure Ni systems present an inductive loop separately at -750 and -730 mV corresponding to the initial deposition potential of Ni.

Obviously, the inductive loop is related to the electrocrystallization process of Ni on the cathode surface. The results of impedance spectra show that the appearance of the characteristic inductive loops represents the nucleation/growth of nickel and the presence of TiO₂ particles reduces the charge transfer resistance of solution. The SEM observation also confirmed that TiO₂ particles can be considered as favorable sites for nickel nucleating [140].

2.5 Strengthening mechanisms in Ni-based composite coatings

For many years, great emphasis was placed on changing the strength of a metal in a targeted manner. In general, strengthening of metallic materials is used in order to specifically improve their properties for the desired application and purpose. With a sufficient strength, an increase of the resistance to plastic deformation can be seen.

Table 2.5 shows the common strengthening mechanisms in materials science.

The basis of strengthening is thus either the hindrance of dislocation motion or a very low dislocation density. In materials science and materials engineering, dislocations are considered the main basis of the plastic deformation and increase in strength. Crystal defects are formed during growth of crystals, under the influence of thermal, mechanical and electrical factors and upon irradiation by neutrons, electrons, X-rays and ultraviolet radiation (radiation effects).

A distinction is made among point (zero-dimensional) defects, line (one-dimensional) defects, defects that form surfaces in the crystal (two-dimensional) and volumetric (three-dimensional) defects. In a one-dimensional defect the size is much greater in one direction than the distance between neighboring like atoms (the lattice parameter), but in the other two directions it is of the same order. In a two-dimensional defect the dimensions are greater in two directions than the distance between the closest atoms and so on.

As it is also seen in the Fig. 2.12, a transfer can be considered as an additional half-plane of particles, which is inserted into a perfect, defect-free crystal. The place where the transfer is complete is called the dislocation line. At this point, the displacement causes the strongest lattice distortion, whereby a high-energy strain field is created around the dislocation line.

The key point of the importance of dislocations is the plastic deformation. This is based on all metals on the generation and movement of dislocations [176, 177].

Name	Characteristics
Solid-solution hardening	introduction of interstitial or substitutional atoms of different kind
Precipitation hardening	distribution of fine precepiatates
Dispersion hardening	distribution of 2nd phase particles
Work hardening	increase in dislocation density by plastic deformation
Fine-grain hardening	reducing grain size (Hall-Petch relationship)
Composites	mixing different materials

Table 2.5 various strengthening methods

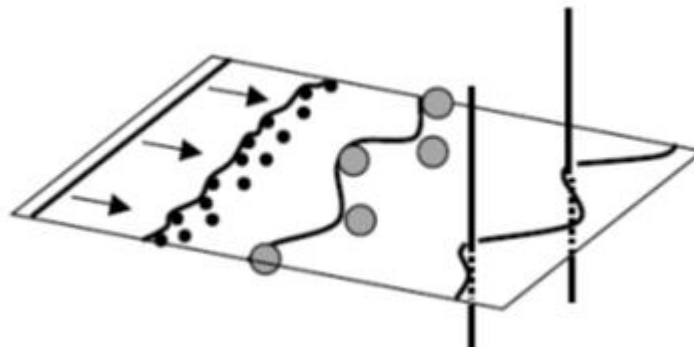


Figure 2.12 Schematic of various strengthening against dislocation motion [176]

2.5.1 Dispersion hardening – Orowan

Dispersion hardening or strengthening of a material means an increased resistance to deformation. The movement of dislocations in the metal facilitates metal deformation. Incorporated particles block the dislocation movement and thus strengthen the metal [141].

The strengthening effect of precipitates or other second phase particles generally becomes more effective, for a given particle volume fraction, as particle size becomes finer.

As schematically shown in Figure 2.13, when a dislocation approaches an array of hard obstacles, their elastic stress field causes the dislocation line to bow between the obstacles. Following Orowan [153], plastic deformation due to long range dislocation motion occurs when obstacles are fully bypassed, i.e.

when the applied stress is sufficient to give a dislocation loop diameter equal to the mean spacing L between obstacles.

Thus :

$$d_d = L \quad (1)$$

The dislocation loop diameter d_d is related to shear stress as

$$T = t b d_d \quad (2)$$

Where t is the shear stress acting on the dislocation, b is the relevant component of the Burgers vector and T is the dislocation line tension energy, which has the simplified form

$$T = \alpha \mu b^2 \quad (3)$$

Where α is a coefficient in the order of unity and μ is shear modulus. On substituting equation (3) into (2), the dislocation loop diameter is obtained as a function of stress

$$d_d = \alpha \mu b / \tau \quad (4)$$

Combining equations (4) and (1), the bypass stress is obtained as

$$\tau = \alpha \mu b / L \quad (5)$$

In this situation, i.e. particle strengthening, the mean particle spacing L is the governing size parameter, stress varying inversely with L . When the volume fraction of particles in the matrix is constant, L scales linearly with particle size, i.e. strength scales inversely with particle size at a fixed particle volume fraction. This theory shows good agreement with the experimental observations by Lloyd [153] of a substantial strength increase in an A356/SiC_p aluminum alloy matrix composite when particle diameter was reduced from 16 to 7.5 μ m at a fixed particle volume fraction of 15 % [142].

A high volume fraction of small particles finely dispersed through the metal matrix will therefore yield optimal hardening. It should be mentioned that there is no unlimited increase in dispersion strengthening with the volume fraction incorporated particles. Brown and Gow [153] found a maximum ultimate tensile strength and hardness for composite at approximately 10 vol% [141].

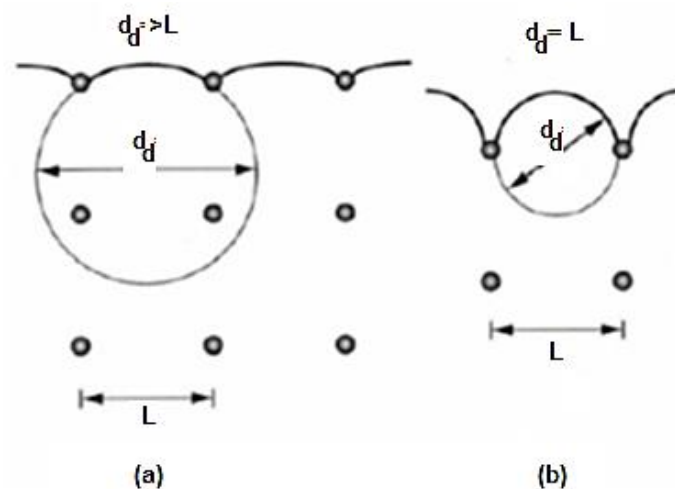


Fig 2.13 Onset of plastic flow controlled by particles in the metal matrix [153]

2.5.2 Grain size effects: Hall-Petch relation

Grain size has long been known to have a significant effect on the mechanical behavior of materials, in particular on the yield stress. In the 1950s, Hall and Petch [153] first established experimentally that the yield strength of iron varied inversely with the square root of grain diameter d_g . This is the so called Hall-Petch effect, expressed as:

$$\sigma_y = \sigma_0 + k d_g^{-1/2}$$

Where σ_0 is termed the friction stress and k is the Hall-Petch slope, considered to be a material constant, which has subsequently been observed for a wide range of materials.

The most common model which describes the effect of Hall-Petch is the slip distance model put forward by Chia et al. [154] in Figure 2.14, which proposes that the presence of grain boundaries reduces the average distance of dislocation motion.

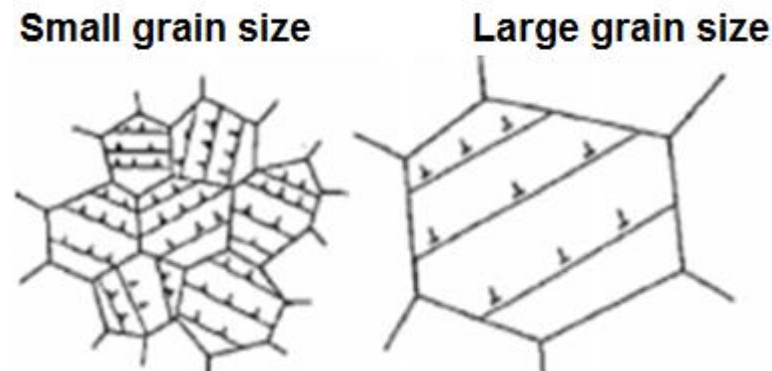


Figure 2.14 Illustration of dislocation mechanism in slip distance model [154]: dislocation-free slip distance is decreased in smaller grain sizes

2.5.3 Solid solution strengthening

There have been a number of papers that have addressed alloying effects on the mechanical properties of nanocrystalline metals [155-157]. For example, in the electrodeposited Ni-W alloys mentioned above, grain size is intimately tied to composition [158], and changing one of these variables tends to cause changes in the other (at least in the as-deposited state). A number of other nanocrystalline alloys, such as Ni-P [159], Pd-Zr [160], and Ni-Fe [161], exhibit a similar dependence of grain size on composition. Detailed studies that isolate the effects of grain size and composition for various systems (solid solution, phase separating, etc.) are needed.

These are, for the most part, somewhat speculative, again because they are generally unable to separate the effects of composition and grain size. At the same time, it is only relatively recent that detailed understanding of the deformation mechanisms of nanocrystalline pure metals has emerged [32,162-165], and many early studies of alloying effects could not benefit from the insights of those works.

As Huang et al. [166] showed in their study, the hardening and softening of the as-plated Ni-P alloys according to phosphorous content generally involves supersaturated solid solution strengthening, Hall-Petch relationship, dispersion hardening as well as the inverse Hall-Petch relationship.

The effect of P content on the microhardness of the as-deposited Ni-P alloys is depicted in Figure 2.15 in terms of the schematic microstructure. At low P contents, the increase of the microhardness is mainly attributed to the supersaturated solid solution strengthening (solubility limit of P in Ni is about 0.17 wt %). As the P content increases, the average grain size of the Ni-P deposit decreases. It has been shown that the hardness of Ni-P alloys is proportional to the square root of grain size ($d^{-1/2}$) at low P contents due to the dislocation pile up in the grain boundary. This is valid for most systems with refined grains and is known as the Hall-Petch relationship. However, for the Ni-P alloy with a composite microstructure consisting of a nanocrystalline phase and an amorphous phase has a maximum hardness of 620 HV as shown in Figure 2.15.

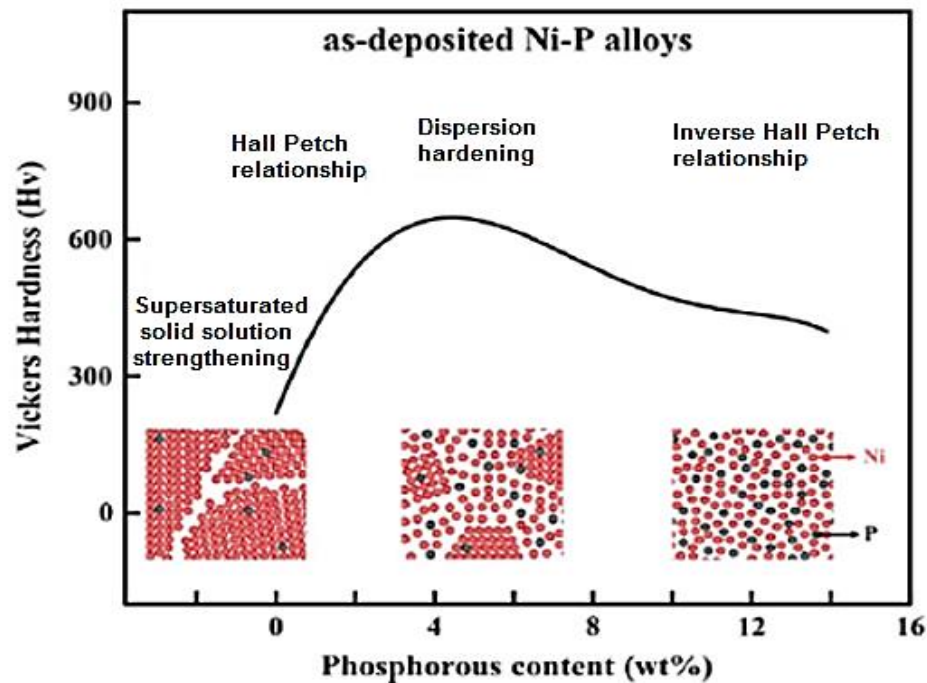


Figure 2.15 Dependences of microhardness of the as-deposited Ni-P films on P content and microstructure [166]

Dislocation movement in crystals can no longer be defined when it encounters with the amorphous matrix. Thus, the Hall-Petch relationship may not be applied to this alloy. Additionally, the average grain size is about 10 nm for the crystalline phase, which is believed to be small enough to be under inverse Hall-Petch relationship. As shown in Figure 2.15, the hardness reaches a peak value for the alloy with a composition at which exhibiting a composite microstructure. Therefore, it is proposed that dispersion hardening may also affect the strengthening behavior of the Ni-P alloys containing mixed nanocrystalline and amorphous phases. More specifically, the nanosized Ni grains are considered as the strengthening particles to the amorphous matrix. The existence of these discontinuous nanocrystalline Ni particles in

the uniform matrix plays an important role in enhancing the resistance to deformation, causing an increase in hardness. This phenomenon has been addressed in some other metallic glass systems, where a second crystalline phase precipitation occurs in the amorphous matrix during crystallization, such as Al base alloys or metallic glass [166].

2.6 Summary of theoretical background

What we learn from the literature is that Ni electrodeposition has currently an extensive application in the microsystem industry. However, the applications in harsh service conditions put forward a requirement of better alternatives. According to literature, alloy electrodeposition and metal matrix composites were introduced as two promising alternatives to pure Ni. Among other binary alloys, Ni-P has been introduced in the literature as a good alternative for the purpose of microsystems compared to pure Ni owing to its interesting functional properties. Meanwhile, many researchers in the last decades have found an obvious increase in the properties of composite coatings, especially strengthening due to the reinforcement with various particles. The properties of composite coatings mainly depend on their composition and structure. Among many other parameters particle characteristics – including type, size and concentration – were found to be crucial to improve the film properties. In order to understand the effect of different particle characteristics on the behavior of the codeposition process, a summary of existing electrodeposition models based on the past investigations were explained. In the following, impedance spectroscopy was introduced as a useful tool for the in-situ study of electrodeposition process. Based on recent literature, EIS technique can be a reliable tool for monitoring the effect of different working parameters on the process of electrodeposition. Finally, due to the significance of strengthening in Ni-based electrodeposited coatings, different hardening models including the effect of grain size, particles existence or type of matrix (Ni-P) were discussed in order to get better insight about the strengthening mechanism of electrodeposited coatings.

2.7 Missing points in the recent studies

Several points are missing in the recent literature reviews which can be described as followed:

- Over the past decades, a number of codeposition mechanisms for the incorporation of particles into the deposit have been proposed. Guglielmi's model is a two-step model that combines the effects of adsorption and electrophoretic attraction and is the first model to arrive at a plausible explanation for the relationship between current density and the volume fraction of the embedded particles [1]. Further models by Buelens, Celis and Valdes assumed that the reduction of the metal ions adsorbed on the surface of the particle (already being adsorbed on the electrode surface) is the determining factor for the codeposition of particles [72]. Although these models can provide us with a good insight into codeposition phenomena, they have mainly been developed on the basis of the investigation of micro sized particles under particular experimental conditions and could not simply be applied to nano sized systems, because, in the nano-range, all the forc-

es act in completely different ways. However, in the recent models proposed by Lee and Talbot [104] the influence of nanoparticles on the codeposition behavior was considered. Nevertheless, the validity of the various theoretical models, underlying particle incorporation in a metal matrix, still requires more empirical laboratory trials.

- Although the galvanic technique is suggested to be the more effective process for producing Ni-P alloy deposits compared to the electroless technique, there are still some challenges with electroplated Ni-P. One of the main challenges - especially for the purpose of MEMS devices - can be the existence of residual stresses in electroplated Ni-P coatings, particularly those with low and medium phosphorous content and electroplated under higher current densities. The existence of internal stress in the coatings appears, finally, as dendrites and cracks on the deposit which would be deteriorating especially for high-strength and high-aspect ratio in micro-nano structures.
- Another missing point is related to the microscopic evolution and strengthening mechanism of Ni-based composite coatings affected by particle characteristics, specifically for electroplated Ni-P deposits. According to the few papers regarding the influence of particles on the properties of electroplated Ni-P coatings, there is still a lack of understanding about the role of particles on the microstructure and strengthening mechanism of electrodeposited Ni-based coatings. Moreover, how would be the possibility of correlating codeposition behavior of particles with different characteristics with incorporation value, microstructure and hardening as a final performance?

2.8 Research objectives

The aims of this work are, on one hand, to substantiate and confirm the past theoretical and semi-empirical suggested models on the electrodeposition mechanism with the help of more empirical results including the characteristics of the layer and an in-situ impedance study of the electrocodeposition process. The influence of particle characteristics including type, size and concentration was investigated on the codeposition behavior of Ni-based coatings with the aid of impedance spectroscopy.

On the other hand, this research aims to build a bridge between impedance and physical properties by relying on the effect of particle characteristics on the layer properties including morphology, microstructure and hardness. In other words, trying to correlate the electrochemical behavior (double layer characteristics) with microstructure features and performance of coatings. Also, this work is aimed to obtain crack-free galvanic Ni-P deposits with the means of particle incorporation and explaining the microstructure evolution and strengthening mechanisms of electrodeposited Ni-based composite coatings affected by the characteristics of difference reinforcements and matrix.

2.9 Work schedule

In an attempt to obtain these aims, the subsequent points are of interest:

- Investigating the impact of particle characteristics, including type and size and concentration, on the behavior codeposition process and the features of doubled layer for Ni-based electrodeposits (Ni and Ni-P) by means of EIS which will help the development of particle selection for the enhanced properties of Ni-based electrodeposition coatings.
- Evaluating the microstructure of coatings including morphology, grain size, texture, internal stress, particle incorporation/distribution, interface of particle with grain using various techniques, such as X-ray diffraction, electron microscopy and spectroscopy, Transmission electron microscopy, EBSD and Optical image analyzer.
- Characterizing the impact of various particle features on the performance of Ni and Ni-P coatings including hardness by means of Martens test and explaining the effective strengthening mechanisms in Ni-based electrodeposited composite coatings.
- Correlating the electrochemical behavior (R_p/C_{dl}) with microstructure features and the performance of coatings.

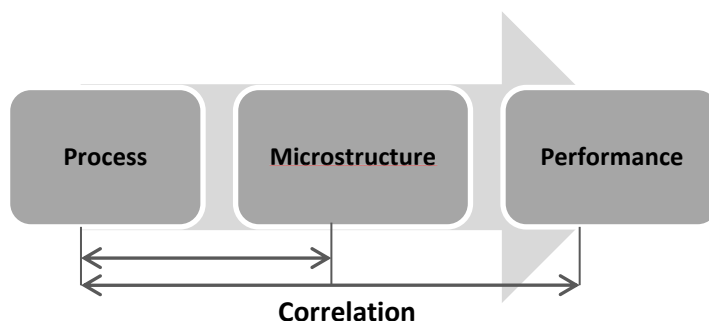


Figure 2.16 Schematic of project

It is hoped that this dissertation provides new insights into the electrodeposition mechanism of Ni-based coatings with the combination of microstructure features and performance. Hopefully, this will help us to establish the scientific principles for rational design of particle selection for improving strengthening performance of electrodeposition systems.

3 Experimental Methods

3.1 Deposition Procedures

3.1.1 Electrolyte Composition and Working Conditions

The electrodeposition Ni coatings were carried out using Watts's electrolyte. For producing Ni-P coatings, sodium hypophosphate, as phosphorous source was added to the Watts bath. The composition of the nickel bath and the operating conditions employed for plating is shown respectively in Table 3.1. All chemicals were p.a. grade and distilled water was used for the preparation of all solutions. Suspensions were prepared by adding a specified amount of particles to the electrolyte.

The particles included Alumina nano size, 13 nm, and micron size, 150-200 nm, for means of particle size effect. For means of comparing particle type Al_2O_3 , TiO_2 and SiC nanoparticles within almost the same nominal grain size: 50 nm, 45 nm, 45-55 nm were chosen respectively.

The dispersion was stirred using a magnetic stirrer for 8 hours in a beaker. The pH of the solution was measured before and after each experiment and if necessary adjusted to pH 3.8 with either NaOH or H_2SO_4 . The electrolyte temperature was maintained at 55 °C using an Ultrasonic bad. The ultrasonic vibration was also applied 1 hour before the first experiment and also during each experiment in order to disperse the particles in the electrolyte.

The experimental design and number of samples produced under different working parameters has been mentioned in Table 3.2. The number of variables and the investigated samples has been designed mainly based on the effect of particles characteristics including different size and type on both Ni and Ni-P matrix.

3.1.2 Impedance investigation

Electrochemical impedance spectroscopy (EIS) experiments were performed to see how the behavior of electrodeposition in Ni-based coatings would change by altering certain working parameters, especially by existence of different particles with characteristics. The concept of EIS method has been already explained in section 2.4.3.2. The procedure of impedance investigation in this work is mentioned as below: A three-electrode cell connected to a work station (IM6- Zahner) was used for both impedance measurements during electrodeposition process. In order to keep the constant distances between anode, cathode and reference electrode, a setup illustrated in Figure 3.1 was chosen. The parameters of impedance experiments are listed in Table 1. By using a constant current density, the constancy of the system over the measuring time was ensured. This was proven by premeasurement of the spectrum of random samples. EIS was conducted directly after the registration of the cell potentials in the galvanostatic mode. EIS data were acquired in the frequency range from 100 kHz to 10 Hz using a sinusoidal signal with 10 mV. In this case, due to the short amount of time needed for each impedance measure-

ment (81 seconds), the test would be less affected under the variations in working parameter like temperature or pH during the deposition time.

The cathodic area of 20 cm² was chosen on one side of the working electrode (carbon steel sheet) and the rest were isolated with special stick band. In order to stabilize the working electrode and to ensure that the system is initially in a stationary state, each sample was pre-deposited before performing impedance tests for 10 minutes in a separated Ni Watts electrolyte under the same working parameters as for the impedance test. After the testing, the sample was again electrodeposited for 5 more minutes in the same electrolyte, which was already used for the impedance test. Between each test cycle, the samples were polarized galvanostatically for 3 minutes under the same current density. For reasons of reproducibility, except performing four cycle tests on each sample, some of the tests were repeated with new samples. In fact, each of the reported values of the impedance experiments represents at the same time the average value of the just-mentioned results. The SIM-Zahner software (Thales box) was used for analyzing the impedance measurements.

Bath type	Ni Watts Bath	Ni-P Bath
Electrolyte composition (1L)	NiSO ₄ .7H ₂ O 250 g/l NiCl ₂ .6H ₂ O 30 g/l H ₃ BO ₃ 30 g/l SDS 0.3 g/l	Ni Watts Bath + NaPO ₂ H ₂ (0.1-10 g/l)
Particle type	Al ₂ O ₃ , TiO ₂ , SiC	
Particle size (nm) - apx.	13, 50, 150	
Temperature (°C)	55	
pH	3.8	
Agitation (rpm)	400	
Applied current density (A/dm ²)	1,2,4	
Codeposition time (min)	90,60,40	
Cathodic area (cm ²)	20	
Anodic area (cm ²)	45	
Cathode-Anode distance (cm)	5.5	

Table 3.1 Electrolyte composition and working condition

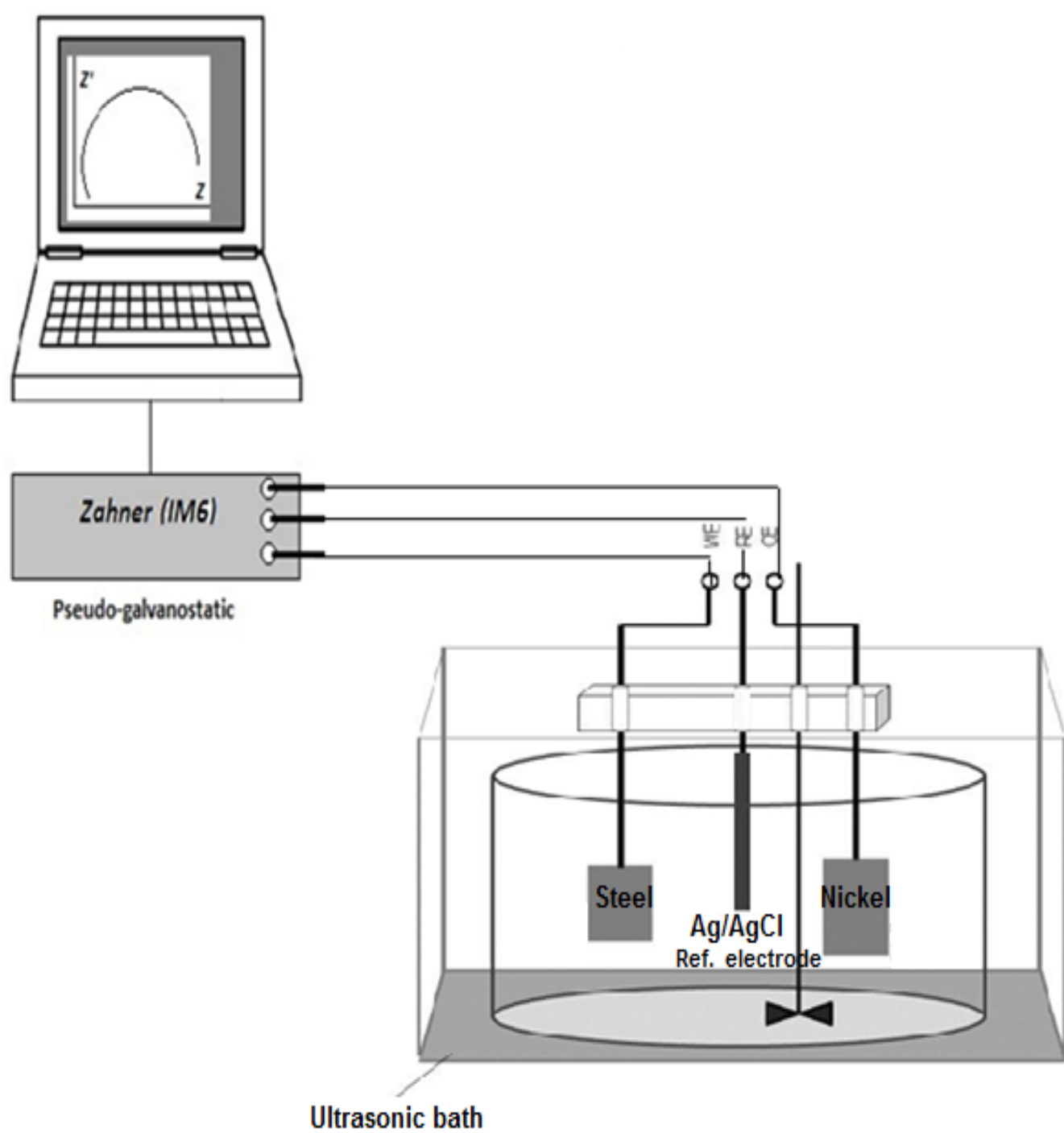


Figure 3.1 Set up of electrodeposition and EIS investigation

Experimental Design					
Run	NaP ₂ H ₂ O (g/l)	Matrix (Ni/Ni-P)	Particle type	Particle size (nm)	Particle concn.(g/l)
1	0	Ni	—	—	0
2	0	Ni	TiO ₂	50	1
3	0	Ni	TiO ₂	50	5
4	0	Ni	TiO ₂	50	20
5	0	Ni	SiC	50	1
6	0	Ni	SiC	50	5
7	0	Ni	SiC	50	20
8	0	Ni	Al ₂ O ₃	50	1
9	0	Ni	Al ₂ O ₃	50	5
10	0	Ni	Al ₂ O ₃	50	20
11	0	Ni	Al ₂ O ₃	13	1
12	0	Ni	Al ₂ O ₃	13	5
13	0	Ni	Al ₂ O ₃	13	20
14	0	Ni	Al ₂ O ₃	150-200	1
15	0	Ni	Al ₂ O ₃	150-200	5
16	0	Ni	Al ₂ O ₃	150-200	20
17	5	Ni-P	—	—	0
18	5	Ni-P	TiO ₂	50	1
19	5	Ni-P	TiO ₂	50	5
20	5	Ni-P	TiO ₂	50	20
21	5	Ni-P	SiC	50	1
22	5	Ni-P	SiC	50	5
23	5	Ni-P	SiC	50	20
24	5	Ni-P	Al ₂ O ₃	50	1
25	5	Ni-P	Al ₂ O ₃	50	5

Run	NaP ₂ H ₂ O (g/l)	Matrix (Ni/Ni-P)	Particle type	Particle size (nm)	Particle concen.(g/l)
26	5	Ni-P	Al ₂ O ₃	50	20
27	5	Ni-P	Al ₂ O ₃	13	1
28	5	Ni-P	Al ₂ O ₃	13	5
29	5	Ni-P	Al ₂ O ₃	13	20
30	5	Ni-P	Al ₂ O ₃	150-200	1
31	5	Ni-P	Al ₂ O ₃	150-200	5
32	5	Ni-P	Al ₂ O ₃	150-200	20

Table 3.2 Table of Experiments

3.2 Layer Characterizations

3.2.1 Scanning Electron Microscopy (SEM)/ energy-dispersive X-ray Spectroscopy (EDX)

Scanning electron microscopy (SEM) can be used for qualitative surface morphology analysis. Energy dispersive X-ray spectroscopic (EDX) is a technique to determine the chemical composition of a material [133]. SEM is a type of microscope that uses a rather light electron-beam in order to obtain an image from the sample. The advantages of SEM include a higher magnification, a larger depth of focus and a greater resolution in comparison to an optical microscope [133].

SEM micrographs combined with EDX studies were done in a SEM, Zeiss NEON 40 EsB with an EDX detector model TSL OIM 5.2. The amount of codeposited nanoparticles in the nickel matrix was evaluated from the aluminum Al, titanium Ti and Silicon Si signal, respectively. The accuracy of EDX analysis was approximately ± 0.5 vol%. The EDX area analyses were performed both on the cross section covering the thickness of deposit at a magnification of 1500-2000x. For the cross section, the samples were embedded in epoxy resin and cut with a diamond saw. After mechanical grinding with 800 to 4000 grade silicon carbide paper and polishing with diamond suspension down to 1 μm . Surface morphology and microstructure of the deposited composites were also analyzed with SEM.

3.2.2 EBSD and TKD

A complete and quantitative representation of the sample microstructure can be established with electron backscattered diffraction (EBSD) [149, 150]. A FESEM NEON40EsB (Zeiss, Germany) was used at 25 kV with a scanning transmission electron microscopy (STEM) detector as well as an EBSD camera (EDAX TSL). For backscattered secondary electron (BSE) imaging, the voltage was lowered to 10 and 5

kV, respectively. Cross sections were prepared with a final oxide polish (OP). EBSD is a powerful microstructural-crystallographic technique used to investigate the crystallographic texture or preferred orientation of any crystalline or polycrystalline materials. For this purpose, an electron beam strikes a tilted sample and the diffracted electrons form a pattern which can be used to determine the crystal orientation, measure grain boundary misorientations, discriminate between different materials, and provide information about local crystalline perfection. The scanning and mapping capabilities of an EBSD system allow for rapid acquisition of data at sub-micron resolutions revealing the constituent grain morphology, orientations, and boundaries of the sample. Corresponding transmission Kikuchi diffraction (TKD) studies were done using the EBSD camera Dig-View in the SEM operated at 25 kV in the high current mode with a 60 μm aperture and a step size of 15 nm and 5 nm. A spatial resolution improvement of up to one order of magnitude for Electron Backscatter Diffraction (EBSD) results can be achieved with the Transmission Kikuchi Diffraction (TKD) technique. TKD uses existing EBSD hardware but requires software adaptations and electron transparent samples, e.g. TEM lamella, free standing films and crystalline nanoparticles.

The difference between these two methods is in the higher transparency of the TKD samples. Moreover, the resolution improves both the EDX elemental analysis as well as the orientation and mapping for the smaller grains detected by the measurement.

Therefore, the main decision-making reason of choosing TKD is being electron transparent, although preparation of samples for TKD is as difficult as for TEM.

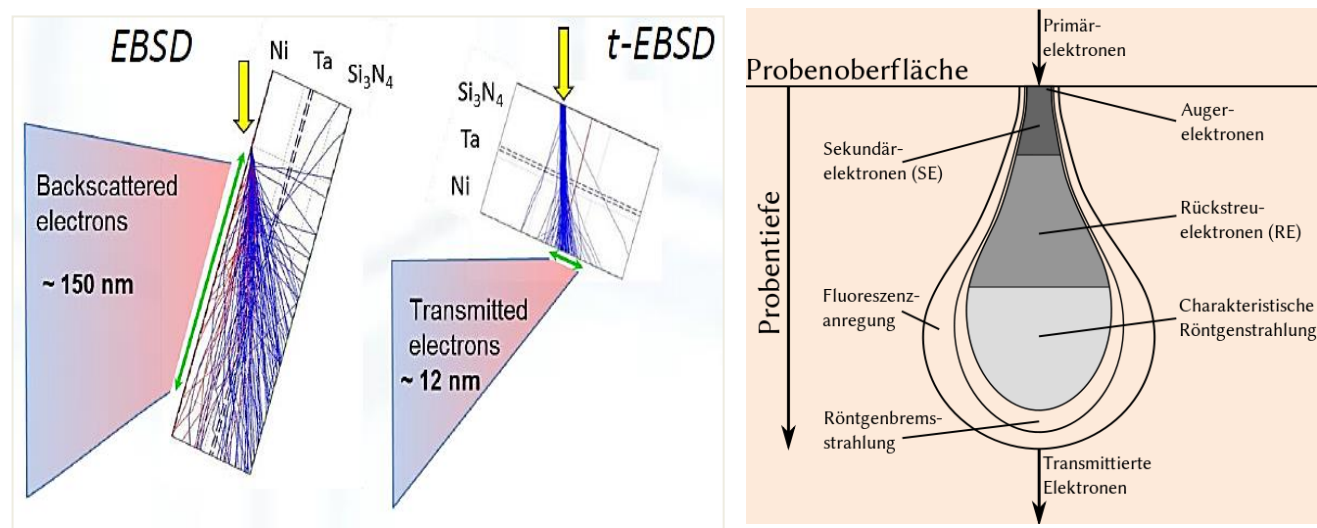


Figure 3.2 Schematic of EBSD and TKD (t-EBSD) analysis

3.2.3 Transmission Electron Microscopy (TEM)

Transmission electron microscopy (TEM) is a microscopy technique in which a beam of electrons is transmitted through an ultra-thin specimen, interacting with the specimen as it passes through it. An im-

age is formed from the interaction of the electrons transmitted through the specimen. The image is magnified and focused onto an imaging device. TEM is capable of imaging at a significantly higher resolution than light microscopes, owing to the small wavelength of electrons. This enables the instrument's user to examine fine details even as small as a single column of atoms, which is thousands of times smaller than the smallest resolvable object in a light microscope.

Bright field (BF) and dark field (DF) are the most commonly used diffraction contrast imaging modes for crystalline materials. A small aperture (5-70 μm diameter) may be inserted in the back focal plane of the objective lens to intercept the diffracted beam and only allow the transmitted beam to form an image. This situation is known as a BF image. Alternatively, the direct beam can be blocked by the aperture while one or more diffracted beams are allowed to pass the objective aperture, this is known as dark field (DF) image. Since diffracted beams have strongly interacted with the specimen, very useful information is present in DF images, e.g. about planar defects, stacking faults or particle size.

The procedure for forming a BF and DF may be better understood with reference to Figure 3.3.

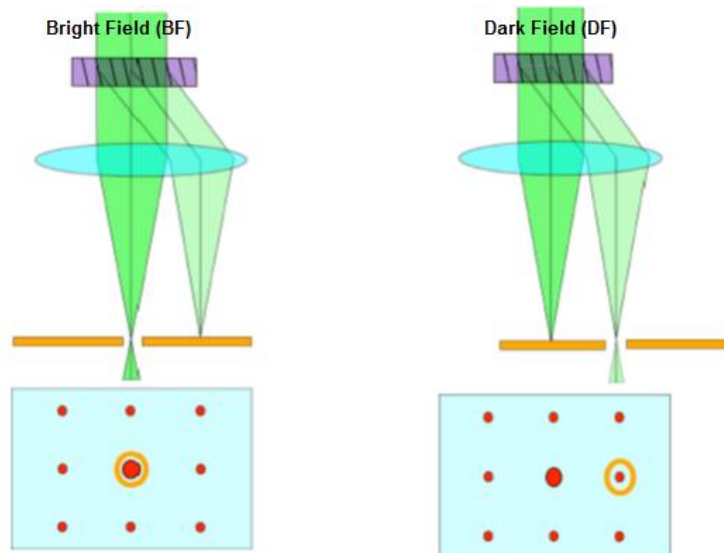


Figure 3.3 the procedure of forming BF and DF in TEM

For the means of TEM experiments, the films were separated from the substrate mechanically. Disks of 3 mm diameter were cut and ion polished by 3kV Ar ions with 6° incidence angle until electron transparency. The utilized TEM (Hitachi 8110) is equipped with a LaB6 cathode and was operated at 200 kV which enables imaging in high resolution complemented by diffraction patterns, bright (BF) and dark field (DF) imaging.

3.2.4 X-ray Diffraction (XRD)

The occurrence of a texture can be easily recognized in an X-ray diffraction pattern by a pronounced enhancement of a certain reflection when compared with a powder pattern of randomly oriented grains. According to Scherrer, the width of the Bragg reflection increases with decreasing crystallite size [152].

X-ray diffraction was utilized to study the texture and crystallite size of the nickel matrix. Diffractograms were recorded at room temperature on a Burker D5000 with a scan rate of $0.12^{\circ} \text{ min}^{-1}$ for two-theta ranging from 10 to 100° . The size of the nickel crystallites was determined from the broadening of the $(2\ 0\ 0)$ and/or $(1\ 1\ 1)$ reflections according to the Debye–Scherrer equation, after background correction and subtracting the instrumental line broadening. However, it has to be emphasized that the crystallite size calculated from the XRD peak profiles refers to the domain sizes that scatter the incoming X-rays coherently. Hence, these values are generally smaller compared to the crystallite size obtained by other techniques such as transmission electron microscopy. An often observed structural feature of polycrystalline electroplated film is that certain crystallographic lattice planes can occur with a greater probability than others, which is called preferred orientation or texture. The preferred crystalline orientation of the nickel films was evaluated by the relative texture coefficients RTC_{hkl} :

$$RTC_{(hkl)} = \frac{I_{(hkl)}}{I_{(hkl)}^0} \left\{ \sum \frac{I_{(hkl)}}{I_{(hkl)}^0} \right\}^{-1} \times 100$$

where the relative intensities of the (hkl) lines are measured in the diffractogram of the nickel films and are the corresponding intensities of a randomly oriented nickel powder sample (JCPDS no. 4-850). The summation was taken for the 4 lines visible in the diffraction spectra, i.e. $(1\ 1\ 1)$, $(2\ 0\ 0)$, $(3\ 1\ 1)$ and $(2\ 2\ 2)$.

3.2.5 Measuring internal stress by XRD

In measuring residual stress using X-ray diffraction (XRD), the strain in the crystal lattice is measured and the associated residual stress is determined from the elastic constants assuming a linear elastic distortion of the appropriate crystal lattice plane. Since X-rays impinge over an area on the sample, many grains and crystals will contribute to the measurement. The exact number is dependent on the grain size and beam geometry. Although the measurement is considered to be near surface, X-rays do penetrate some distance into the material: the penetration depth is dependent on the anode, material and angle of incidence. Hence, the measured strain is essentially the average over a few microns depth under the surface of the specimen.

3.2.6 Martens test

The mechanical property is an important factor in surface finishing for the implementation in industrial processes. The determination of the microhardness is often the method of choice for a straightforward screening because it is relatively inexpensive, easy to use and almost non-destructive.

For detecting the hardness value, instrumented indentation (HM2000XYm, HELMUT FISCHER GmbH) is applied on the cross-sections of the deposits by applying a 25 mN force for 30 s loading time, 30 s holding time and another 30 s unloading time on a Vickers indenter. The final value quoted for the hardness of a deposit represents the average of 5 measurements.

4 Results and Discussion

4.1 Layer Characterization of Ni electrodeposited from Watts electrolyte

According to XRD results in Figure 4.1 and 4.2, it is apparent that the diffraction pattern of pure Ni deposit is generally characterized by the intense (2 0 0) diffraction line corresponding to a (1 0 0) texture, where the diffraction pattern of Ni at current density of 2 A/dm² is mainly characterized by (3 1 1) and (1 1 1) lines which are considered as the most effective directions on the strengthening of deposits. Moreover, the grain size of Ni deposit achieved from Debby-Scherer's law, in Figure 4.3 shows a decline at current density of 2 A/dm² and again increases at higher current density of 4 A/dm². Based on Martens results, in Figure 4.4, it is seen that increasing current density to 2 A/dm² caused an improvement of hardness, while at higher current density of 4 A/dm² a reduction in hardness is observed.

The behavior of hardness with increased plating current density can be explained as followed: At low plating current density of 1 /dm², the plating is limited by the reaction rate at the interface between solution and sample. There is a sufficient supply of Ni ions to the cathode, and the reduced Ni atoms have sufficient time to migrate to a relaxed position and to fill any remaining pores and gaps. The deposited Ni film is therefore dense and possesses the bulk value of Martens. As the plating current density increases to 2 A/dm², the plating rate rises, and the nucleation rate of Ni is faster which leads to growth impediment of Ni crystals, and finally, finer grains and higher strengthening due to the Hall-Petch mechanism [145-147]. By further increasing the current density to 4 A/dm², the limited supply of Ni ions to the cathode leads to the formation of a depletion layer of Ni ions near the cathode surface: the so-called mass-transport limitation. Any incoming Ni ions will be captured by outgrowing microstructures, leaving behind pores and gaps in the film. The deposited layer is porous, rough and possesses a tensile residual stress [144].

The microstructural change is believed to be responsible for the change in Martens results observed here. The surface of electroplated Ni films at lower current densities of 1, 2 and 4 A/dm² have been investigated by SEM (Figure 4.5), and no cracks and pores were found under a magnification of 2K while at current of 4 A/dm² pores and gaps are visible. Most of these pores are in the nanometer range or even smaller.

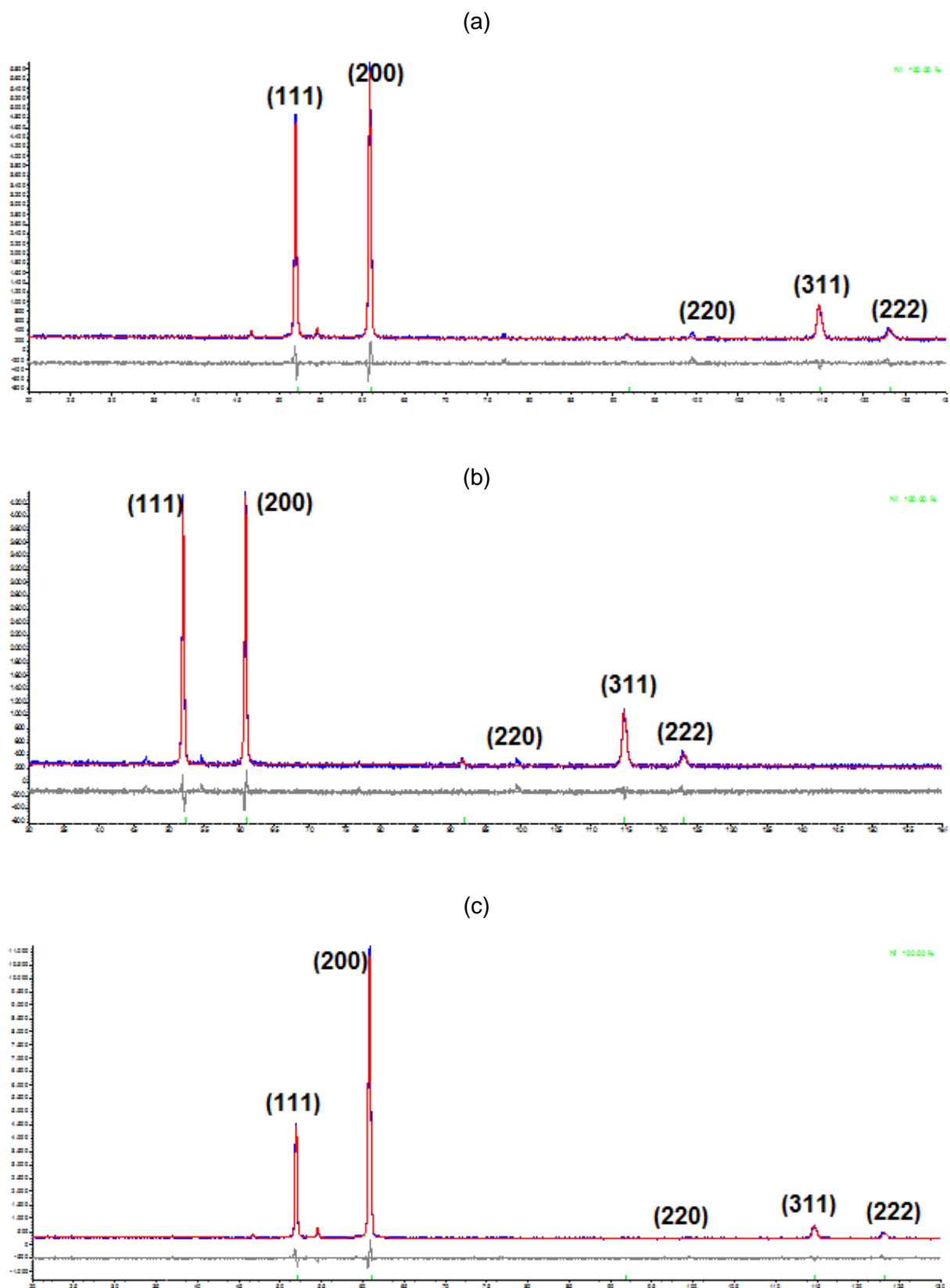


Figure 4.1 XRD results of Ni electrodeposited from Watts Bath in different current density: (a) 1, (b) 2 and (c) 4 A/dm²

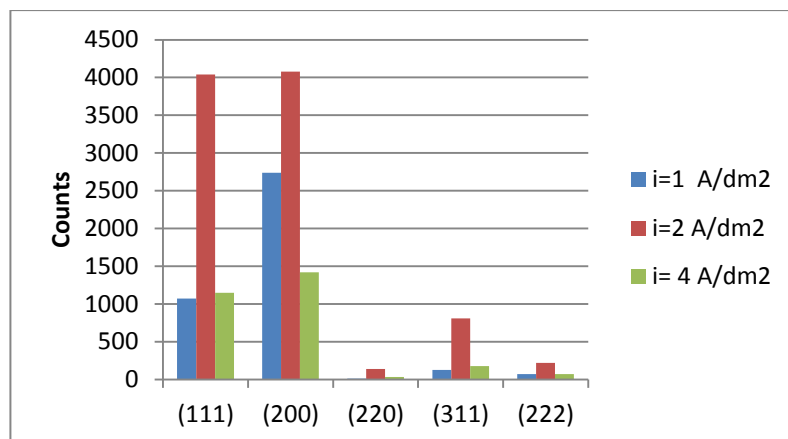


Figure 4.2 Effect of current density on texture of Ni electrodeposits

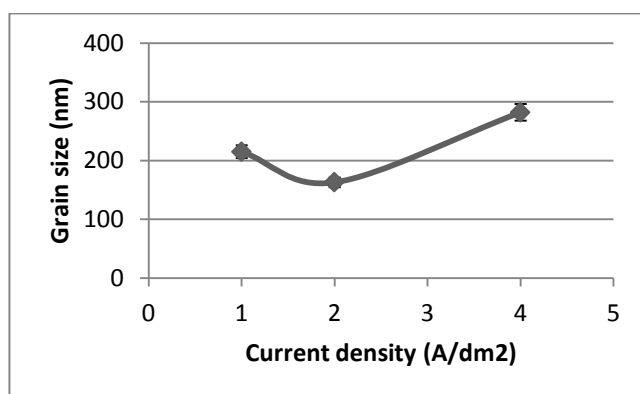


Figure 4.3 Effect of current density on grain size of Ni electrodeposited in different current density of 1, 2 and 4 A/dm²

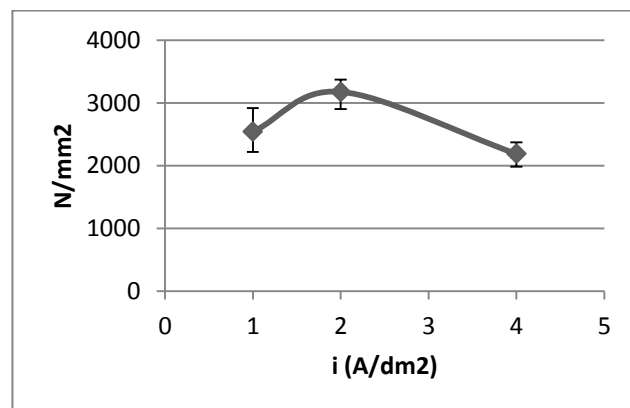


Figure 4.4 Effect of current density on Martens hardening of Ni electrodeposited in different current density of 1, 2 and 4 A/dm²

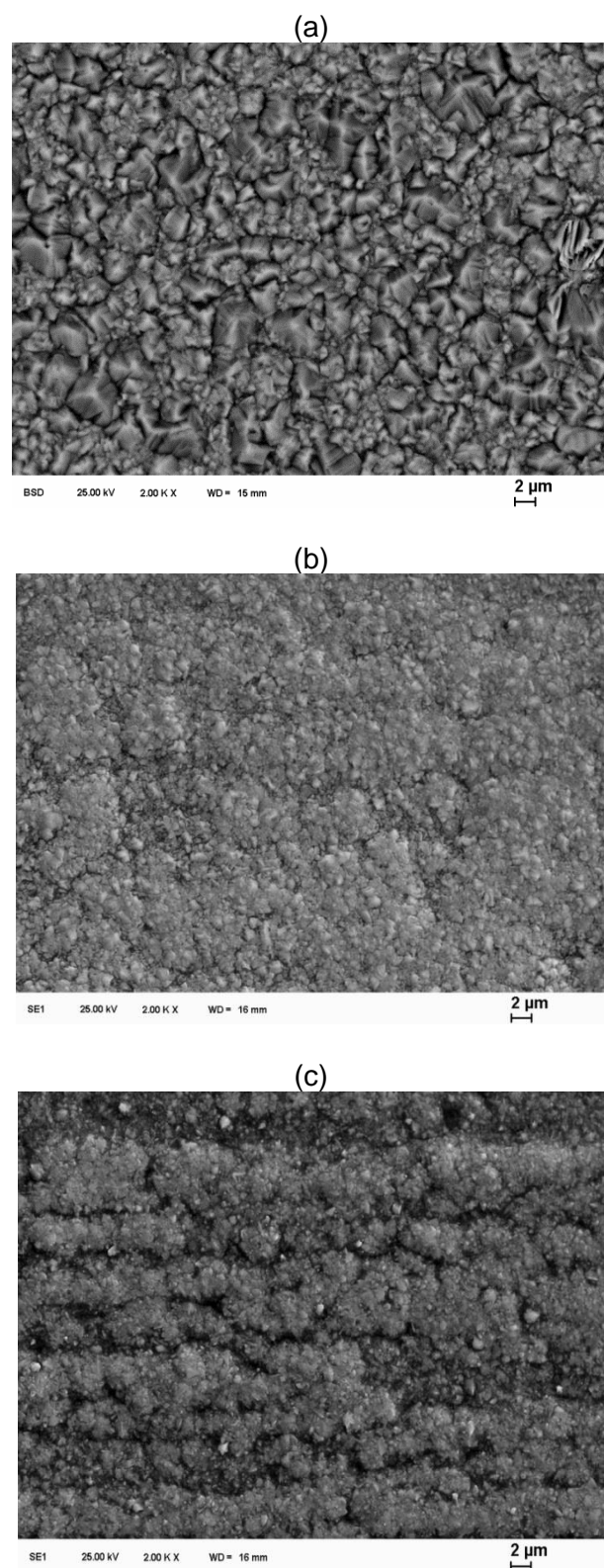


Figure 4.5 SEM morphology images of Ni in different current density: (a) 1, (b) 2 and (c) 4 A/dm²

4.2 Electrodeposition behavior of Ni electrodeposited coatings by means of EIS

According to the results of the polarization in Figure 4.6 a), the cathodic potential values rise by increasing the applied current density. Furthermore, impedance measurements for Ni, electrodeposited under different current densities as represented in Figure 4.6 b), showed that the current density has a significant impact on the impedance behavior of the Ni deposits. As can be seen, all the spectrums show a single capacitance loop in high and medium frequencies while at higher current densities an inductive loop can also be obtained in lower frequencies. According to achievements of other researchers, especially those of Wiart and others [119-124], an equivalent circuit model, which can explain a nickel electrodeposition process, usually, includes three main elements of R_s , R_{dl} and C_{dl} : R_s is the solution resistance between the reference and working electrodes and represents the resistance of the ions in an electrolyte transfer to the electrodes. R_{dl} is the resistance against charge transfer through the double layer at the electrode/electrolyte interface. C_{dl} , in the form of a constant phase element (CPE), shows the double layer capacitance of the interface of the electrode/electrolyte. The use of a CPE is required because of inhomogeneity and moderate deformations existent in the semicircles. The roughness factor of CPE elements was neglected in this study. The inductive loop has also been included by other researchers [119, 120, 124]. Although the nature of this behavior is not totally clear yet, some researchers [106] proposed that the inductive loop indicates the presence of the intermediate, whereas others [121-124] believe that this loop is related to the adsorption/desorption process of intermediates on/from the cathode surface. Therefore, with the exclusion of the inductive loop in lower frequencies, the simple model in Figure 4.7 is proposed for this study, which could be achieved faster in a shorter range of frequencies and provided us with information about the charge transfer and double layer capacity, which can be directly referred to the reduction rate of nickel. As can be seen in Figure 4.8, the increase in current density leads to a decline in charge transfer resistance, which behaves reciprocally to the current density. The charge transfer resistance and the cathode double layer are inversely proportional to the current density, as explained in detail in [148]. This inverse proportional relation between current density and charge transfer resistance, which was also found for high polarization [122] for a nickel sulfate electrolyte, leads to an interesting prediction concerning the system's behavior under high polarization. In fact, increasing current density leads to an increase in nucleation rate, an increase in current efficiency and rate of cathodic deposition.

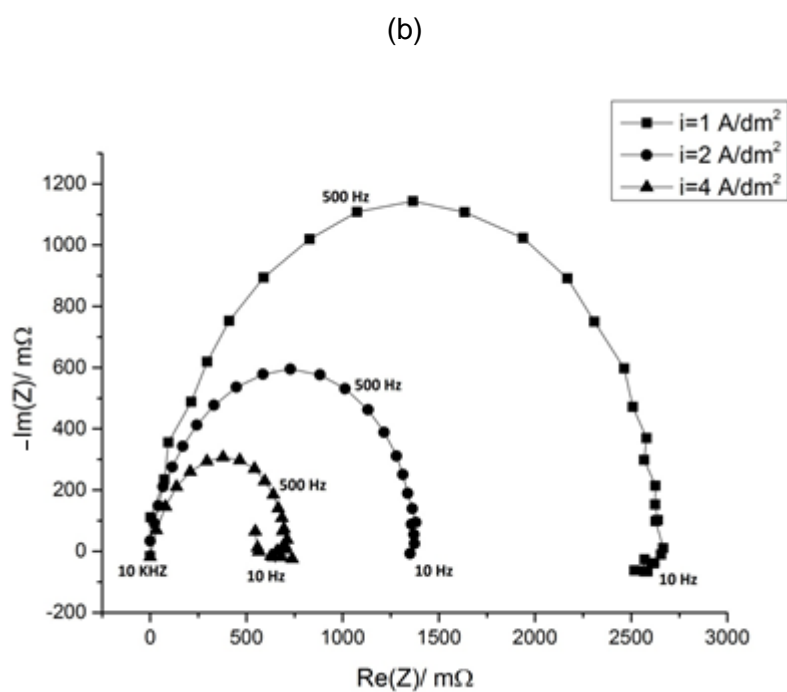
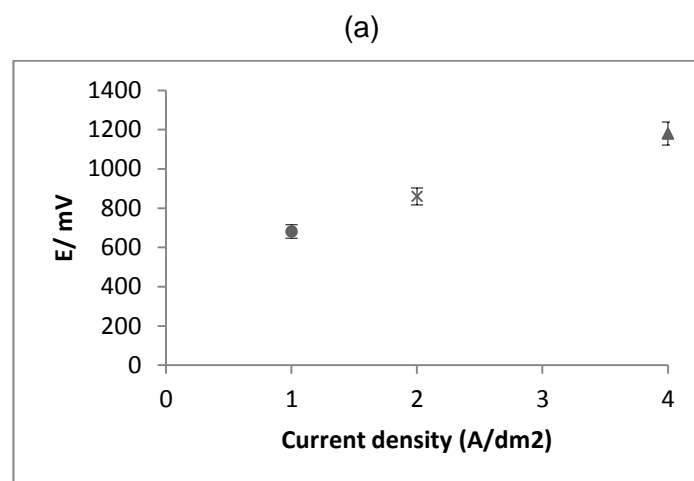


Figure 4.6 Galvanostatic polarization (a) and Nyquist spectrums (b) of Ni deposition in current densities of 1, 2 and 4 A/dm^2 vs Ag/Ag/Cl

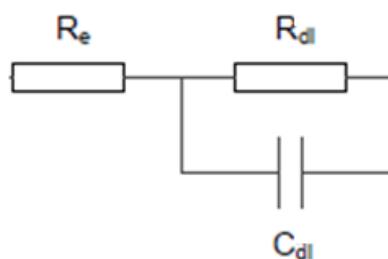


Figure 4.7 Simple circuit model for the Ni electrodeposition from Watts's electrolyte.

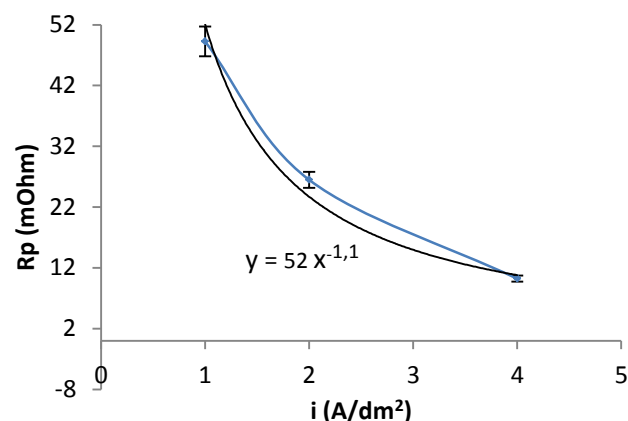


Figure 4.8 Charge transfer vs current density for electrodeposition of Ni from Watts's electrolyte

4.3 Effect of particle properties on the electrodeposition behavior of Ni-Al₂O₃ composite coatings and its layer properties

4.3.1 Effect of alumina particle size on the morphology, microstructure and mechanical properties

As illustrated in Figure 4.9, Ni-Al₂O₃ composite coatings show different morphology compared to pure nickel coatings. With the addition of Al₂O₃ particles in the electrolyte, the borders of the Ni grains become fuzzy and more compact in comparison to pure Ni with no particles. In the case of adding nano-Al₂O₃, the morphology seems to be even more compact and homogenous. Moreover, for the coating electrodeposited with submicron particles, it is obvious that the particles were mainly incorporated within a certain gap from the Ni matrix and growth of nickel around the particle becoming rough. This behavior can be related to the non-inductive nature of alumina particles, as it was also mentioned by [99]. Furthermore, according to the cross-section backscatter SEM images shown in Figure 4.10, it is observed that the “dark” spherical Al₂O₃ particles are uniformly distributed in the “white” nickel matrix, thanks to the use of ultrasound during the deposition process. Nevertheless, because of the higher surface energy of nanoparticles, agglomeration at higher particle concentrations is still unavoidable despite the application of ultrasound.

The EDS analysis in Figure 4.11 displays the atomic percentage of Al for Ni-Al₂O₃ composite coatings electrodeposited from Watt's bath including nano- and submicron Al₂O₃ particles with different particle concentrations in the electrolyte. As can be seen, under the same conditions, the atomic percentage of Al for submicron particles is higher than the coatings prepared with nanoparticles. In addition, in both cases, the incorporation value of particles rises with increasing the loading of particles in the electrolyte.

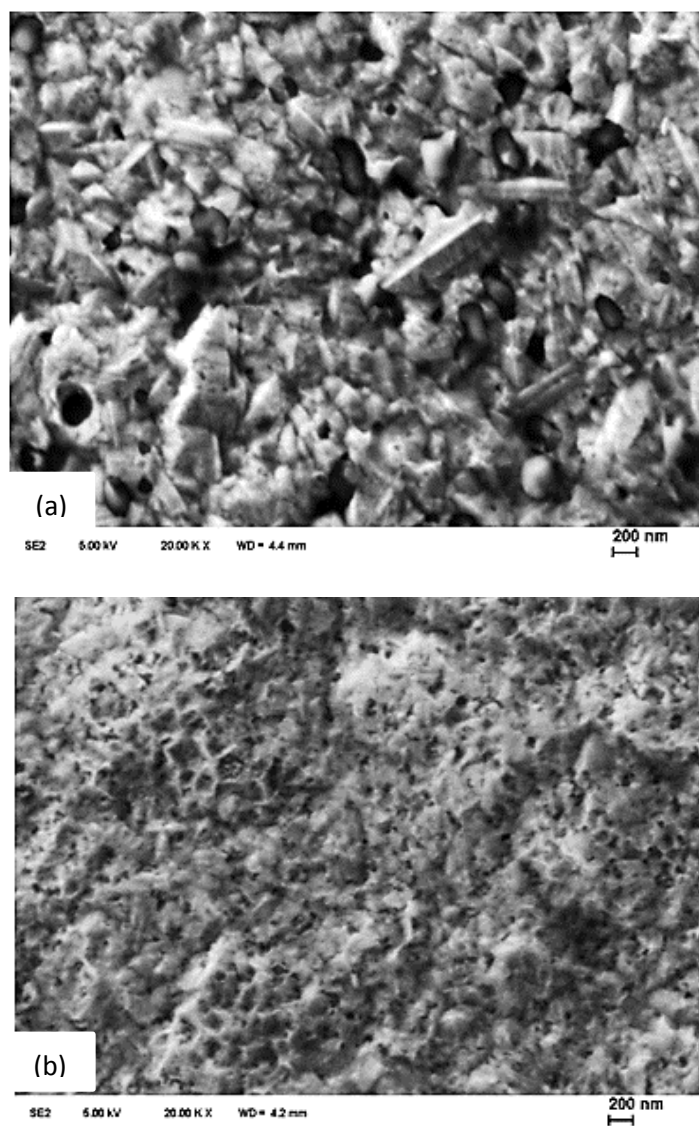


Figure 4.9 SEM images of the surface morphology: (a) Ni-sm Al_2O_3 20 g/l (cb) Ni-n Al_2O_3 20 g/l electro-deposited at $i = 4\text{A/dm}^2$ for 40 min

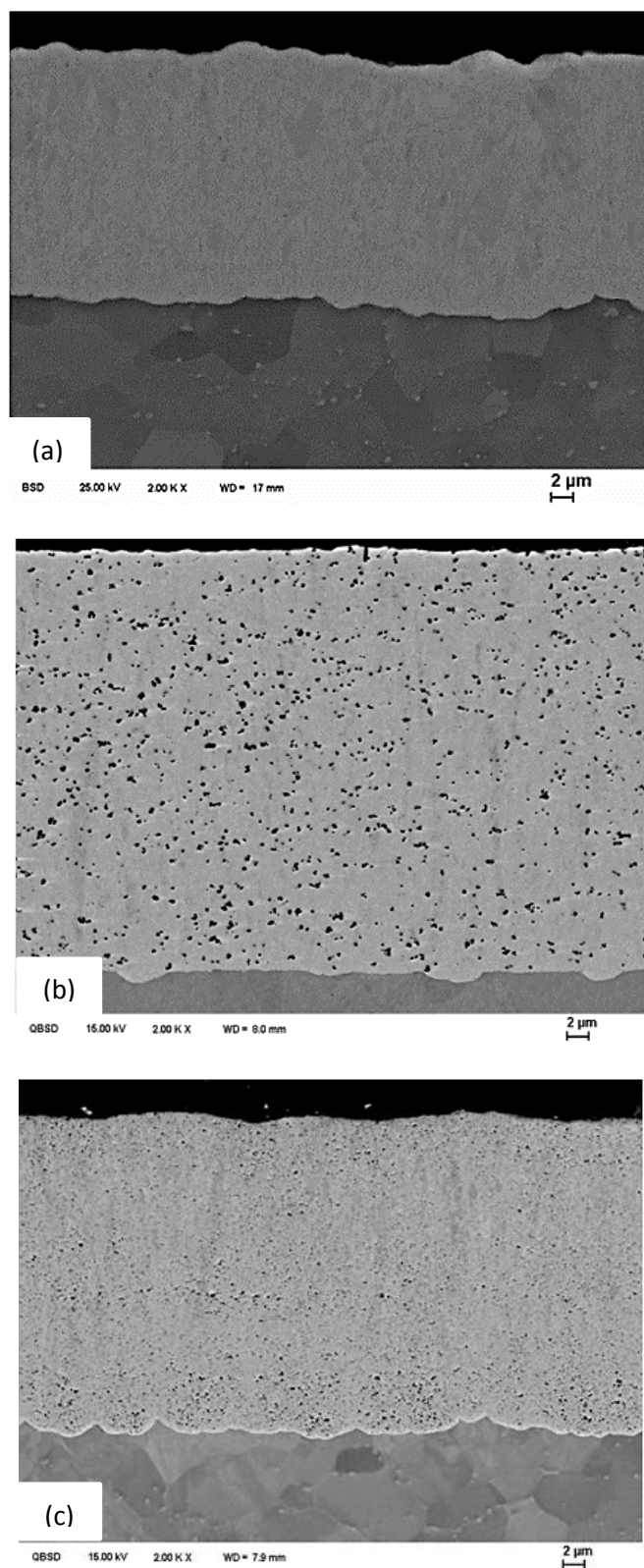


Figure 4.10 SEM images of cross-section: (a) Ni, (b) Ni-sm Al₂O₃ 20 g/l (c) Ni-n Al₂O₃ 20 g/l electrodeposited at $i=4\text{A/dm}^2$ for 40 min

However, as plotted in Figure 4.12, the measurement of the volume percentage of particles in a certain surface by means of the image analyzer shows that, under the same working conditions, the number of incorporated particles - in the case of adding nanoparticles - is slightly higher compared to the addition of

submicron particles, namely 5.1 to 4.6 vol%. The same behavior was detected for Al_2O_3 50 and 300 nm by Vereecken et al. [132]. In fact, by reducing the particle size, the number of the particles codeposited into the matrix is higher; but - due to the smaller size - the atomic percentage would be lower.

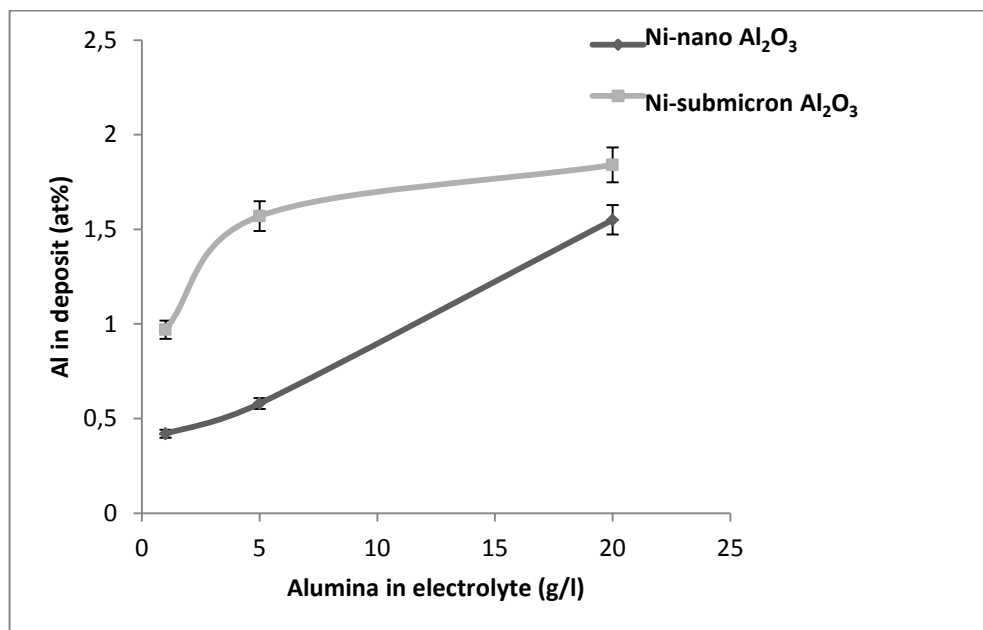


Figure 4.11 Effect of particle size and concentration on the incorporation value of particles achieved from EDX mapping analysis from the thickness of the deposits

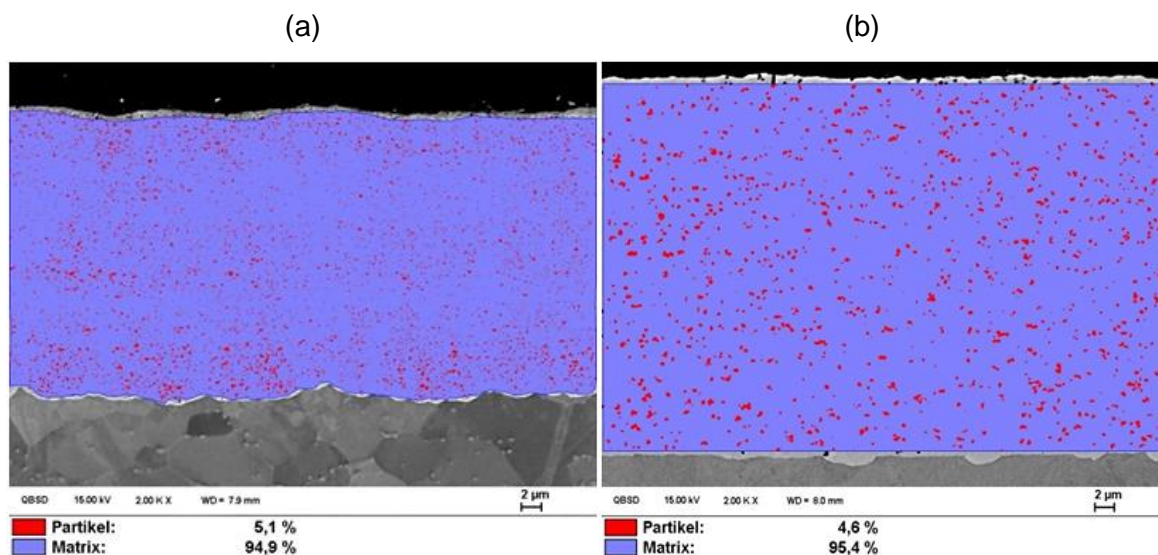


Figure 4.12 Volume percentages (vol %) of alumina particles estimated by image analyzer software: (a) Ni-nano Al_2O_3 20 g/l (b) Ni-submicron Al_2O_3 20 g/l electrodeposited under the same working conditions

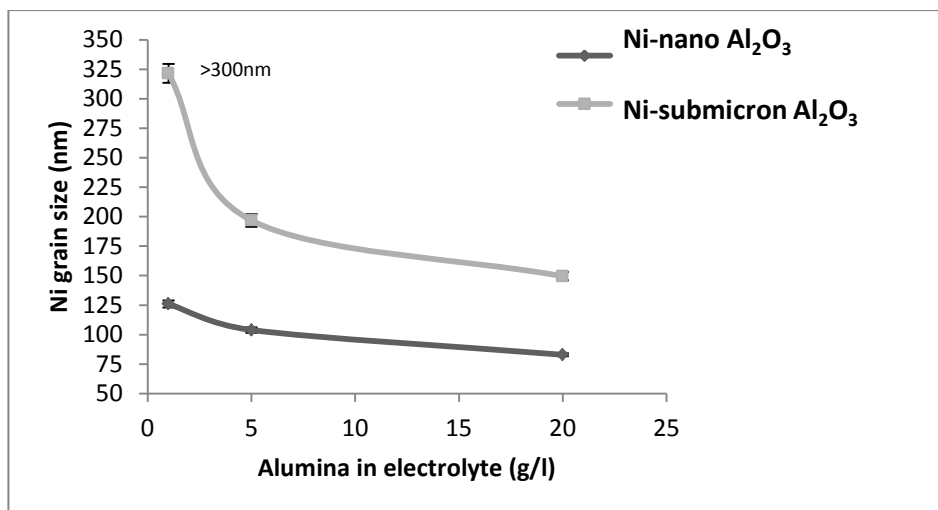


Figure 4.13 Effect of particle size and concentration on the Ni grain size

Figure 4.13 exhibits the grain size of the Ni matrix for the samples estimated from Scherrer's equation using the XRD peak width. In fact, the reduction in the grain size of the Ni crystal by adding particles approves the compactness of the coatings as also confirmed by the results of the morphology. It can be seen that, by increasing the concentration of particles in the electrolyte, on one hand, the incorporation value for the case of submicron particles is higher than when nanoparticles were used, but on the other hand, the grain size value reduced more when nanoparticles are added into the Ni matrix. The difference in microstructure and grain size of Ni matrix for Ni- Al_2O_3 composite coatings with both nano- and submicron particles are more observable in EBSD results of Figure 4.14.

The reason here is that smaller particles can offer more sites for nucleation, which is detrimental for the growth of Ni crystal while on larger particles, therefore, Ni crystal finds more opportunity to grow. One possible mechanism to explain the codeposition behavior of particles here is the phenomenon proposed by Guglielmi [1]. In the first step, the particles in the electrolyte are clouded by nickel ions and due to the agitation in the electrolyte, clouded particles approach the cathodic surface and there, a certain amount of particles can be trapped and buried by reducing new ions over them. According to the thickness measurements in Figure 4.15, it is understandable that in lower particle concentrations till 5 g/l, the possibility of transferring Ni ions through the particles is high such as the value of the thickness at the given concentration is large, namely around 65 μm . At the higher concentration of 20 g/l, however, the thickness values for both particle types showed a declining trend. It is possible that the addition of more particles into the solution could block the cathodic surface and, therefore, a more active area for the reduction of Ni ions.

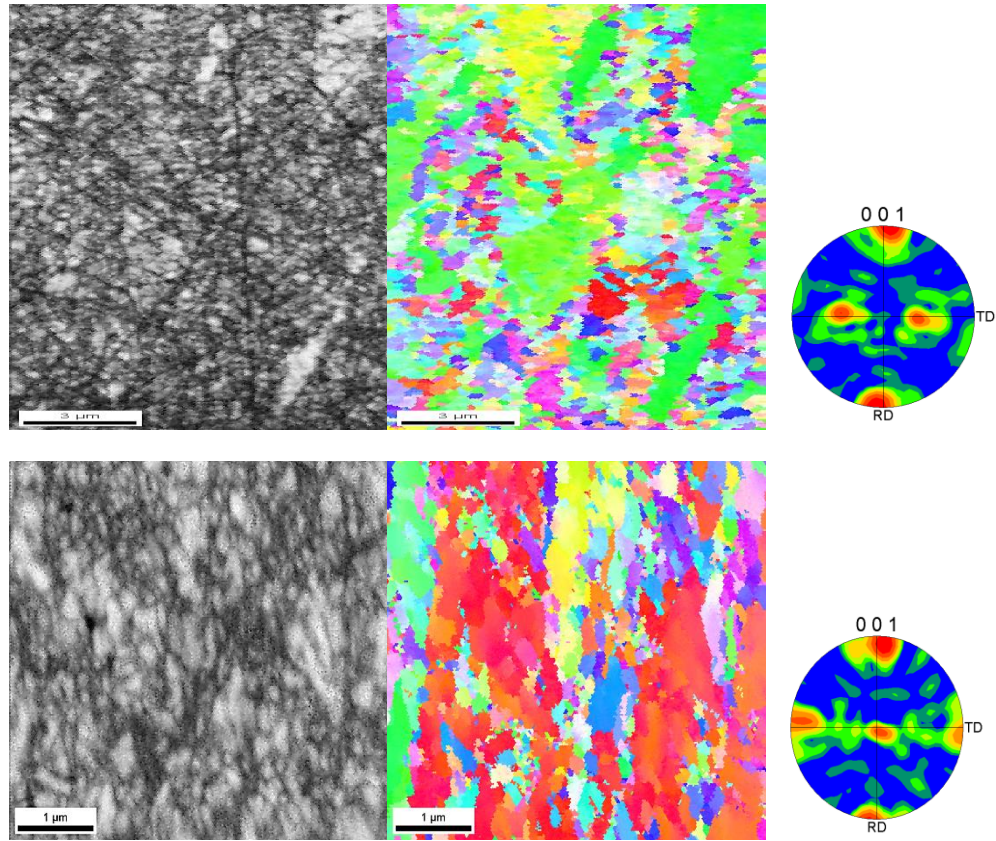


Figure 4.14 EBSD texture of Ni-nano Al_2O_3 and Ni-sm Al_2O_3 with 20 g/l under other same working parameters

Nevertheless, at the higher concentration of 20 g/l, the thickness of the layer deposited with submicron particles is higher than the layer deposited with nanoparticles, 37 ± 0.7 and 25 ± 1.2 μm respectively. The reason here, as explained above, can be the better opportunity of Ni crystals to grow on larger particles rather than on smaller ones. Since the particle hinders the current flow, the local overvoltage should rise respectively, thus the number of crystallization sites would be increased.

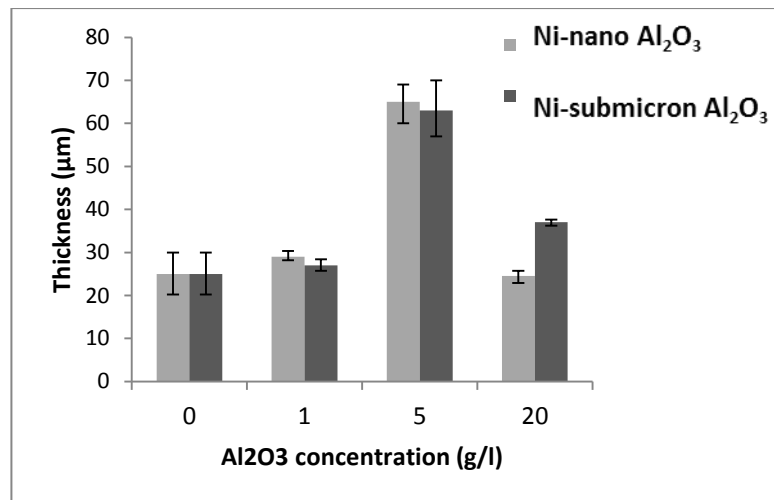


Figure 4.15 Effect of particle size and concentration on the thickness value of the deposits electrodeposited under the same conditions

Figure 4.16 shows comparable XRD-patterns depending on the particle size and content at the deposited layer. Ni coating exhibited a preferential growth on the crystal face (2 0 0), once nano- Al_2O_3 was co-deposited, the growth orientation of the Ni/ Al_2O_3 composite coating was changed from crystal face (2 0 0) to (1 1 1) for nanoparticles and remains (2 0 0) for submicron particles, although the relative intensity of both directions increases by adding more particles into Ni matrix. The codeposition of Al_2O_3 obviously affects the relative intensity corresponding to different crystal faces, with increase of Al_2O_3 in the coatings, the relative intensity corresponding to crystal face (1 1 1) increases, but the relative intensity of crystal face (2 0 0) decreases. For composite coatings with nanoparticles, the peak of crystal face (2 2 0) is more obvious. It seems that also the peak of (3 1 1) becomes stronger with increasing of Al_2O_3 content. Erler et al. [162] demonstrated that the XRD patterns of nickel nanocomposite coatings indicate changes in texture of such coatings which are dependent on the particle content in electrolyte. Chang et al. [163] has also presented similar results.

The Martens hardness of Ni- Al_2O_3 composite coatings was also carried out on the cross section of the layers by means of the Martens test as it was already explained in the experimental section. According to the results of the Martens hardness presented in Figure 4.17, it can be discerned that the Martens hardness of the Ni- Al_2O_3 composite coatings electrodeposited with both nano- and submicron particles follow an increasing trend by increasing the particle concentration in the electrolyte. It is obvious that the addition of nanoparticles leads to a higher Martens hardness at each single concentration in contrast to the addition of submicron particles. According to the results of the Martens test and the suggested codeposition mechanism, it can be concluded that, even though the codeposition can arise easier for the larger particles, the nucleation rate of nickel and subsequently the hardness value should not necessarily be higher. The reason of higher incorporation value in case of submicron particles can be related to easier transfer of the larger particles from the double layer to the surface.

The Martens hardness can be controlled by dispersion hardening or the amount of dispersed particles embedded in the layer based on the Orowan mechanism [153]. As it could be seen, by increasing the concentration of particles in the electrolyte, the incorporation value for submicron particles will be higher than that of nanoparticles, but on the other hand, the number of incorporated particles in the case of applying nanoparticles is higher. This means that the possibility of hindering the dislocations in the coating deposited by nanoparticles is higher. Moreover, as it was already seen, the grain size of the nickel matrix is smaller in the case of nanoparticles. This means that the grain size of the matrix, based on the Hall-Petch effect [154], plays an important role in the hardening mechanism of coatings.

In order to shed more light on assumptions about the codeposition behavior of alumina particles with different sizes and concentrations, impedance spectroscopy was used to explain the effect of particle features on the behavior of the charge transfer and double layer capacity for the Ni electrodeposition.

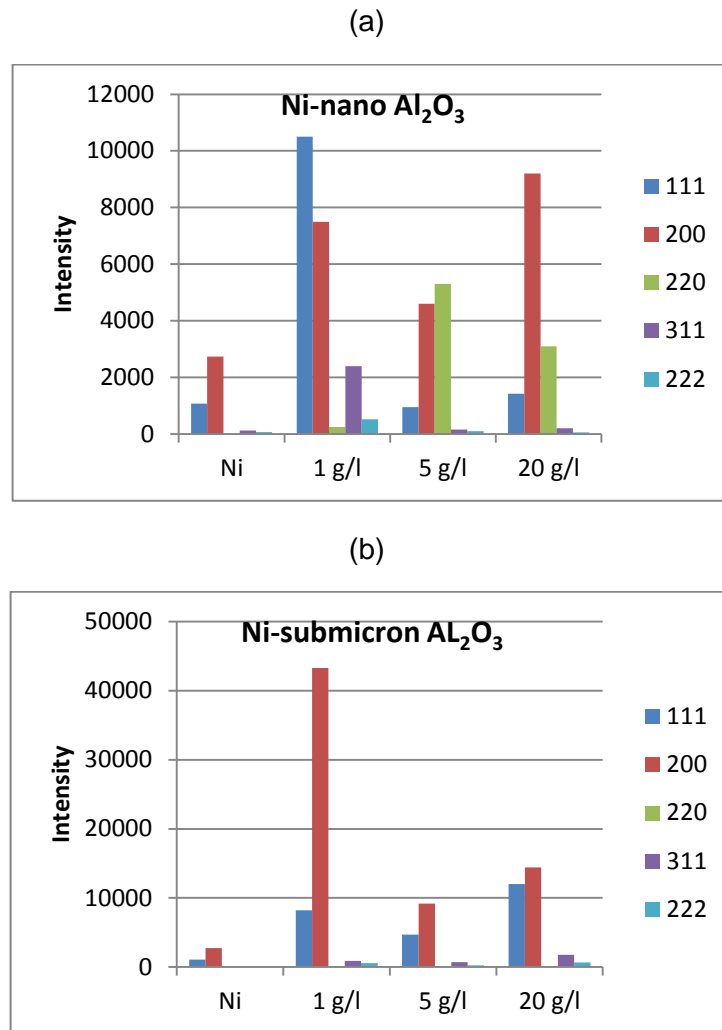


Figure 4.16 Texture values in (a) Ni- Al_2O_3 13 nm (b) Ni- Al_2O_3 200 nm electrodeposited at current density of 4A/dm^2 with 20 g/l particle concentration into Watts's electrolyte

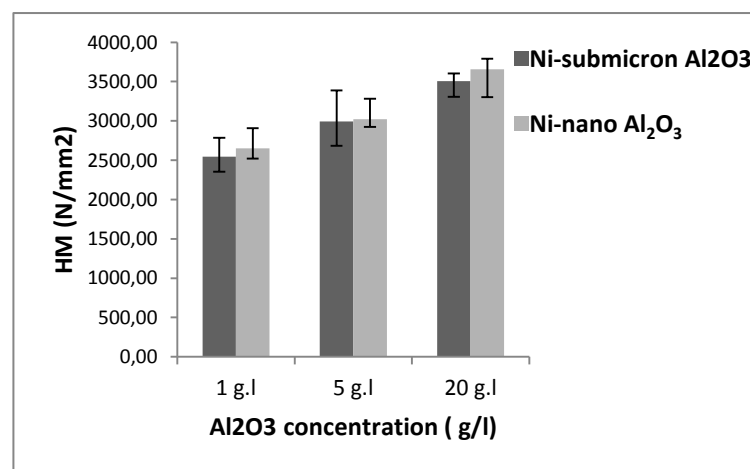


Figure 4.17 concentrations including the effect of grain size and particle content

4.3.2 In-situ EIS study of Ni-Al₂O₃ electrodeposition

Figures 4.18 (a-c) show the Nyquist plots from electrochemical impedance spectroscopy results during the electrodeposition process for Ni and Ni-Al₂O₃ with particle nano- and submicron particles and different concentrations of 1, 5 and 20 under the same deposition conditions. The impedance data comprises of a single capacitance loop in high and medium frequencies and an inductive loop in lower frequencies.

According to the mechanism of Ni electrodeposition proposed by Epelboin and Wiart [122, 124], the simple circuit model in Figure 4.19 is suggested for the impedance results of this study. In this study, the inductive loop was excluded in very low frequencies. Therefore, the impedance measurements could be achieved much faster within a shorter range of frequency which provide information about charge transfer and double layer capacity, which can be directly related to the Ni reduction. Nevertheless, the trace of inductive loops is indeed visible in rather lower frequencies. In this model, C_{dl} is the double layer capacitance of the interface of the electrode/electrolyte, and R_{ct} is a resistance against the charge transfer through the double layer at the electrode/electrolyte interface.

As it was seen in Figure 4.17, the loop size for both particle sizes was found to decrease with increasing particle concentration till 20 g/l. Additionally, as it is seen in the Figure 6c, at the concentration of 20 g/l, the usage of submicron particles caused higher shrinkage in the semicircle of Nyquist spectrums compared to the addition of nanoparticles to the electrolyte.

Increasing the concentration of the particles resulted in the decrease of the charge transfer resistance or the increase of the double layer capacity, as it was also shown by Benea or Dolati for SiC particles [106, 131]. As it can be deduced from the impedance results in Figure 10a and 10b, a descending trend in the impedance of the charge transfer as well as an ascending trend in the doubled-layer capacity was observed by increasing the Al₂O₃ particle concentration till 20 g/l. According to the impedance results, by the increase in the concentration of the particles in the electrolyte, the possibility that nickel ions are transferred by means of the particles towards the cathodic surface is higher. In other words, the decline in thickness of the double layer can finally influence the nickel reduction. Moreover, according to the results of Figure 4.20 (a and b), the value of the charge transfer resistance for submicron particles is lower than that of nanoparticles, and the double layer capacity for larger particles is moderately higher compared to smaller particle sizes. This means that the thickness of the double layer on the cathodic surface is less than that of nanoparticles in the case of adding submicron particles. Thus, as it is illustrated in the schematic of Figure 4.21, submicron particles can be easier incorporated into the deposit than nanoparticles due to having a larger active surface for free ions and a higher mass transfer.

Nevertheless, the deposition of nickel at the higher concentration of 20 g/l arises faster due to the higher charge transfer and double layer capacity. The reason for the decline in the thickness of coatings or for the reduction of the thickness of deposits at the higher particle concentration of 20 g/l, as it is seen in

Figure 4.21 (b), can be partly related to the blocking of the active surface of the cathode due to the accumulation of particles on the surface which should be avoided.

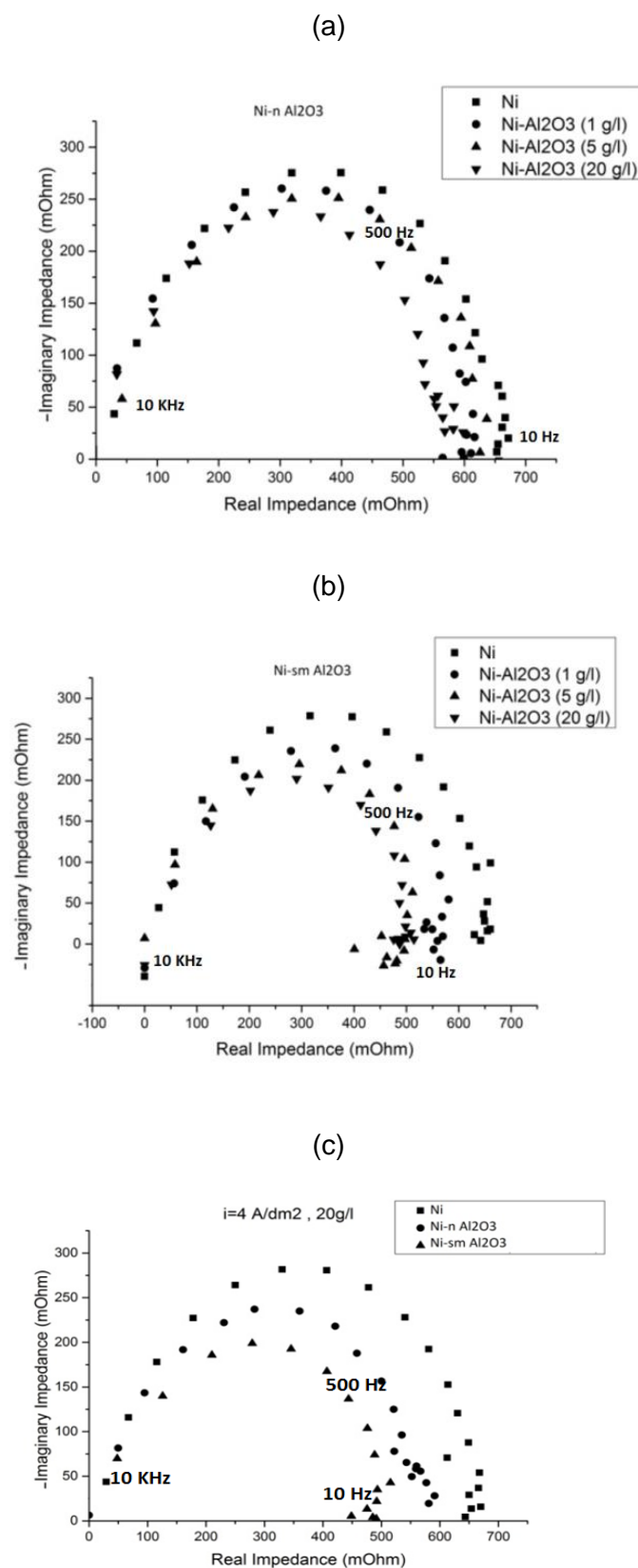


Figure 4.18 Effect of particle size and concentration on the Nyquist spectrums: (a) Ni-nano Al_2O_3 (b) Ni-submicron Al_2O_3 (c) comparison at the concentration of 20 g/l

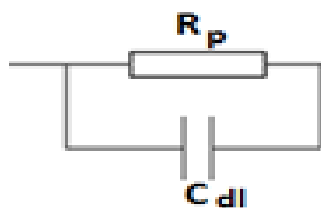


Figure 4.19 Circuit model used for impedance measurements for the frequency range of 10 kHz-10 Hz

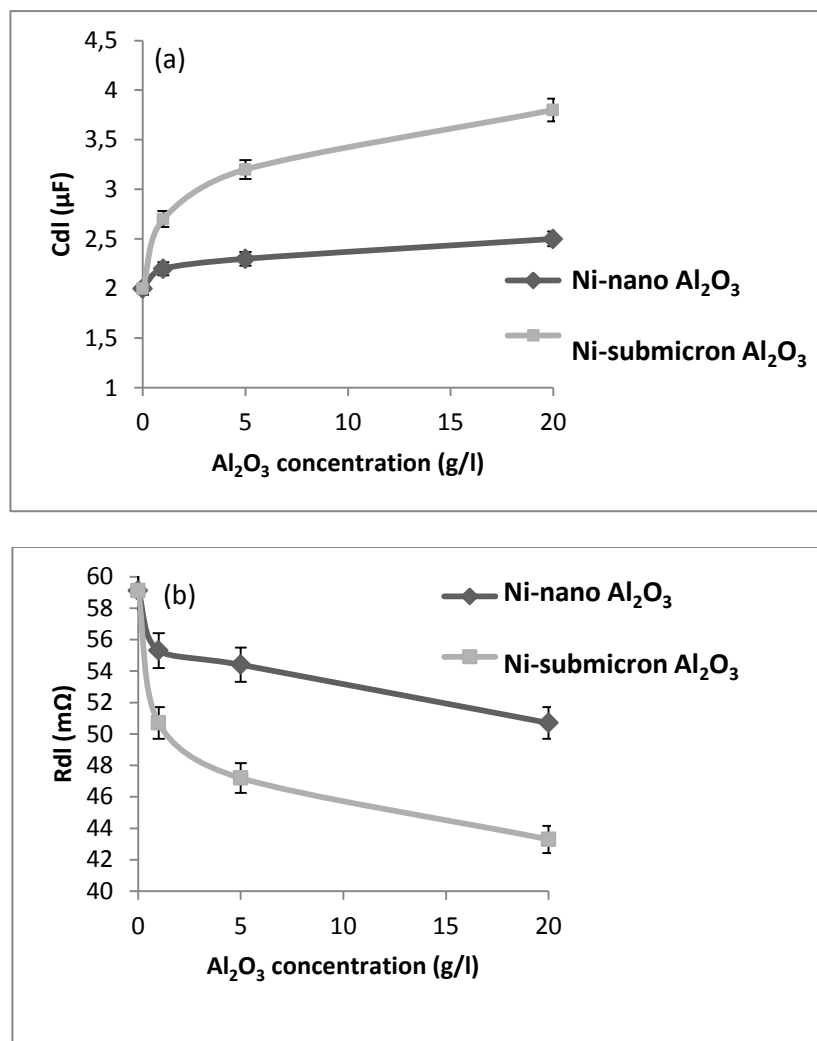


Figure 4.20 Results of C_{dl} (a) and R_{dl} (b) calculated by fitting the impedance results with the suggested circuit model by means of Matlab

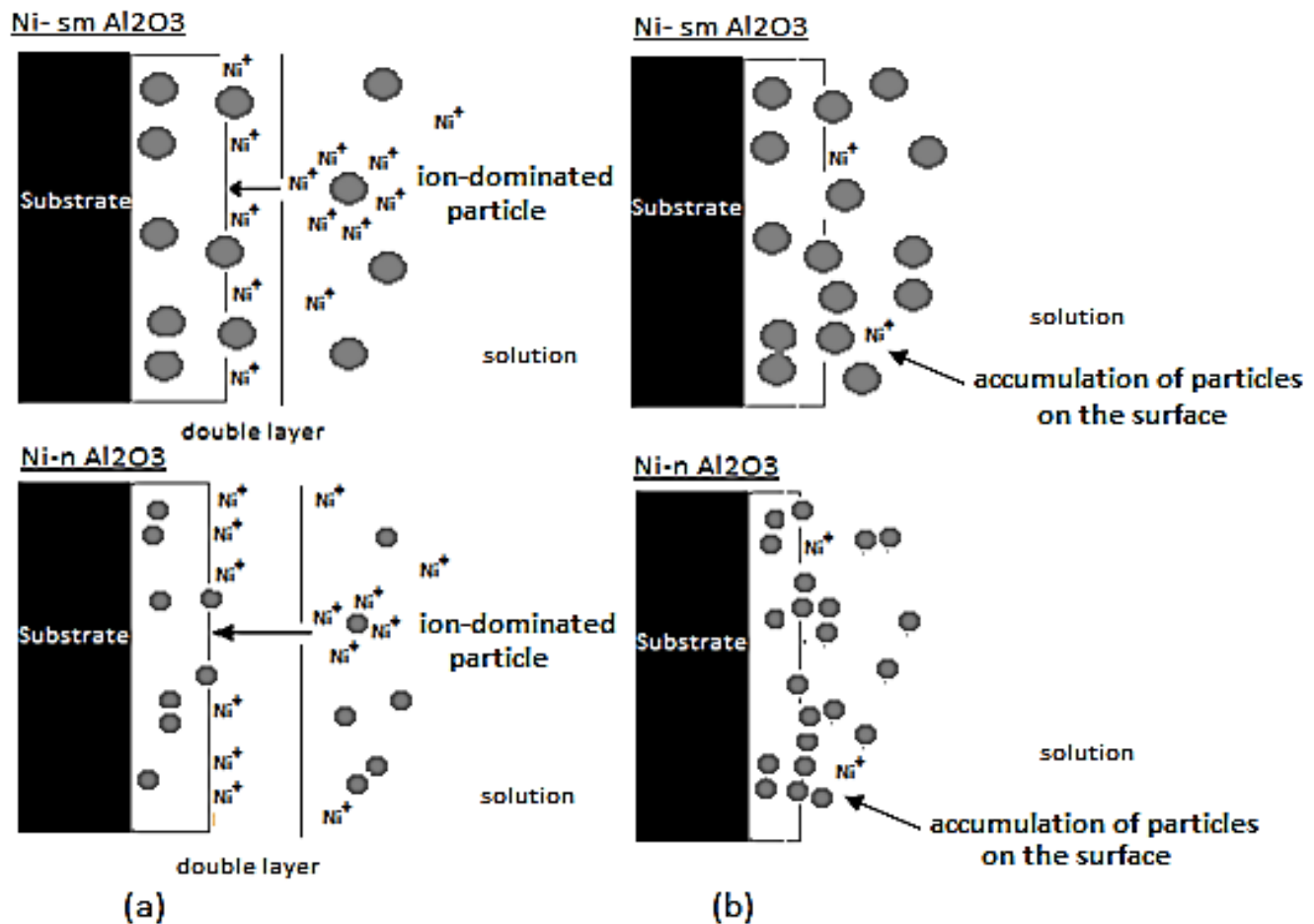


Figure 4.21 Schematic of the particle incorporation mechanism based on particle size and concentration:

(a) at low concentration of particles (b) at high concentration of particles

4.3.3 Effect of particle type on the morphology, microstructure and mechanical properties

As illustrated in SEM images in Figure 4.22, the morphology of Ni composite coatings are different compared to a pure nickel coating. With the addition of particles in the electrolytic, the borders of the Ni grains become fuzzy and more compact in comparison to pure Ni with no particles. In fact there is a transition in the morphology from columnar to equiaxial crystal growth. With addition of particles in solution, these particles precipitate in grain interfaces and obstacle grain growth. Thus, the structure transforms from pyramidal to global. In the case of adding Al₂O₃, the morphology seems to be even more compact and homogenous compared to the coatings deposited with SiC and TiO₂ under the same working conditions.

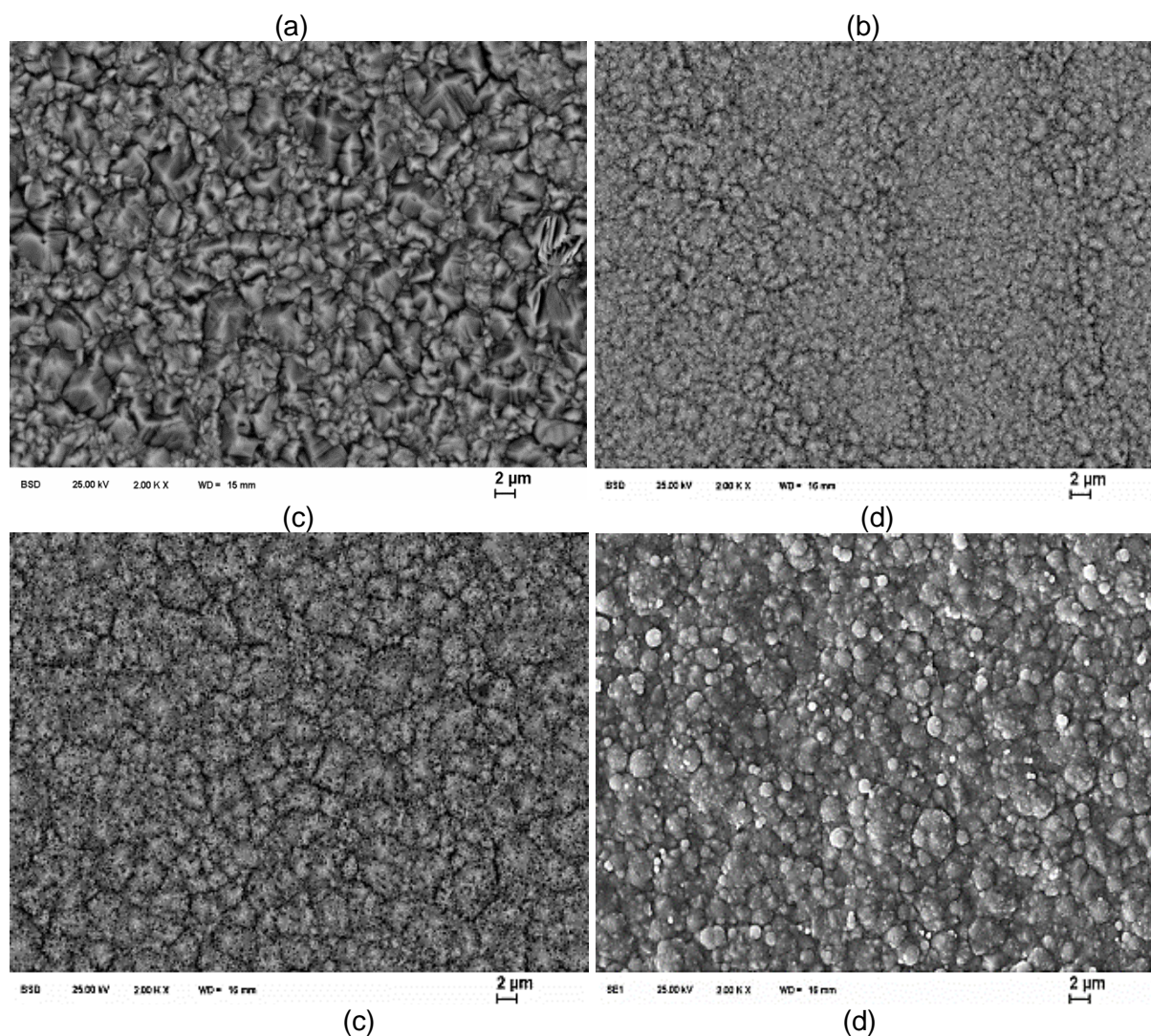


Figure 4.22 SEM images from the surface morphology of Ni coatings with different type of particles electrodeposited under the same working conditions: (a) Ni, (b) Ni-Al₂O₃, (c) Ni-TiO₂, (d) Ni-SiC

The SEM cross-section examination in Figure 4.23 reveals that all deposits (regardless of particle type) were crack free, homogenous and well adherent to the steel substrate. According to the cross-section SEM images, the influence of particle concentration for Al₂O₃, SiC and TiO₂ particles have been shown on the incorporation value of particles in the Ni deposit. The nickel deposits present a pseudo-columnar structure with the columns oriented on the direction of the electrical field, while the codeposition of particles leads to the interruption of the columnar growth. It is observed that the incorporation value for TiO₂ is much higher than Al₂O₃ and SiC for the coatings electrodeposited under the same conditions, especially incorporation value for SiC despite of 20 g/l particle concentration in the electrolyte, seems to be very dispersed and negligible.

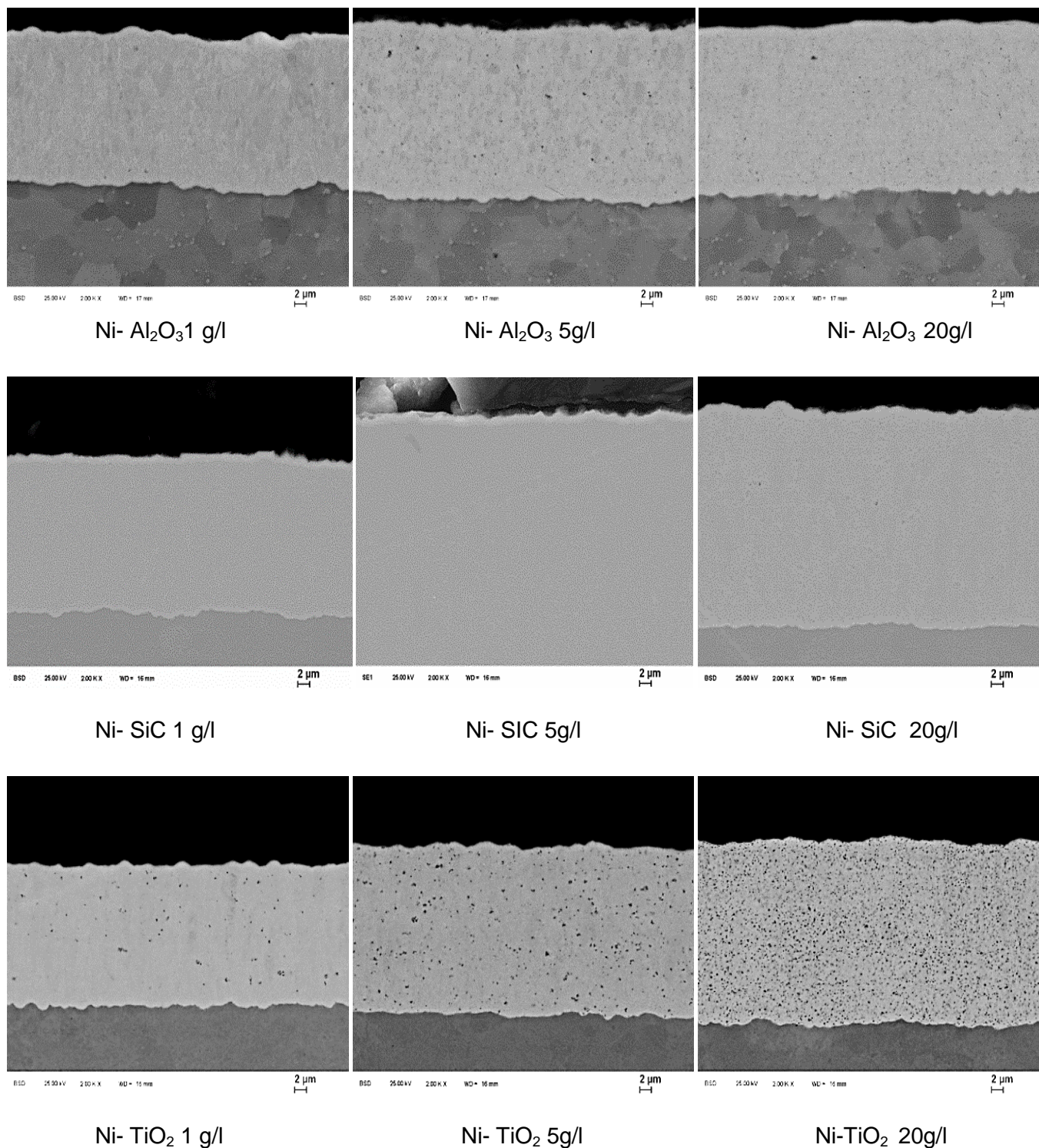


Figure 4.23 SEM images from cross-section of Ni coatings with different particle type and particle concentration, electrodeposited under the same working conditions and same particle size

According to the thickness measurements in Figure 4.24, it is seen that by adding Al_2O_3 and TiO_2 into the electrolyte, the thickness values of the deposits are almost constant, about 25 μm and do not change noticeably. On the other hand, the coating electrodeposited with only 5g/l SiC particles in the electrolyte shows the largest thickness value compared to other coatings deposited under the same electroplating

conditions, about 45 μm , while this value decreased to about 30 μm by adding 20 g/l particles into the electrolyte.

In fact in lower particle concentrations up to 5 g/l, the possibility of transferring Ni ions through the particles is higher such as the value of the thickness at the given concentration is large, especially for SiC particles with conductive nature has better opportunity for Ni crystals to grow rather than on Al_2O_3 or TiO_2 particles with rather inert behavior. At the higher concentration of 20 g/l, the addition of more particles into the solution would block the cathodic surface and therefore, a more active area for the reduction of Ni ions.

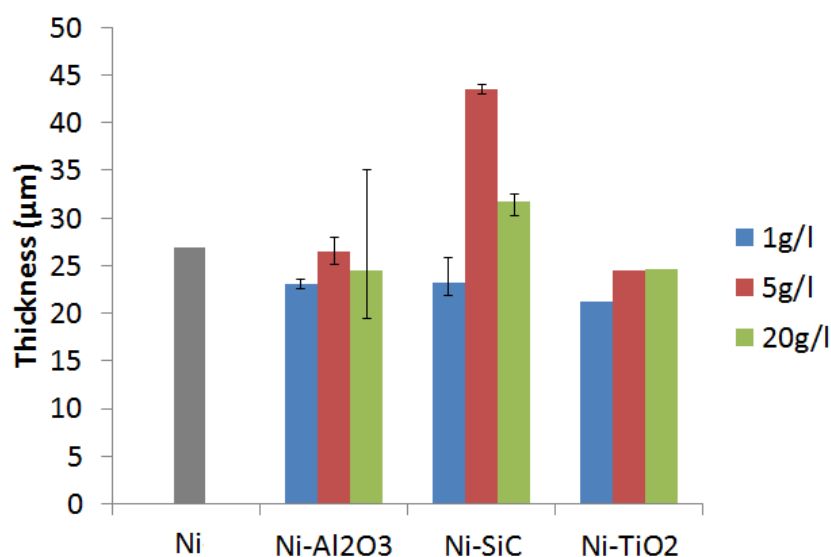


Figure 4.24 Thickness results of Ni coatings with different type of particles electrodeposited under the same working conditions

The EDS analysis in Figure 4.25 reveals the particle concentration in the coatings electrodeposited from Watt's bath outlined in terms of atomic percentage for titanium oxide, alumina and silicon carbide with 50 nm particle size, respectively. The data are calculated from the measured Ti/Ni ratio (Al/Ni and Si/Ni, respectively) assuming the stoichiometric composition, since light elements, especially carbon, hardly can be analyzed quantitatively by EDX.

It is seen that generally, the incorporation value of particles increases by increasing the particle concentration in the electrolyte. Adding SiC particles showed insignificant changes and also the lowest amount of incorporation value compared to Al_2O_3 and TiO_2 . The highest incorporation value relates to the coatings electrodeposited with TiO_2 particles. The EDS results correspond well with the SEM cross-section images from the coatings.

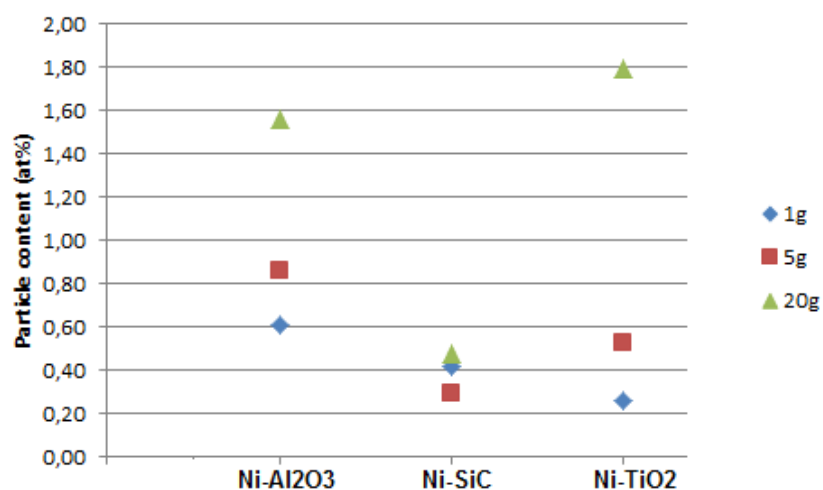


Figure 4.25 Particle content VS particle concentration/type for Ni electrodeposited composite coatings

According to the results of Ni grain size achieved from XRD results and estimation of Scherrer's law, first of all, it is observed that, the grain size of deposited coatings getting smaller by increasing the particles concentration in the electrolyte for all three particle types. Moreover, it is obvious that the coatings deposited with Al₂O₃ particles showed finer microstructure at each single concentration compared to the coatings deposited by SiC and TiO₂. Although incorporation value for TiO₂ was much higher than SiC, the effect of TiO₂ particles on crystal growth and refinement was almost the same as coatings with the low amount of SiC particles.

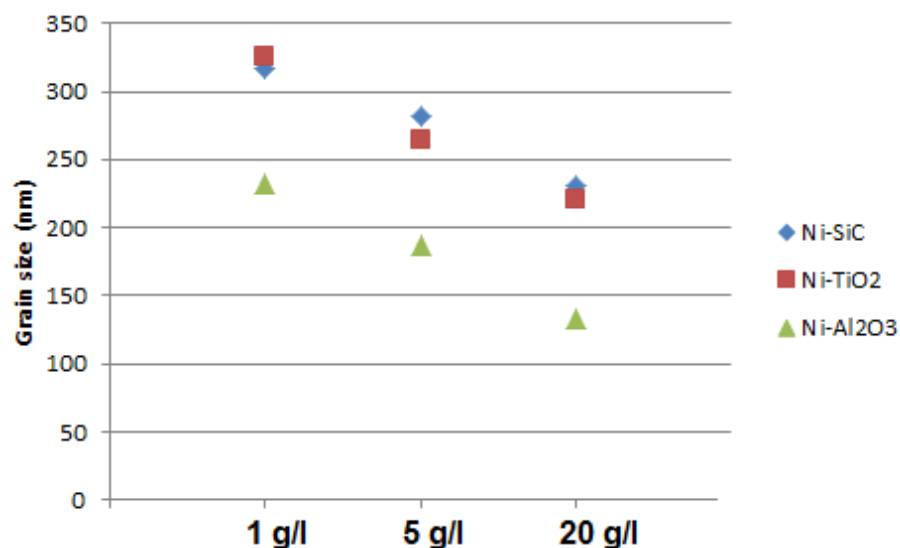


Figure 4.26 Grain size results for $i=4 \text{ A/dm}^2$, from XRD

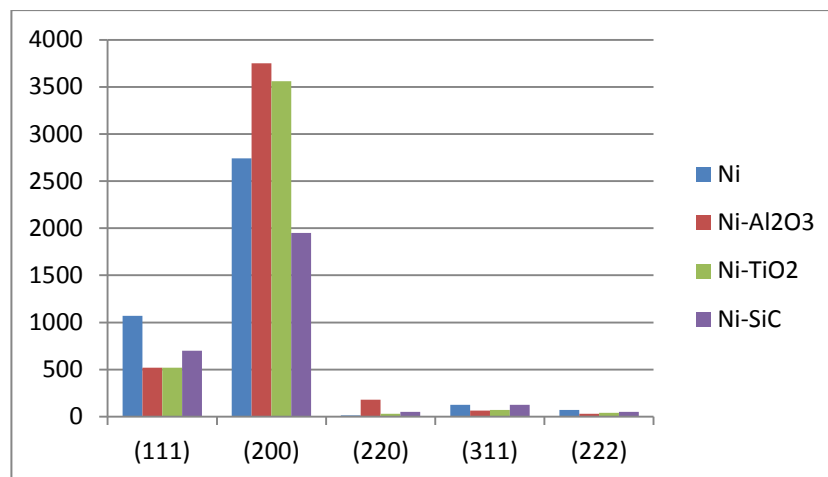


Figure 4.27 Texture values in Ni electrodeposited coatings with different particle type

Pure electroplated nickel films typically reveal a columnar crystal growth. Codeposition of particles can change the plating conditions and create additional nucleation sites. However, different texture transitions are not seen in the Ni composite coatings with different type of particles with 20 g/l concentration in the electrolyte. Meanwhile, the relative intensity of (1 1 1) for the composite coatings decreased almost to half of the value compare to Ni. Moreover, there is an improvement in the direction of (2 2 0) observed by adding Al₂O₃ and TiO₂ particles. The highest relative intensity among these three particle types relates to alumina in (1 0 0) and after that TiO₂ and SiC respectively. The same trend has been seen by others [62].

The results of internal stress for Ni composite coatings achieved from XRD, shows that adding particles into Ni Watts's electrolyte reduces residual stress in the deposited composite coatings, whereas under the same working conditions adding 20 g/l TiO₂ particles reduces the stress, to a minimum of approximately 230 N/mm² at 4 A/dm². The grain size of nickel might be smaller with high Al₂O₃-particle content in the electrolyte, so that residual stress of the first order cannot accumulate as much as with TiO₂.

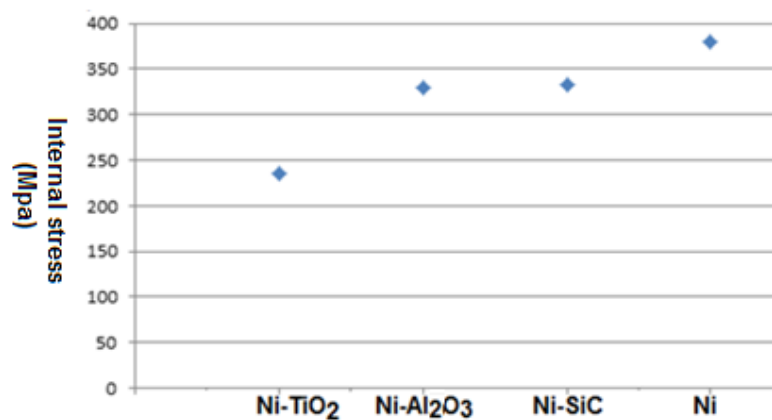


Figure 4.28 Internal stress in Ni electrodeposited composite coatings with different particle types measured with XRD technique

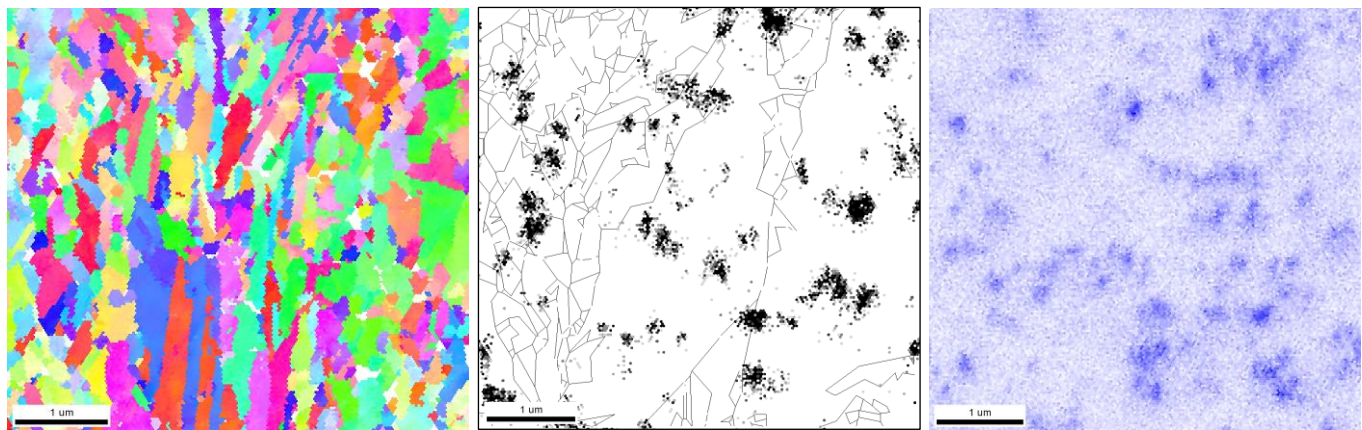
The results acquired in Figure 4.29- 4.31 could illustrate more clearly the microstructure of coatings electrodeposited with different particles types. Compared to electron backscattering images of nickel films, EBSD and TKD studies give a rather accurate picture of the grain size since quality maps are composed in terms of crystallographic orientation. It is observed that due to the higher surface energy of nanoparticles, despite the application of ultrasound, agglomeration at higher particle concentrations is still unavoidable. It is observed that Al_2O_3 influenced more intensely on the refining of Ni grains compared to SiC and TiO_2 . Furthermore, Figure 4.29 shows a fairly random TiO_2 distribution with particles located near the reconstructed grain boundaries as well as incorporated in nickel crystals. While Al_2O_3 and SiC are preferentially incorporated in the vicinity of grain boundaries.

EBSD maps indicate that the alumina nanoparticles are predominantly incorporated in the grain boundary zone. It is apparent that the alumina particles terminate the columnar nickel crystals and consequently affect the growth direction. The different influence on crystal growth by codeposition of semiconducting particles like silicon carbide compared to nonconductive particles like alumina is striking, and should be estimated under the aspect of particle conductivity. Otherwise the incorporation of SiC particles does not change the columnar growth of nickel.

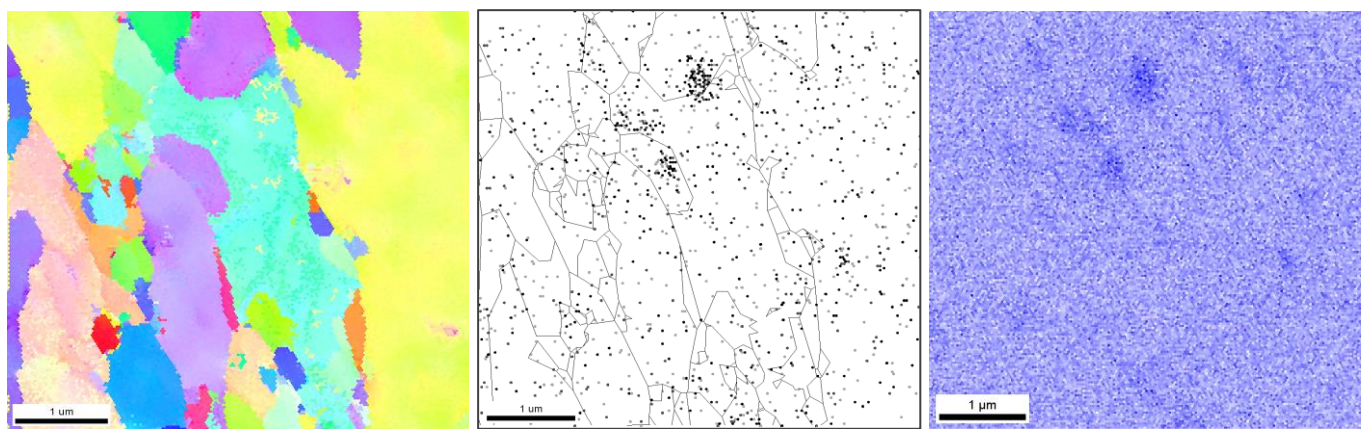
The particles intersect the crystalline columns and do not provide additional nucleation sites for electrocrystallization. A survey of different models of electrolytic codeposition is given in reference [169]. By analyzing theoretical and experimental results, the authors point out the effect of current distribution at the cathode which is remarkably different for conducting or non-conducting particles. The small crystals on top of the particles are unoriented. In accordance with reference [169], it is assumed that the different influence of nonconductive and conductive particles on the primary current distribution at the cathode changes the nickel deposition around the adsorbed particles. Electrical isolating and conductive particles have different impacts on the primary current distribution at the cathode and change the nickel deposition around the adsorbed particles. Behind non-conductive particles like TiO_2 , the remarkably decreased current facilitates nickel crystal growth around the particle. In contrast, semi-conductive particles like SiC leave the current distribution fairly unchanged.

The results of Martens test in Figure 4.32 indicate that adding 1 g/l of each type of particles had no considerable effect on strengthening of deposit while after adding 5 g/l particles in the electrolyte, Martens hardening increased. Although the Martens hardening did not change any more with increasing more concentration of Al_2O_3 and SiC, this value increased even more by increasing concentration of TiO_2 particles in the electrolyte and respectively in the deposit.

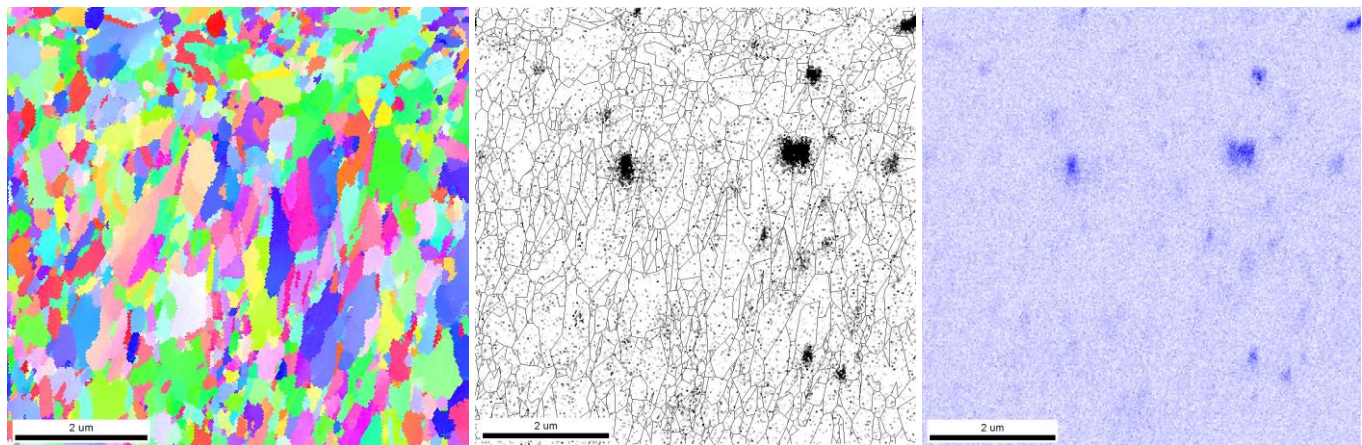
The results revealed that the fine particles incorporated within the Ni matrix could restrain the growth of Ni crystals and impede the motion of dislocations, by way of grain refining and dispersive strengthening effects.



Ni-TiO₂

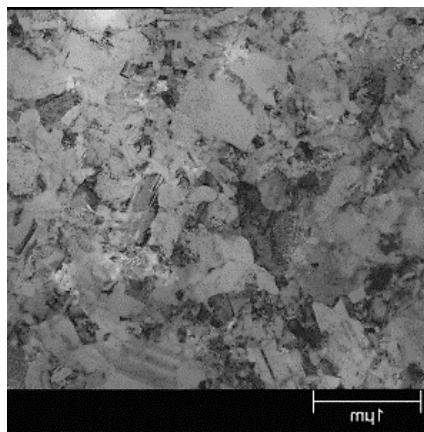


Ni-SiC

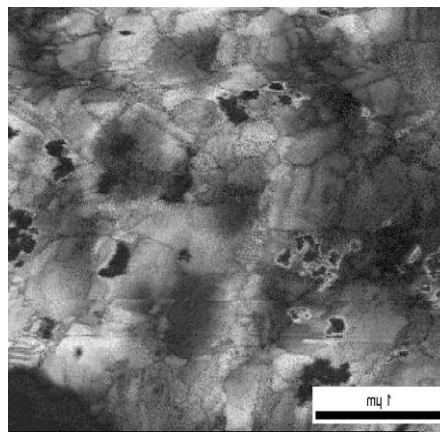


Ni-Al₂O₃

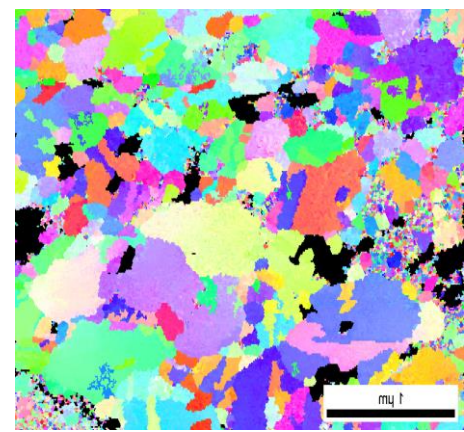
Figure 4.29 EBSD images of Ni composite coatings with different particle type electrodeposited under same working conditions



Ni-TiO₂



Ni- SiC



Ni- Al₂O₃

Figure 4.30 TKD images of Ni composite coatings with different particle type and same particle size electrodeposited under same working conditions

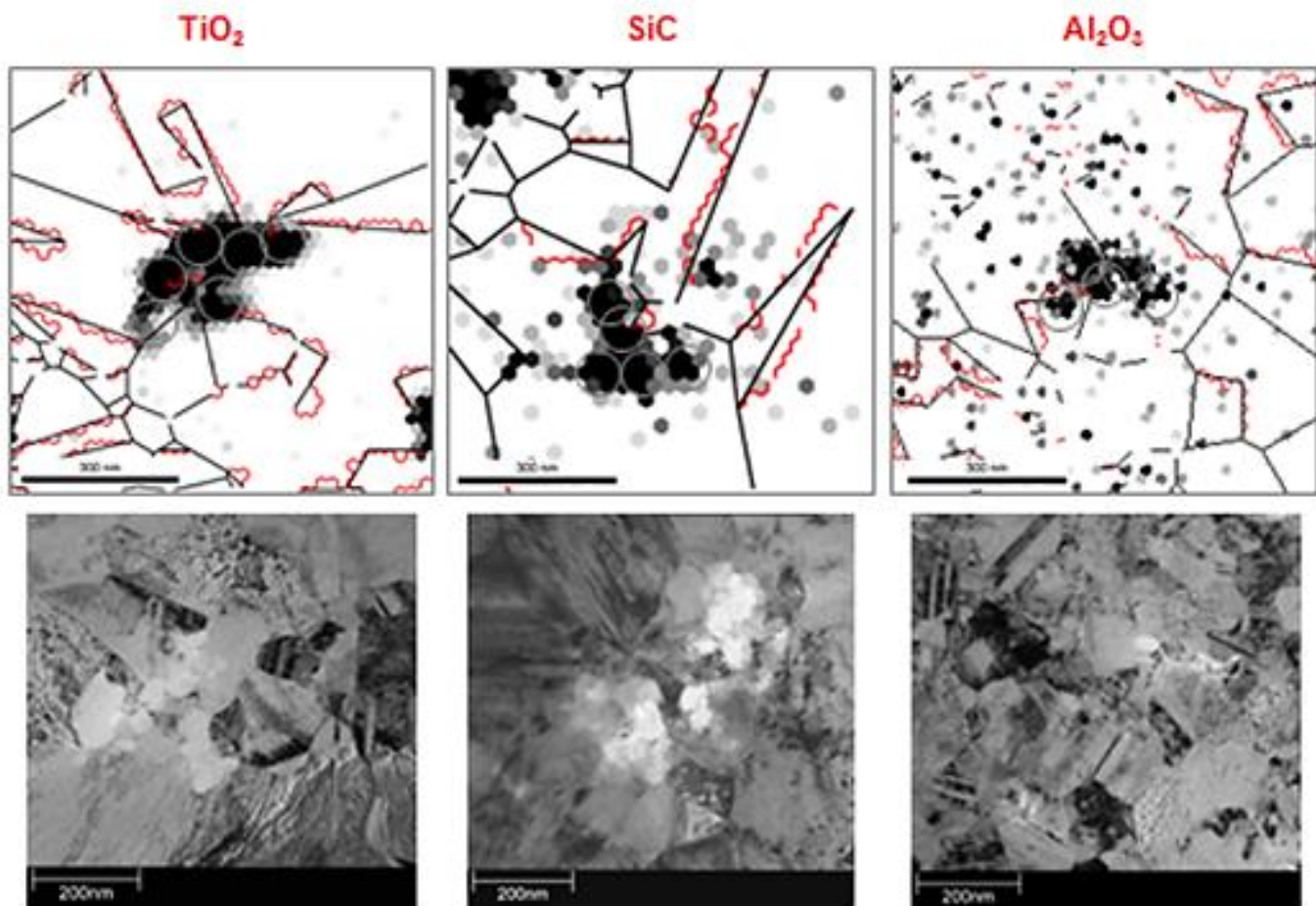


Figure 4.31 Comparison between TEM and TKD images for Ni composite coatings with different particle type electrodeposited under same working conditions

This means that the mechanism of Orowan and dispersion hardening plays a specific role for the coating with TiO_2 particles according to particle number and better distribution. On the other hand, accumulation of SiC particles has lower effect on the hindrance of dislocations. Moreover, the dominating mechanism of strengthening in Ni- Al_2O_3 composite coatings is mainly due to the Hall-Petch effect and grain refining rather than particles incorporation and Orowan mechanism.

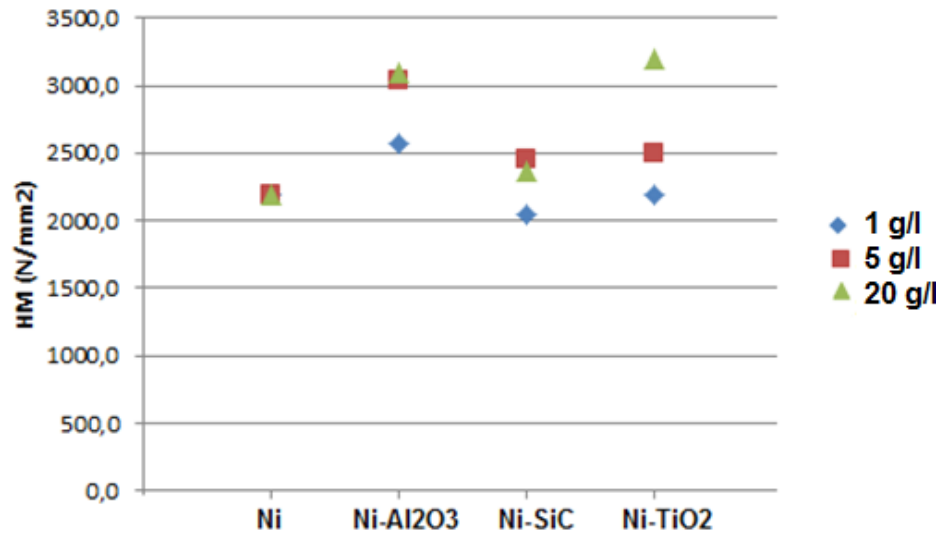


Figure 4.32 Hardness versus particle concentration/particle type

4.3.4 In-situ EIS study of Ni electrodeposited with different particle type

Figure 4.33 shows the Nyquist plots from electrochemical impedance spectroscopy results during the electrodeposition process for Ni- Al_2O_3 , Ni-SiC and Ni- TiO_2 with three different particle concentrations of 1, 5 and 20 g/l electrodeposited under the same deposition conditions. It is seen that the size of Nyquist semicircle for the coating with alumina particles at lower concentration of 1 and 5 g/l is smaller than the coatings with SiC and TiO_2 particles, while the one including TiO_2 particles shows the larger semicircles for the concentration of 1 and 5 g/l. On the other hand at higher concentration of particles in the electrolyte, 20 g/l, the size of semicircle for the Ni coating including TiO_2 gets rather small compared to the other two coatings with Al_2O_3 and SiC particles. As already discussed before, the main physical elements describe the behavior of Ni electrodeposition at middle and high frequencies, including C_{dl} which is the double layer capacitance of the interface of the electrode/electrolyte, and R_{dl} that is a resistance against the charge transfer through the double layer at the electrode/electrolyte interface.

By correlating the results of particle content from EDX with the results of impedance spectroscopy, it is observed that particle content in composite coatings corresponded well with the impedance value achieved from EIS results. It means that at lower particle concentration of 1 and 5 g/l TiO_2 content is lower than SiC and Al_2O_3 respectively and this is equal to higher charge transfer resistance for TiO_2 compare to SiC and Al_2O_3 particles.

On the other hand, the particle content for Ni-TiO₂ at concentration of 20 g/l was higher than Al₂O₃ and SiC and in the meantime the charge transfer for this coating showed lower resistance compared to the coatings electrodeposited under the same conditions with Al₂O₃ and SiC. Since the size of these particles is in the same range, this behavior is clearly related to the intrinsic characteristics, for example differences in particle density and surface composition which can finally affect the charge transfer and respectively particle content. The incorporation of particles into the film may involve physical adsorption or chemisorption of particles, or electrochemical reactions of species adsorbed at the particle surface. Various models have been proposed that take these effects into account [169,170]. For instance, charged surfactants adsorbed on codepositing particles influence the particle composite content through the particle surface composition, but this is not determined by the particle charge. Other interaction forces, like the London-Van der Waals force or hydration force, dominate and are responsible for the effect of particle material on particle composite content. Apart from the surface composition the bulk properties of a particle material will affect composite deposition. Particle mass transfer and the particle-electrode interaction depend on the particle density, because of gravity acting on the particles. Since the particle density cannot be varied without changing the particle material, experimental investigations on the effect of particle density have not been performed. However, it has been found that the orientation of the plated surface to the direction of gravity combined with the difference in particle and electrolyte density influences the composite composition. In practice it can be difficult to deposit composites with homogeneous composition on products where differently oriented surfaces have to be plated.

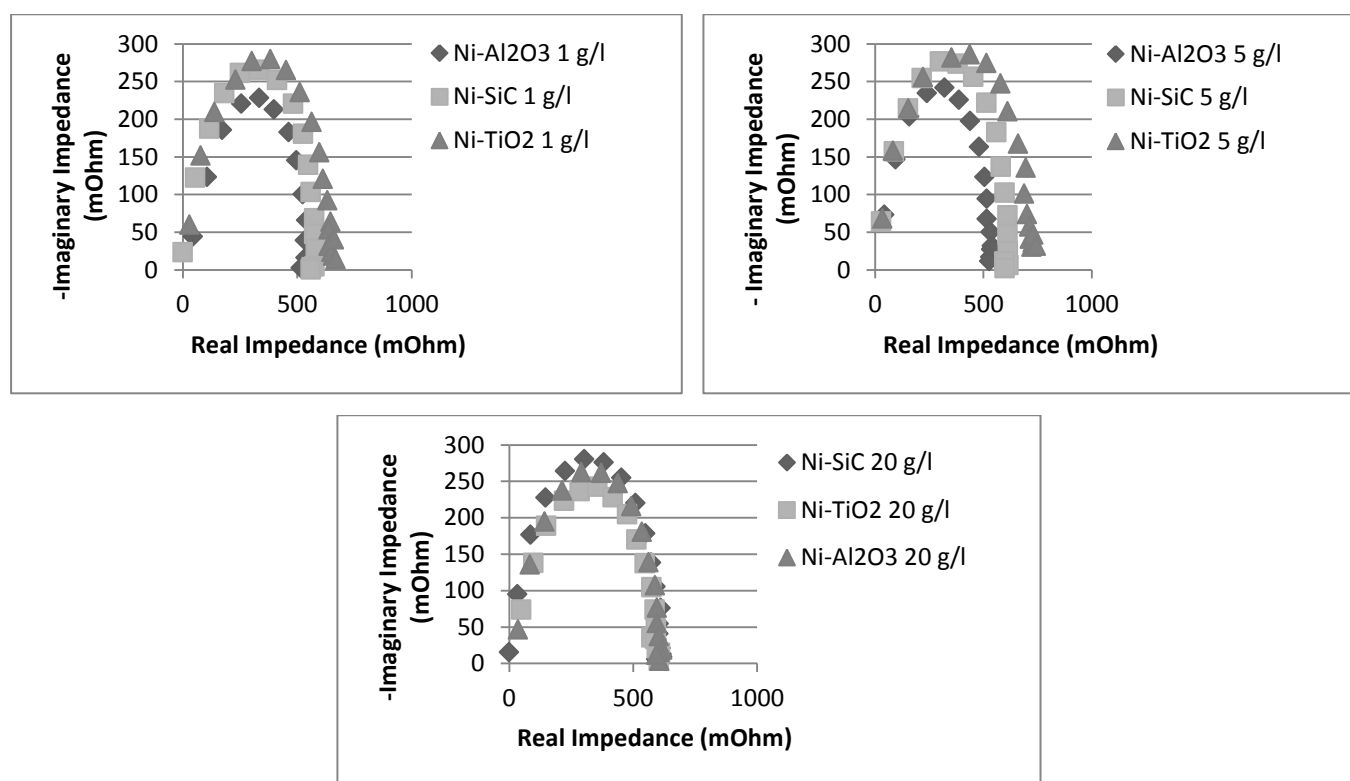


Figure 4.33 EIS results from the effect of particle type on the electrodeposition behavior of Ni

4.4 Investigation on electrodeposition behavior of Ni-P and Ni-P composite coatings

4.4.1 Layer Characterization of Ni-P electrodeposited coatings

Ni-P coatings were electrodeposited from the modified Watts Electrolyte under the same working conditions with different concentration of sodium hypophosphate and different current densities. As it is seen from EDX and GOEDS results in Table 4.1 and also in Figure 4.34 the phosphorous content in Ni-P coatings changes with the phosphorous source in the electrolyte and also current density. Increasing the phosphorous source and decreasing the current density both caused higher phosphorous content in Ni-P deposits. The content of phosphorus in the deposits electroplated from the low phosphorus baths did not vary appreciably with current density. The deposits from the high phosphorus-nickel bath, Ni-H, showed a decrease in content of phosphorus as the current density was raised. With the P incorporation suspected to be rather constant, the Ni deposition is favored with increasing current density thus controlling the Ni/P ratio. Similar results have been discussed in a number of publications [164].

Nº	[NaP ₂ H ₂ O] (g/l)	Current density (A/dm ²)	EDX: [P] (wt %)	GOEDS: [P] (wt %)
1	0,1	1	1,1	1,2
2	0,1	2	0,7	1,2
3	0,1	4	0,6	0,7
4	0,5	1	3	3,2
5	0,5	2	2,4	2,7
6	0,5	4	1,7	2
7	1	1	5,3	4
8	1	2	3,1	3,4
9	1	4	2,6	2,6
10	5	1	8,8	7,7
11	5	2	7,7	6,5
12	5	4	5,8	4,5
13	10	1	9	7,2
14	10	2	8,2	6,8
15	10	4	7,2	4,9

Table 4.1 Effect of NaP₂H₂O₂ and current density on the phosphorous content of Ni-P electrodeposits measured by EDX and GODES

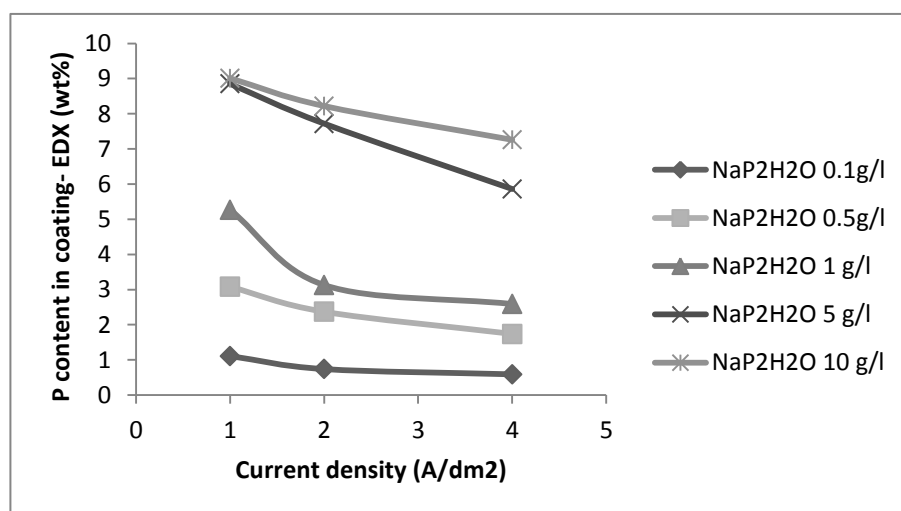


Figure 4.34 Correlation of phosphorous content in Ni-P deposit with current density and NaP₂H₂O₂ as Phosphorous source in Watts Ni bath

The X-ray diffraction analysis (Figure 4.35) shows the difference in microstructure of Ni-P regarding P content. The transition of the crystalline state towards a less ordered state is characterized by broader and less intense peaks which can continue until disappearing according to increasing phosphorus content. Thus, only deposits with less than 5 g/l $\text{NaP}_2\text{H}_2\text{O}_2$ are crystalline containing 5.8 wt. % of phosphorus are crystalline, even microcrystalline taking into account the extinction and the widening of the whole of the peaks. On the sample without phosphorus, the smoothness of the peaks is the result of strong crystallinity of the deposit for this composition, as has been shown previously. On the other hand, the inversion of the intensities of the peaks (1 1 1) and (2 0 0) for the sample with 5 g/l $\text{NaP}_2\text{H}_2\text{O}_2$ deposited at current density of 4 A/dm² could be explained by a change of crystalline texture with the phosphorus incorporation: the deposit without phosphorus presents a preferential orientation of the (2 0 0) plane parallel to the surface whereas the one with phosphorous favors the plane (1 1 1). This result was already observed by Lewis and Marshall [27]. They assign this privileged orientation of the planes (1 1 1) with increasing phosphorus content in the deposits due to the fact that the deformations of the crystallites are more important according to the crystalline planes (2 0 0) compared of the planes (1 1 1).

Beyond the phosphorus content of 5.8 wt. %, all the other samples become amorphous: the diffraction peaks decline, widen and then disappear. Phosphorus dissolves in solid solution in the nickel mesh and therefore does not appear on the X-ray diffractions.

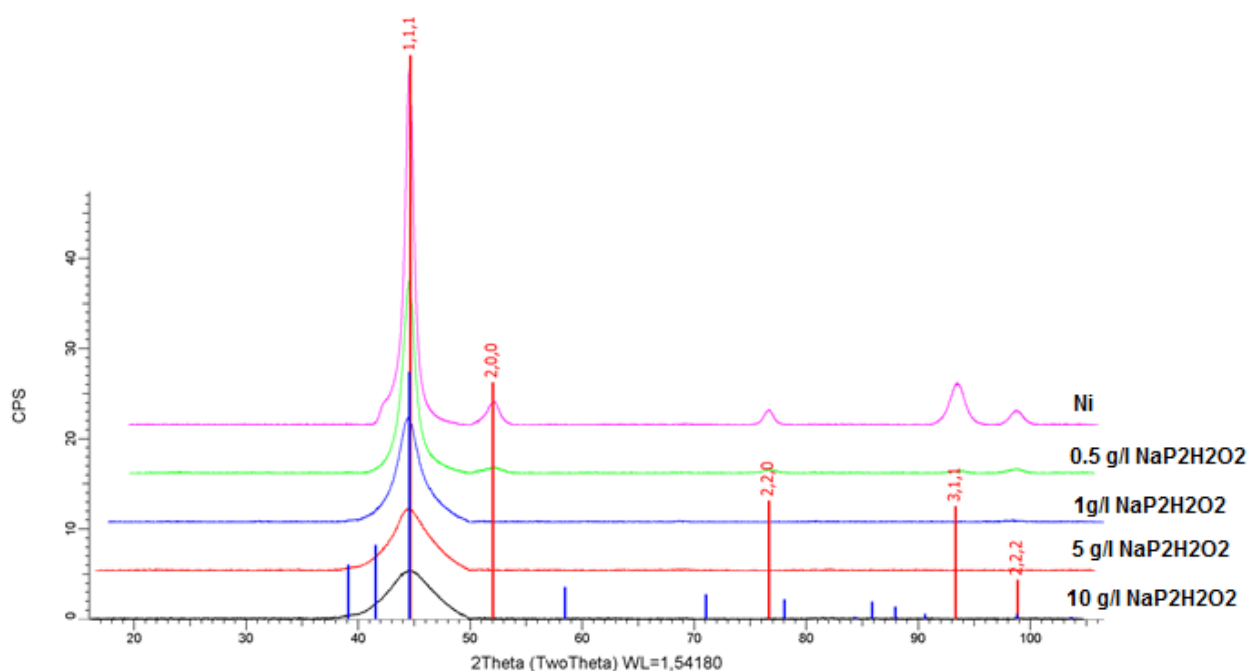


Figure 4.35 Effect of phosphorous source concentration on the crystallinity of Ni deposit indicated by XRD. Coatings electrodeposited at $i=4$ A/dm² and under same working conditions

Figure 4.36 shows the effect of phosphorous on the morphology of Ni deposit. The coatings deposited without phosphorus, pure Ni, as we have seen, showed pyramidal grains with characteristic of a crystalline structure, whereas the deposit elaborated in the presence of $\text{NaP}_2\text{H}_2\text{O}_2$ has a globular morphology which would return rather to an amorphous structure (Figure 4.3). This levelling according to the $\text{NaP}_2\text{H}_2\text{O}_2$ content of the bath is explained by a radical change of the morphology of the deposits.

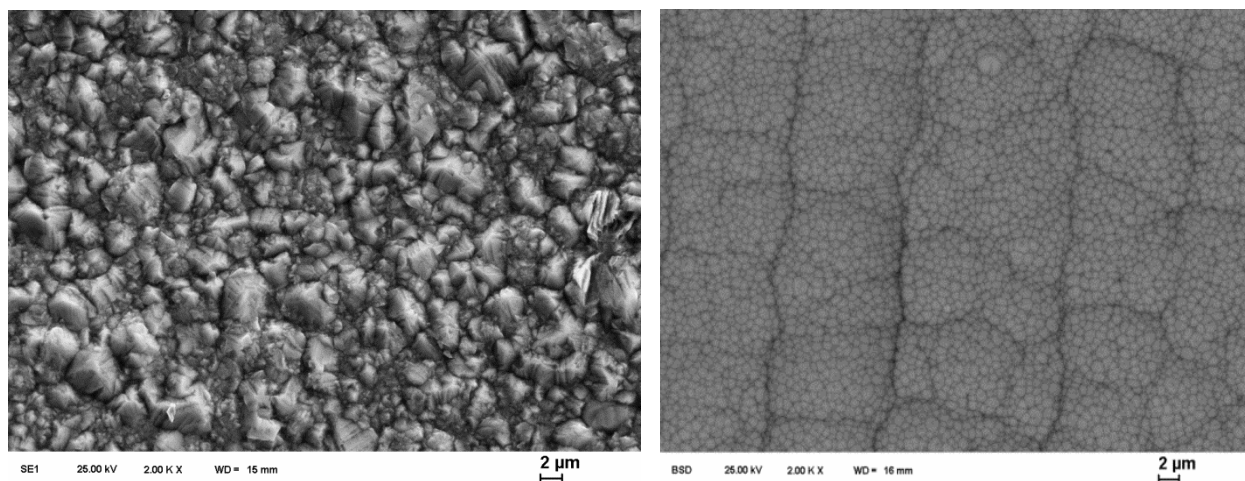


Figure 4.36 Morphology of Ni deposit with (right) and without (left) phosphorous source in Watts Ni

According to EIS results in Figure 4.37, it is observed that under the constant current density, by increasing the phosphorous source in the electrolyte, the impedance semicircle gets shorter. In other words, increasing the phosphorous content leads to reducing of charge transfer impedance and declining of double layer capacity for Ni deposition. As it is known by increasing P content, the microstructure of deposits from crystalline inclined towards nanocrystalline and amorphous structure. This evolution in microstructure has been attempted to be corresponded with the impedance results. According to impedance investigations, it seems that there could be a relationship between P content in deposits and value of charge transfer (R_p). Impedance results are mostly comparable in lower current of 1 A/dm^2 but in 2 and 4 A/dm^2 we have usually dispersion in impedance, probably due to the changes and variations in potential values (Figure 4.38).

Variations in the potential value, as indicated in voltammetry results (V-t) in Figure 4.39, can be due to the changes in interfacial pH by time which finally leads to formation of lamellar layers (Figure 4.40). This occurs mainly in low P content or higher current density, as mentioned in our already published paper [32].

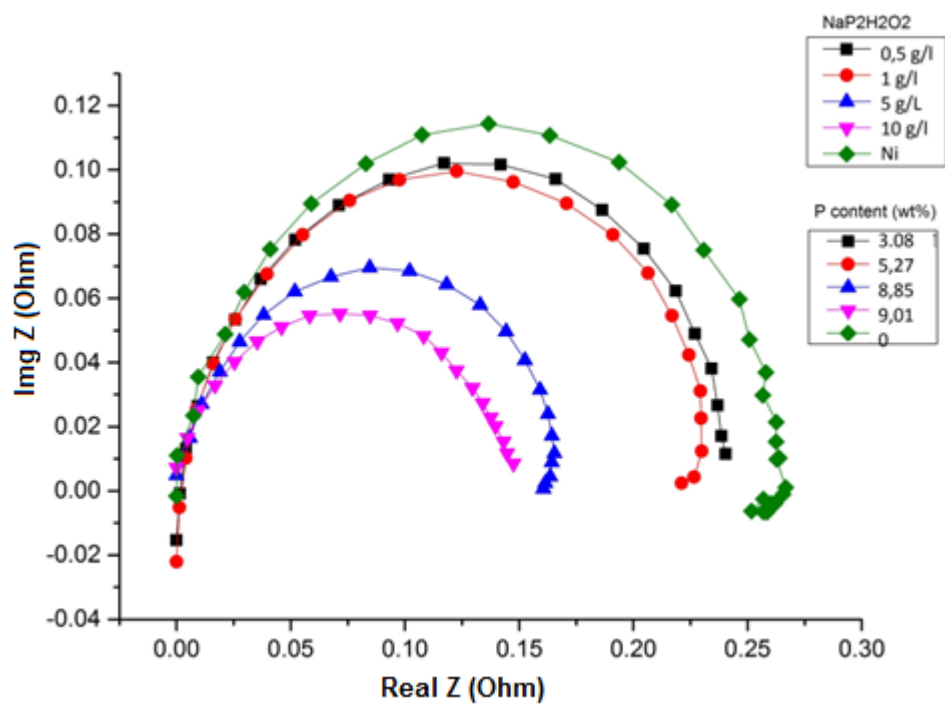


Figure 4.37 Effect of $\text{NaP}_2\text{H}_2\text{O}_2$ concentrations on the impedance behavior of Ni-P deposit (Ohm)

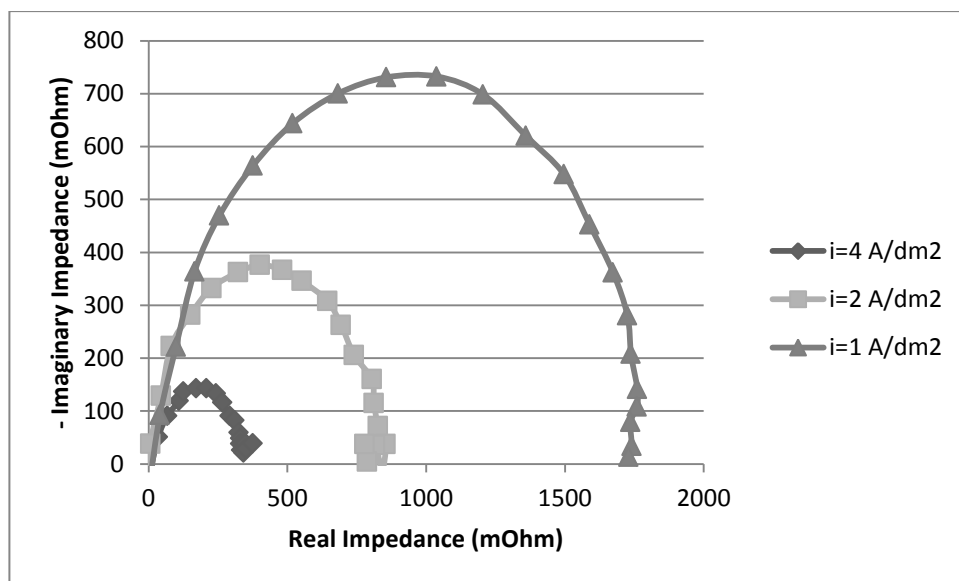


Figure 4.38 Effect of current density on the impedance behavior of Ni-P electrodeposited under the same $\text{NaP}_2\text{H}_2\text{O}_2$ concentration: P content 8.25, 7.5, 5.75

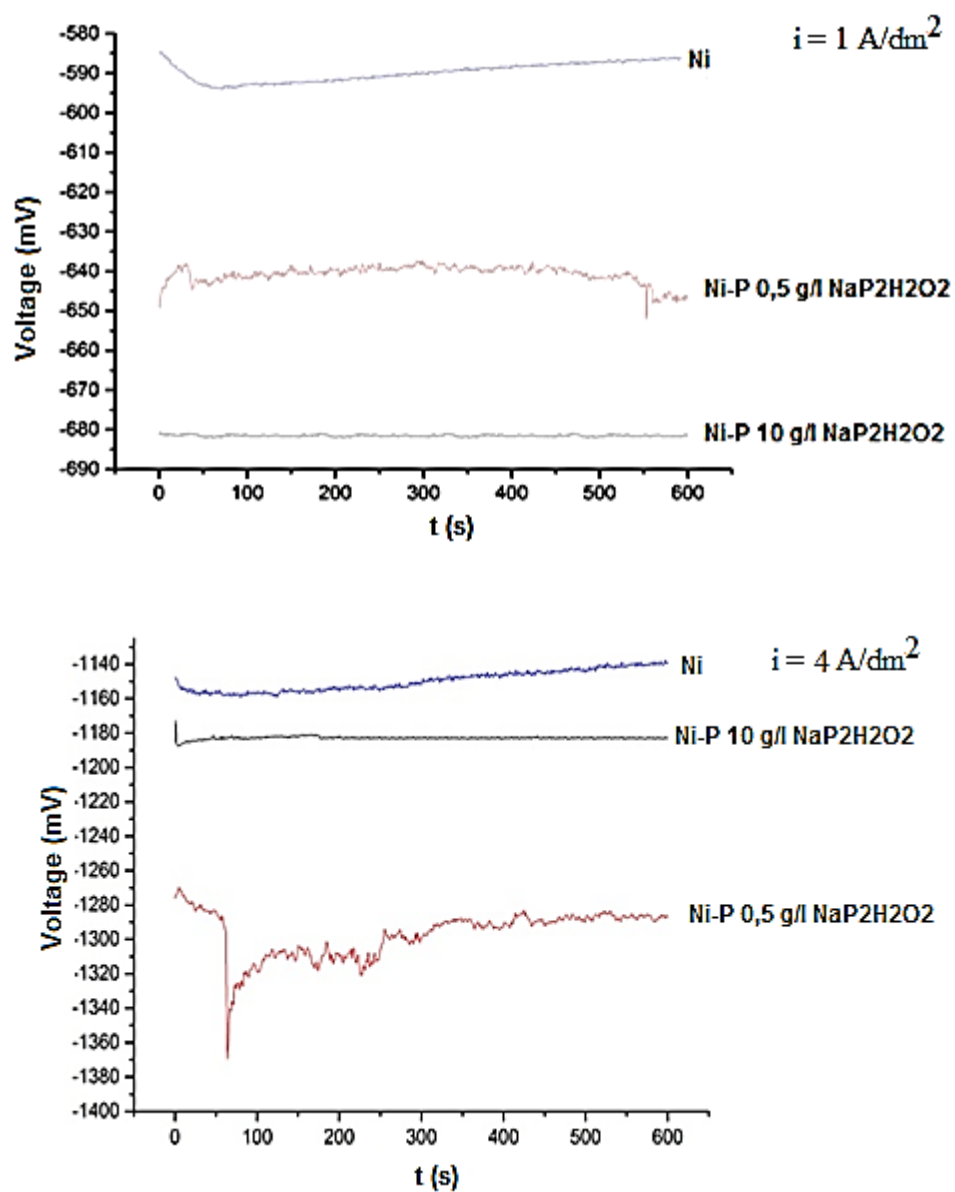
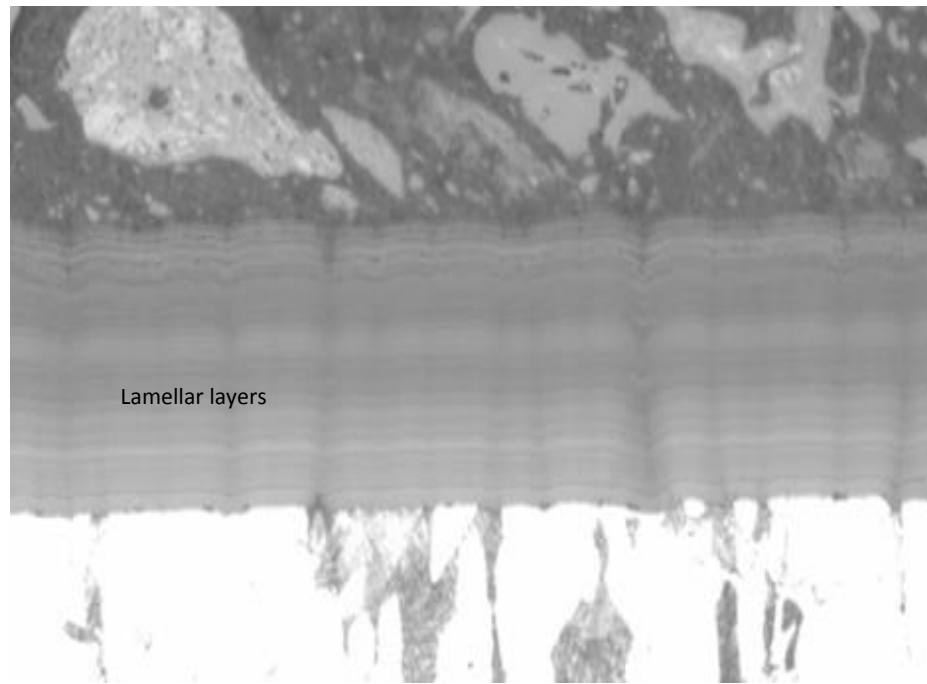
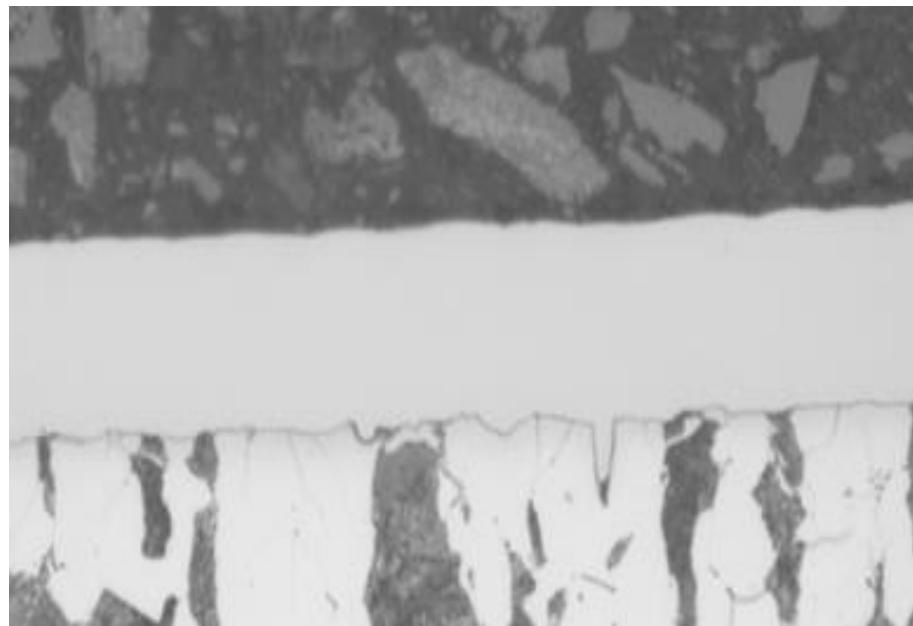


Figure 4.39 Effect of Lamellar layers in Ni-P on the potential during deposition



Ni-P low/medium phosphorous (lamellar)

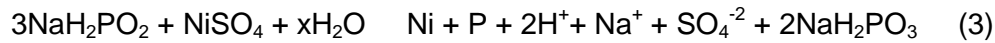
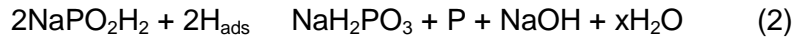
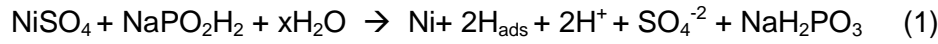


Ni-P high phosphorous (amorphous)

Figure 4.40 Effect of phosphorous content on the microstructure of Ni-P electroplated coating

Elemental mapping confirms an inhomogeneous phosphorus distribution over the cross-section (Figure 4.40). Inserted in this figure, the line scan shows vertical fluctuations of about 10 % of the total P concentration which is also comparable to the mean deviation of the overall matrix composition. It should be noted that the thickness of the lamellas varies between 100 nm and some μm . The micron-sized variations have been observed frequently in electroplated and electroless deposited Ni-P coatings, for exam-

ple in [41] and [165]. According to the deposition mechanism via oxidation of the sodium hypophosphite and reduction of the nickel ions, the incorporation of phosphorus in the deposit depends on the pH, i.e. proton concentration. Therefore, local pH variations cause the variation in the deposit phosphorus content. The fine variations of about 100 nm, which reveal the compositional contrast in Morphology (Figure 4.41).



The deeper insight about such lamellar behaviors has been explained extensively in our publication [138].

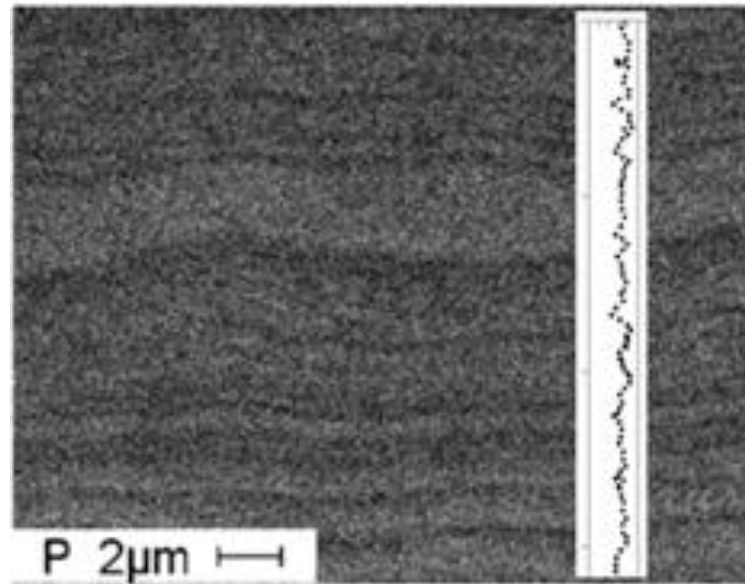


Figure 4.41 Elemental EDX shows phosphorus distributions in the cross-section of Ni-P galvanic coating

4.4.2 Effect of Particles incorporation in Ni-P galvanic coatings

4.4.2.1 Effect of particle size on the layer characteristics and electrodeposition behavior of Ni-P electrodeposited coatings

It was found that adding alumina particles in the plating bath electrodeposited under current density of 4 A/dm² leads to the reduction in crack phenomenon of Ni-P coatings surface (Figure 4.42).

Mizushima et al. [167] have noticed that the microcracks are caused by the relaxation of internal tensile stresses. They suggested that the hydrogen ingress into the deposit occurs during the electrodeposition and its subsequent release creates a high tensile stress which can develop the microcracks in deposit.

In fact when particles are added into the bath, they may absorb hydrogen ions near the cathode, preventing the ions from being reduced to nascent hydrogen. It is noticeable that higher current densities cause more nascent hydrogen to be accumulated at the cathode surface before it is evolved.

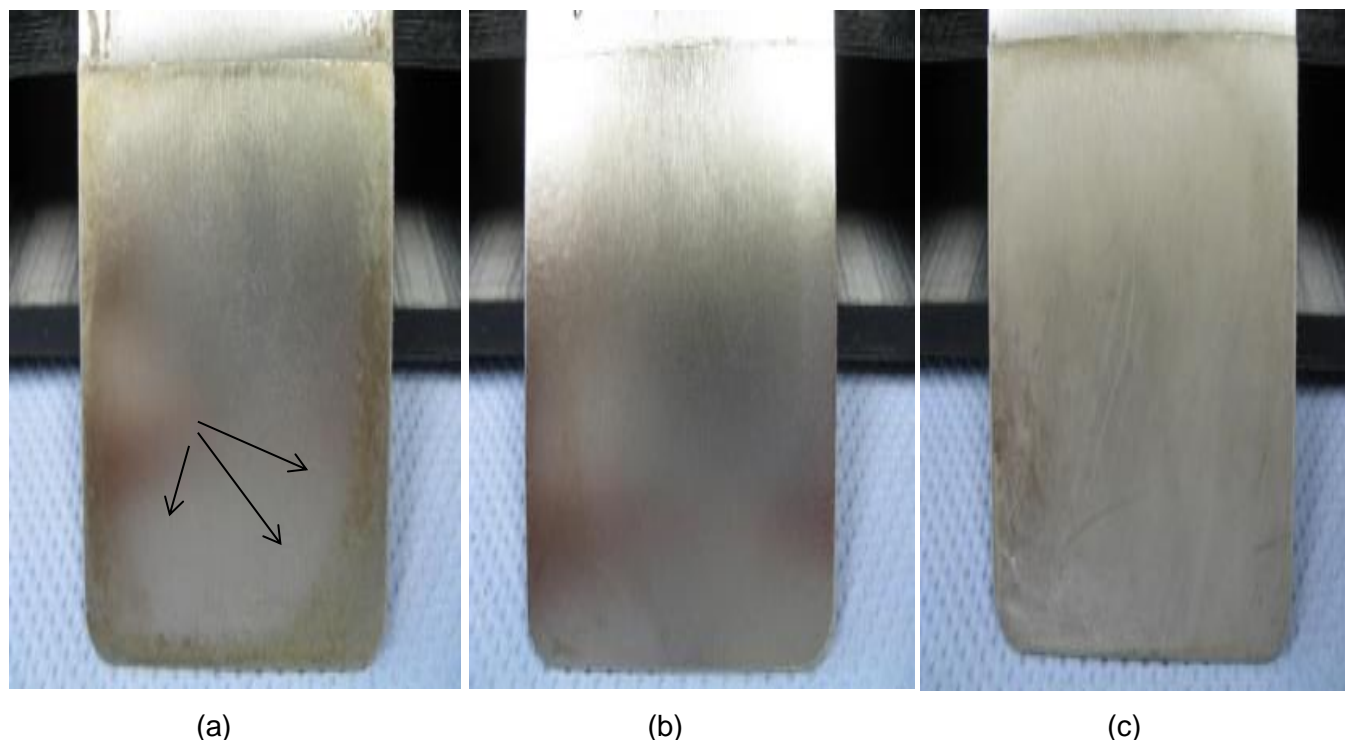


Figure 4.42 Photos from samples Ni-P (a) and Ni-P-Al₂O₃ 13nm (b), 200nm (c) electrodeposited under same working conditions

Additionally, the indirect reaction mechanisms for Ni-P codeposition shows that hydrogen ions absorbed by Al₂O₃ may prevent the reduction of phosphorous acid to phosphorus, lowering the phosphorus content and hence lowering the residual stress and cracks.

The morphology of the Ni-P coatings without particles and with alumina particles of nano and submicron size has been shown in Figure 4.43. All the coatings show a nodular surface structure. They have a light gray color with a luster effect. The morphology of the Ni-P-Al₂O₃ coatings consists of a homogeneous fine globular structure with embedded Al₂O₃ particles appearing as black spots.

The presence of Al₂O₃ in the Ni-P layer affects heterogeneity of the surface and increases the number of boundaries between Ni and other particles in the matrix. It can also be found that surface morphology has changed from a smooth state to a non-smooth state with a nodular appearance. Rezrazi believes that changes in surface morphology depend on phosphorus content in composite coating [168]. The plates with high phosphorous content were found to have smooth and uniform morphology, indicating the amorphous nature. Figure 4.44 provides the SEM micrographs showing the cross-section of the deposit plating at current density of 4 A/dm² at 20 g/l Al₂O₃ 13 nm and 200 nm.

The composite coatings were compact and without cracks, as depicted in surface images (Figure 4.43) and corresponding cross-sectional profiles (Figure 4.44).

It is observed that particles were dispersed homogeneously in the matrix and adding submicron particles lead to higher value of incorporation compared to nanoparticle.

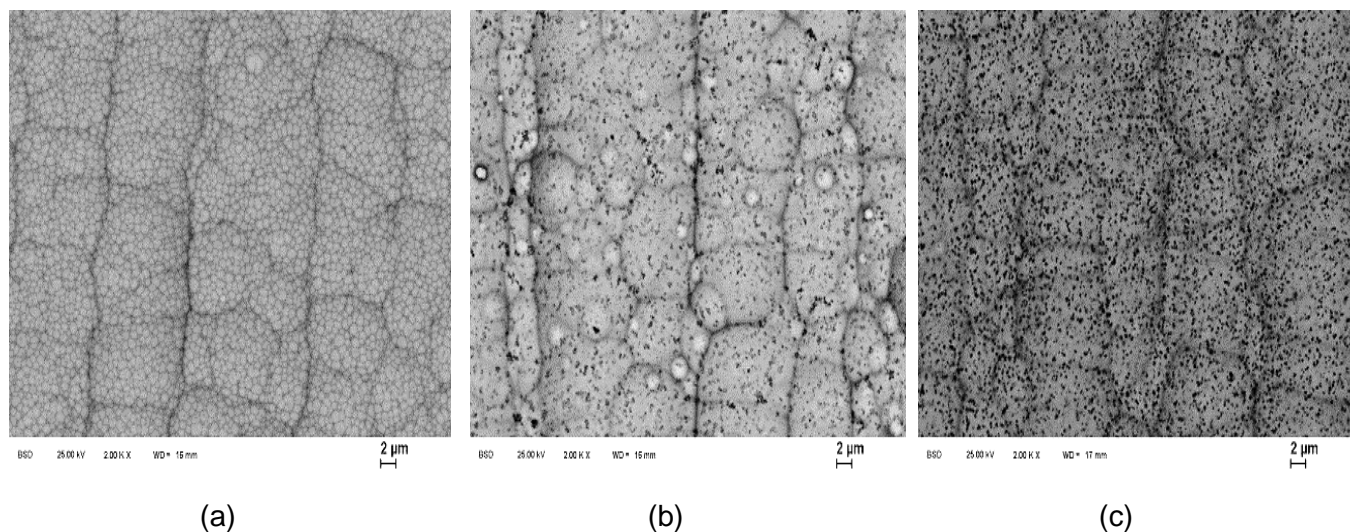


Figure 4.43 Morphology of Ni-P (a) and Ni-P-Al₂O₃ 13 nm (b), 200nm (c) electrodeposited under same working conditions

It is seen that under the same working conditions adding submicron particles into the electrolyte lead to a large difference in the incorporation value compared to nanoparticles, about 7 times as it was detected by EDX in Figure 4.45. On the other hand, P content in the coating with submicron particles decline more than the coating electrodeposited with nanoparticles (Figure 4.45).

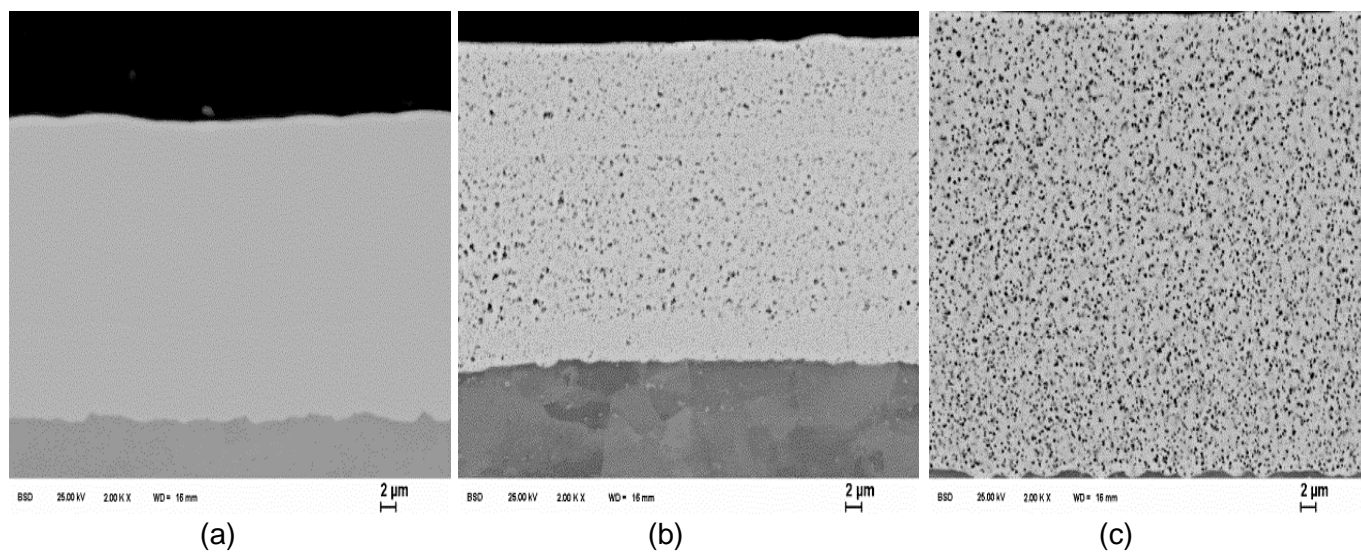


Figure 4.44 Cross section SEM images of Ni-P (a) and Ni-P-Al₂O₃ 13 nm (b), 200 nm (c) electrodeposited under same working conditions

It is apparent that the observed decrease of P content in the alloy matrix attributes to the presence of Al_2O_3 particles. It is known that in plating bath operating at low pH values, an increased amount of protons are adsorbed on Al_2O_3 particles [170,172,173] and consequently, results in increased hydrogen evolution. Therefore, Al_2O_3 particles catalyze hydrogen evolution by changing the reduction paths during Ni-P electrodeposition [131] through the enhancement of molecular hydrogen against nascent hydrogen production [129, 130, 138]. According to the indirect reaction mechanism for Ni-P codeposition nascent hydrogen is necessary for the reduction of phosphorus source to phosphine [38]. Thus, the presence of Al_2O_3 particles could reduce the P content in the deposit by restriction of phosphine production.

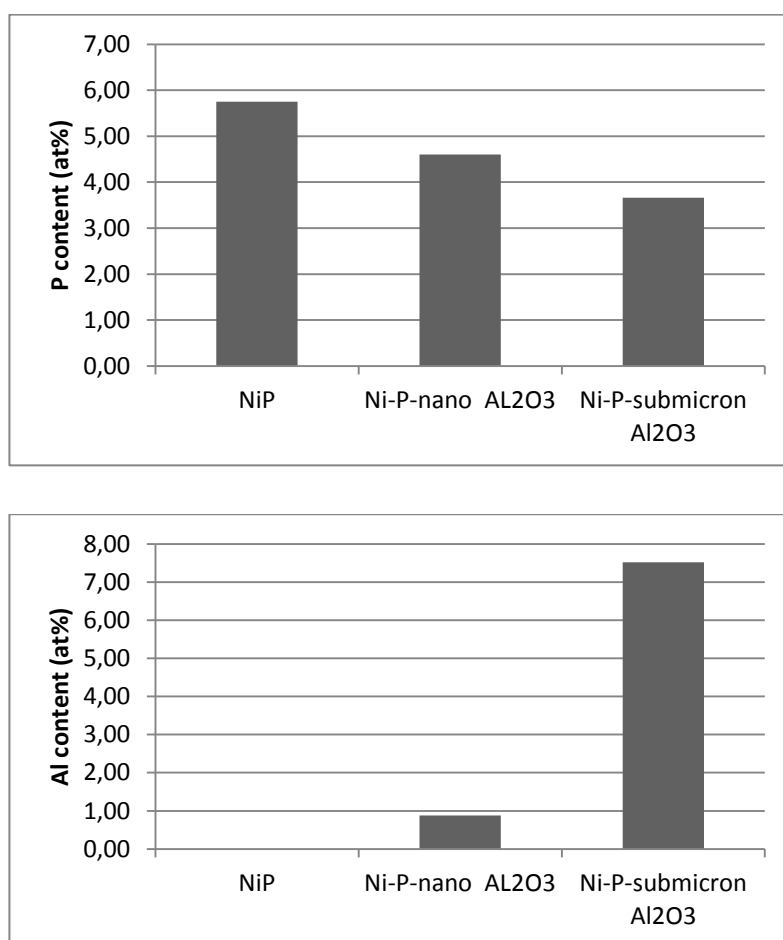


Figure 4.45 EDX results from P content and particle incorporation in Ni-P composite coatings electrodeposited with nano and submicron particles

As it is seen from the thickness results in Figure 4.46, the thickness of Ni-P coatings increase with adding particles into the electrolyte. The coating electrodeposited with submicron particles was even higher than the one deposited with nanoparticles. It is understandable that by adding particles, hydrogen ions absorbed by Al_2O_3 , prevent the reduction of phosphorous acid to phosphorus and, according to the indirect mechanism of Ni-P formation, lead to a lowering in phosphorus content. As already discussed the microstructure of Ni-P is directly dependent on P content. In other words, at lower P content, the micro-

structure is more crystalline and there is more possibility for growth of the Ni grains. Therefore, the thickness of layer would be larger than the coating with higher P content and would rather have an amorphous structure.

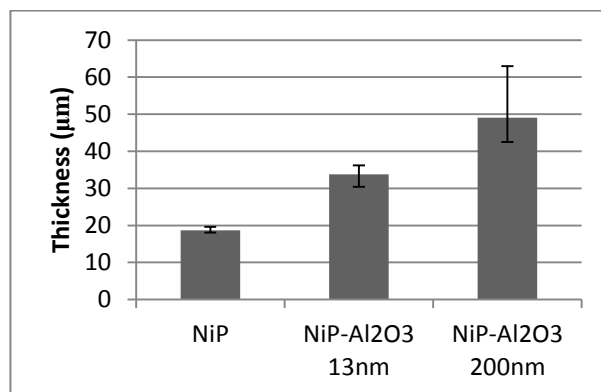


Figure 4.46 Thickness results of Ni-P and Ni-P-Al₂O₃ with nano and submicron particles electrodeposited under same working conditions

According to the XRD results in Figure 4.47, the internal stress in the Ni-P coatings before and after adding particles after annealing and crystallization were measured. It was seen that adding particles in both cases leads to a decline in internal stress, and for submicron particles even the internal stress is 5 times less than Ni-P without particles. There can be two reasons for the decreasing in internal stress in Ni-P composite coatings. Firstly, the main reason for formation of cracks and stress in Ni-P coatings especially in higher current densities initiates from hydrogen evolution during electrodeposition process. Therefore adding particles itself in the electrolyte, adsorbed the hydrogen ions around themselves in which the amount of this adsorption depends on the characteristics of particles like size, concentration and also their zeta potential in the electrolyte. Secondly, like Ni composites incorporation of particles in the matrix hinders the dislocations movement according to Orowan's mechanism and declines the stress in the matrix. In this case, size and incorporation value are the most important factors influencing on the residual stress of Ni-P coatings. The latter effect is attributable to formation of structural defects that inhibit postelectrolysis relaxation, which in turn induces volume changes in the deposit and prevents propagation of the brittle cracks. This hypothesis was confirmed by XRD analysis, which revealed the changes in the microstress conditions of the Ni-P matrix following particle incorporation.

In the EBSD images in Figure 4.48 a) and b) from the Ni-Al₂O₃ composite coatings with nano- and submicron particles the distribution of particles in the matrix are clearly observed. Despite of annealing and recrystallization, the size of incorporated particles is a lot larger than the size of Ni or Ni₃P grains. There is no reliable evidence for crystallinity as the Confidence index (CI) must be greater than 0.1. It can be concluded that the dispersion hardening plays almost no role on the strengthening mechanism of Ni-P

composite coatings. However, the hardness of ceramic particles itself as a hardening phase can intervene the strengthening of the deposit.

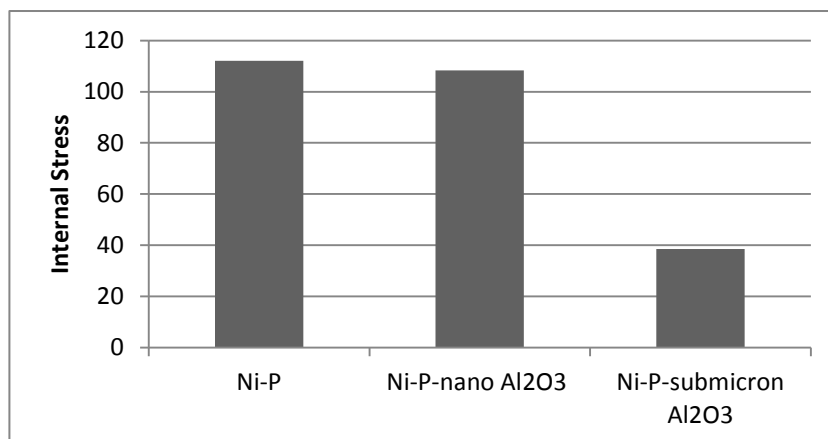
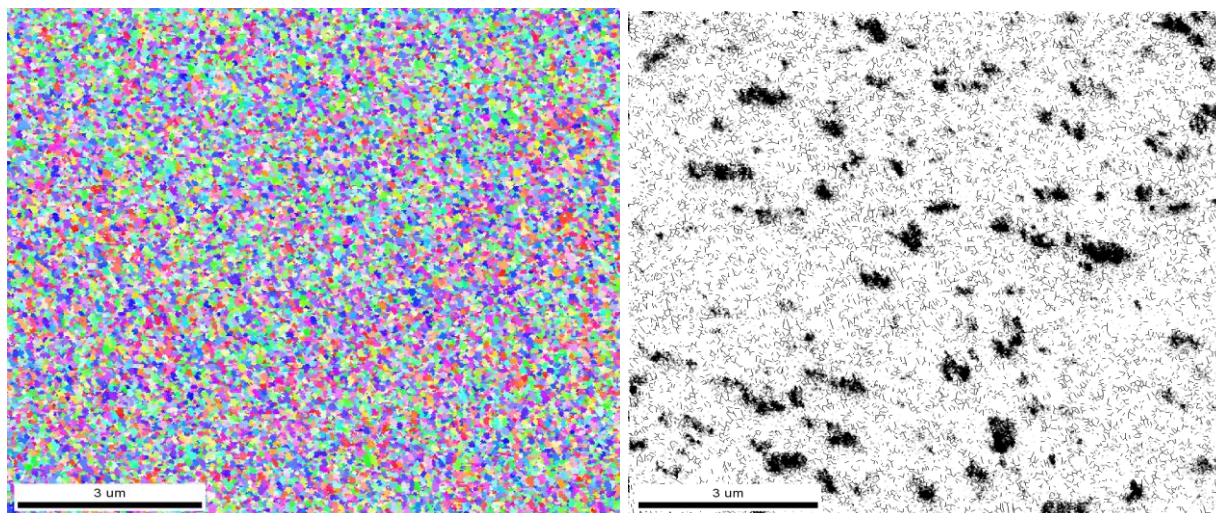
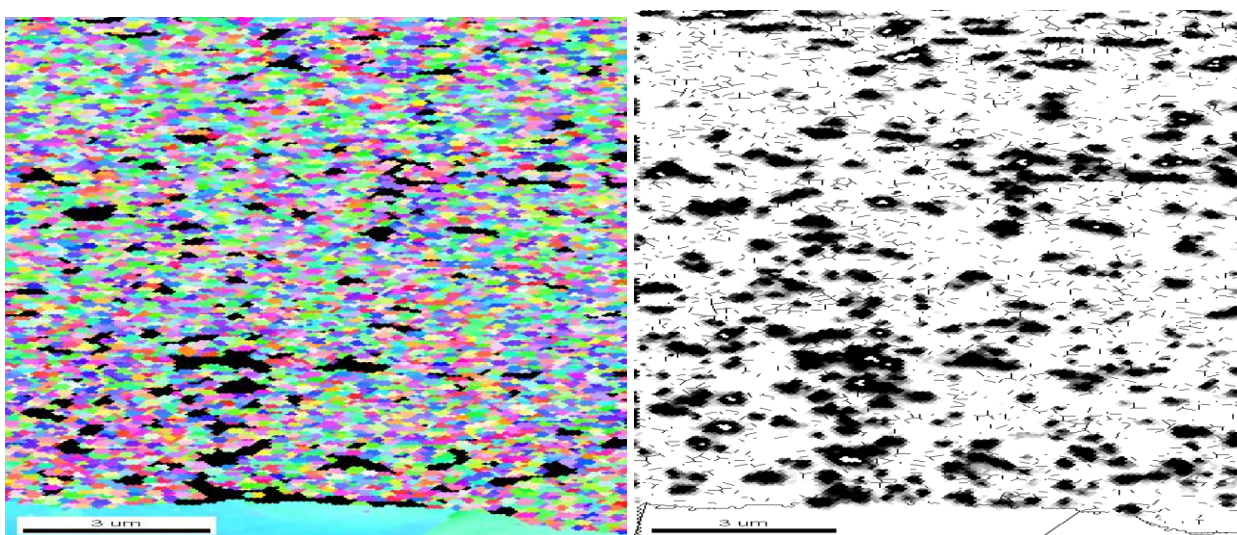


Figure 4.47 Internal stress of Ni-P and Ni-P-Al₂O₃ electrodeposited with nano and submicron particles measured by XRD



Ni-P-nano Al_2O_3



Ni-P-submicron Al_2O_3

Figure 4.48 EBSD images of Ni-P-nano Al_2O_3 and Ni-submicron Al_2O_3 composite coatings

Figure 4.49 shows the results of Martens test for Ni-P and Ni-P- Al_2O_3 composite coatings electrodeposited under the same conditions for both nano and submicron particles size. As it is seen, when particles are added into the electrolyte the Martens hardness decreased compared to Ni-P without particles. As already explained in the literature reviews, the hardening and softening of the as-plated Ni-P alloys according to phosphorous content generally involves supersaturated solid solution strengthening, Hall-Petch relationship, dispersion hardening as well as the inverse Hall-Petch relationship. Here the P content of Ni-P and Ni-P- Al_2O_3 composite coatings both are less than 7 wt. % and the microstructure of the deposits contain the mixture of nanocrystalline and amorphous. Despite the effect of supersaturated solid solution strengthening due to the existence of phosphorous, the Ni grain size would be also finer by increasing P content. Therefore, according to Hall-Petch law the hardness should be higher. Moreover,

the influence of dispersion hardening due to the existence of nanocrystalline phase in the amorphous matrix is higher. As mentioned before, adding particles leads to a phosphorous reduction in Ni-P coatings and, therefore, in the as-plated coatings with particles the hardness would be less than pure Ni-P without particles. On the other hand, it is seen that although adding particles lead to a decline in microhardness for as-plated Ni-P coatings, but the hardness of coating includes submicron particles is higher than the coating including nanoparticles electrodeposited under the same working condition and the same amount of particles concentration in the electrolyte. In fact, this can be related to the effect of incorporation value and distribution of particles in the Ni-P matrix, and finally, hindering the movement of dislocations by means of P. After annealing at 400°C, the deposits exhibited enhanced values of microhardness compared to the corresponding values of the as-plated form, as shown in Figure 49 a) and b). This increase in microhardness is caused due to the crystallization of amorphous phase of Ni-P matrix and especially due to the precipitation of hard intermetallic compounds of Ni₃P and Ni₂P [38, 85]. For the majority of composites, an explicit dependence of the microhardness values against the applied plating conditions after thermal treatment was not evident. This could be attributed to the fact that probably the precipitation hardening mechanism overlaps the Al₂O₃ particle hardening effect, and thus the hardness of composite coatings does not directly depend on the codeposition percentage of particles.

“Strengthening by annealing” phenomenon has been reported for metals produced by electrodeposition [63,175] and severe plastic deformation [174]. Wang et al. [175] suggested that the relaxation at nonequilibrium grain boundaries on annealing makes it more difficult for them to dislocate. Upon annealing, the grain boundaries turn into well-defined high angle boundaries and interior defect density is also decreased significantly.

In addition, phosphorus was found to segregate to the boundaries. Therefore, it can be argued that the increase in the hardness and the Hall-Petch slope upon annealing is a consequence of grain boundary relaxation, phosphorus segregation and reduction of interior defects. The strengthening may also result partly from an increase of density owing to the degassing of hydrogen. The addition of phosphorus in Ni has a direct contribution to its strength on increasing the frictional stress, refining grain size and segregation to grain boundaries.

All coatings were transformed to a polycrystalline Ni/Ni₃P alloy by heat treatment. The fraction of Ni₃P/Ni and the mean crystallite size of the Ni₃P and Ni crystals have been derived from XRD and are summarized in Table 2.

Phosphorus	Ni ₃ P/Ni fraction	Mean crystallite size Ni ₃ P [nm]	Mean crystallite size Ni [nm]
Ni-P	0.66	85	75
Ni-P-nano Al ₂ O ₃	0.59	44	61
Ni-P-submicron Al ₂ O ₃	0.54	50	67

Table 4.2 Crystalline phase fractions and grain sizes of the composites after heat-treatment

There is a good understanding of how to modify mechanical properties of Ni-P and Ni/Ni₃P coatings via microstructure evolution and phase formation during deposition and annealing by variation of their P content [95]. Consequently, dispersion and precipitation hardening due to the formation of the Ni₃P phase in the matrix determine the properties of the annealed medium phosphorus composite coatings. This was similarly observed for the Ni-P composite coatings in this study. The incorporated particles in their agglomerated form are about four times larger compared to the mean matrix grain size. Therefore, their contribution to the dispersion hardening of the composite is limited (Table 4.2). Remarkably, the microhardness of the annealed composite coatings remains higher than Ni-P without particles but higher phosphorous content. This can be related to the particle incorporation in the matrix, which inhibits the coarsening of the Ni₃P crystals during annealing. Thus, the improved hardness of the composites is a result of the nano-grained microstructure of the matrix accompanied by the high fraction of reinforcing hard particles.

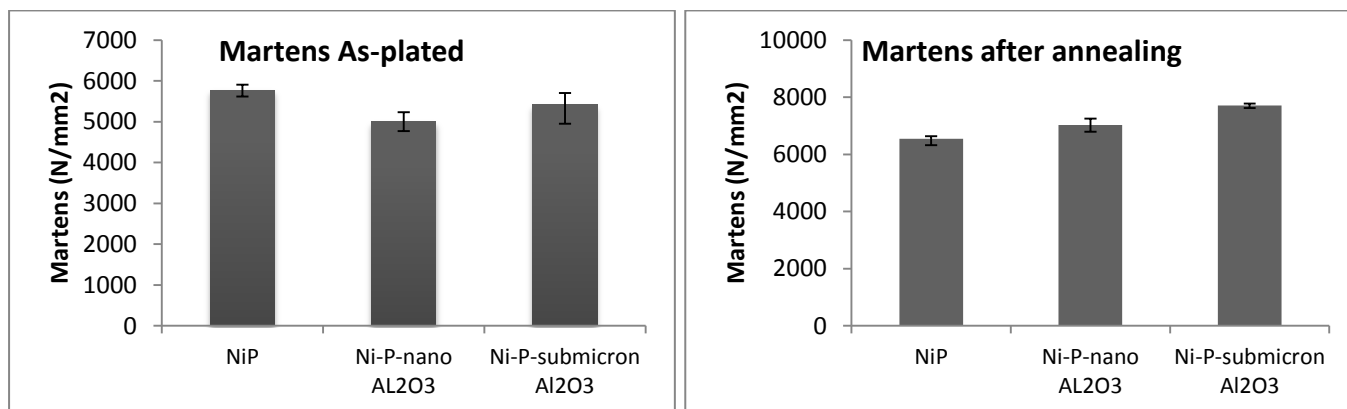


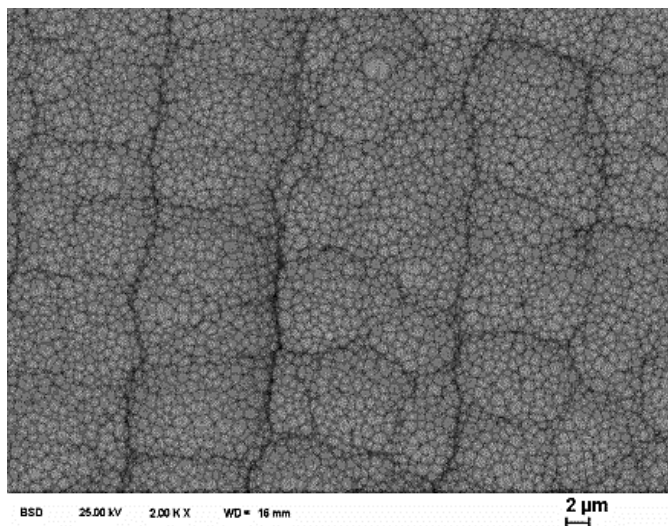
Figure 4.49 Martens results of Ni-P, Ni-P-nano Al₂O₃ and Ni-P-submicron Al₂O₃ composite coatings as-deposited and after annealing at 400 °C, 1 hr.

4.4.2.2 Effect of particle type on the layer characteristics and electrodeposition behavior of Ni-P electrodeposited coatings

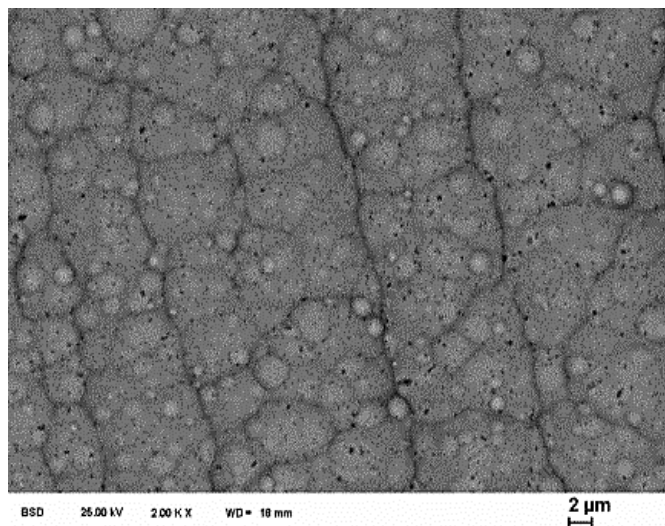
Adding each three types of particles Al_2O_3 , SiC and TiO_2 into Ni-P bath also conducted to Ni-P composite coatings without cracks. As already mentioned the reason here is related to prevention of the ions from being reduced to nascent hydrogen due to adding particles into the electrolyte.

From morphological SEM images in Figure 4.50, it is seen that Ni-P coating shows a cauliflower-like morphology while embedded particles on the matrix of deposited shows a homogeneous finer global structure.

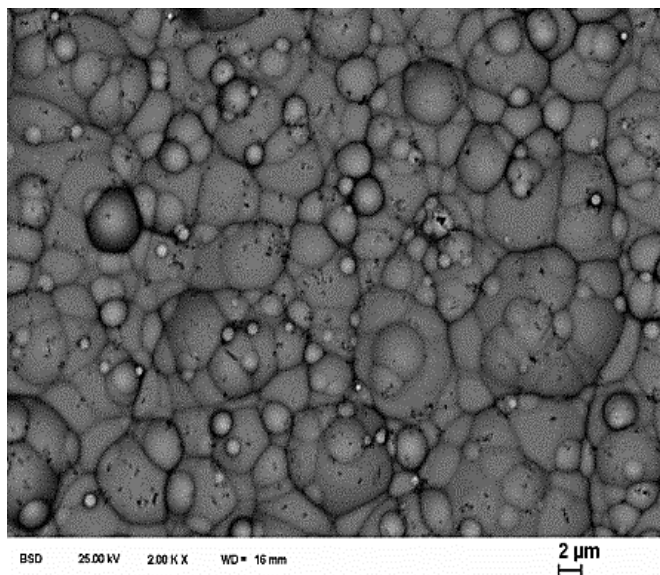
The surface distribution of Ni-P composite coating layers is virtually homogeneous which is due to a molecular mixing of the amorphous nickel matrix with the particles (Figure 4.51). The incorporation value and distribution of different particle type in Ni-P matrix are illustrated clearly in cross-section SEM images. As it is seen the accumulation of TiO_2 particles in electrodeposited Ni-P seems to be much higher than Al_2O_3 or SiC particles under the same working condition.



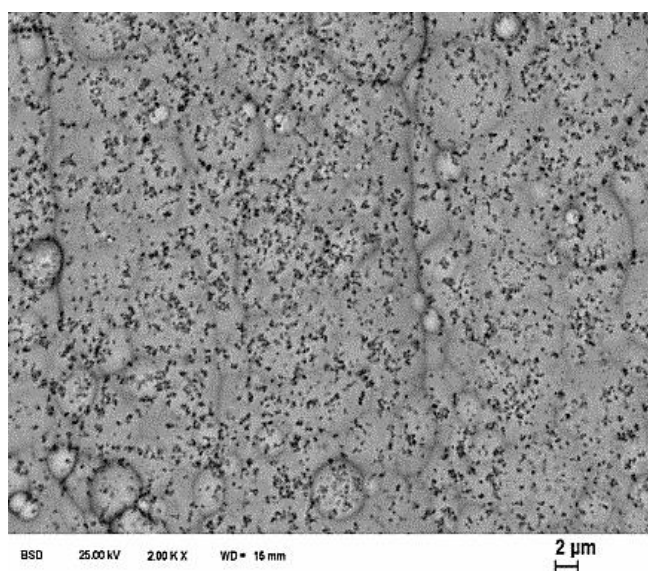
Ni-P



Ni-P-Al₂O₃



Ni-P-SiC



Ni-P-TiO₂

Figure 4.50 Morphology SEM images of Ni-P deposit and Ni-P composite coatings electrodeposited with different particle types under same working conditions

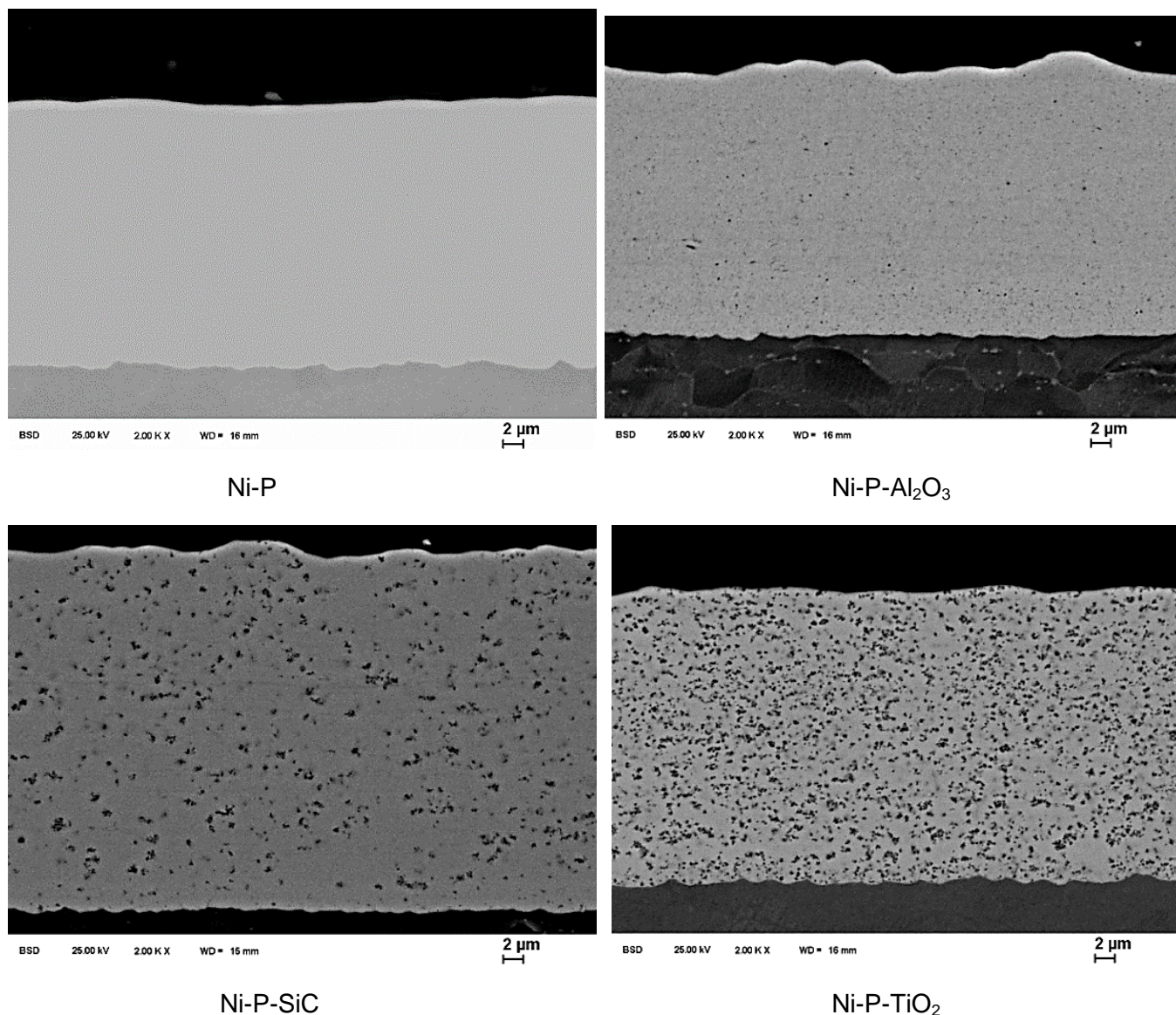


Figure 4.51 SEM images from cross-section of Ni-P deposit and Ni-P composite coatings electrodeposited with different particle types under same working conditions

Figure 4.52 a) and b) show the content of incorporated Al₂O₃ particles and P content in the Ni-P composite coatings as a function of the particle type detected by EDX analysis. Under the same working conditions and same concentration of particles in the electrolyte, the incorporation value for the coating with TiO₂ is approximately two times more than the coatings electrodeposited with SiC and Al₂O₃.

Adding all type of particles leads to a decline in P content of deposits. It is apparent that the observed decrease of P content in the alloy matrix attributes to the presence of particles. It is known that in nickel plating baths operating at low pH values, an increased amount of protons are adsorbed on particles [48, 171,172] and consequently, results in increased hydrogen evolution.

Therefore, particles catalyze hydrogen evolution by changing the reduction paths during Ni-P electrodeposition [129] through the enhancement of molecular hydrogen against nascent hydrogen production [67, 129,130]. According to the indirect reaction mechanism for Ni-P codeposition nascent hydrogen is

necessary for the reduction of phosphorus source to phosphine [38]. According to the results, it seems that the value of particle incorporation between different particle types has no significant influence on declining of P content. By the way, by adding particles there is more possibility for growth of the Ni grains and therefore the thickness of layer would be larger than the Ni-P coating without particle and rather amorphous structure (Figure 4.53). In other words, current efficiency of Ni-P electrodeposition increases by adding particles which leads to thicker layer under the same working conditions. As already discussed, this relates to the adsorption of producing hydrogen on the particles. There is less possibility for hydrogen ions to hinder the deposition process on the cathodic surface. Therefore, it is understandable that the higher value of thickness relates to the Ni-P coating with TiO_2 particles and the highest amount of incorporated value compared to Ni-P- Al_2O_3 and Ni-P-SiC with lower amount of codeposited particles.

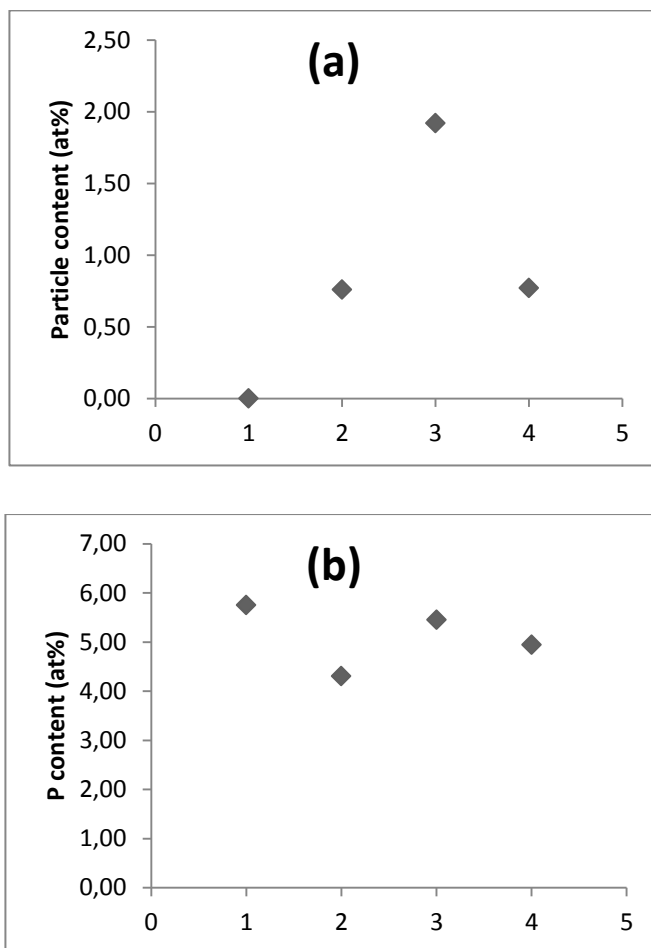


Figure 4.52 EDX results of Ni-P deposit and Ni-P composite coatings electrodeposited with different particle types under same working conditions: (a) particle content (b) phosphorous content

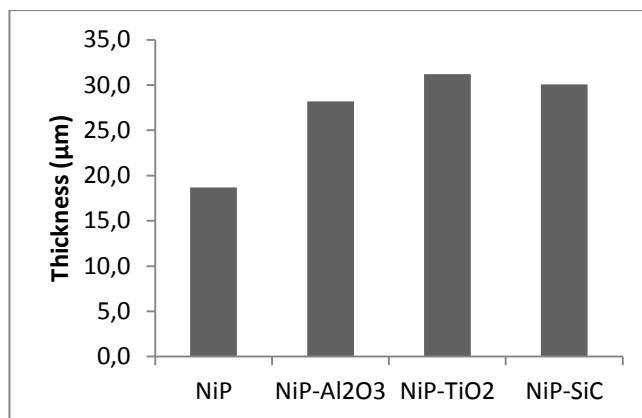


Figure 4.53 Thickness of Ni-P deposit and Ni-P composite coatings electrodeposited with different particle types under same working conditions at current density of 4 A/dm²

According to results of internal stress in Figure 4.54, it was seen that adding TiO₂ particles leads to an incredible decline in residual stress of Ni-P coating after annealing, while by adding the same amount of Al₂O₃ or SiC into Ni-P electrolyte, the internal stress did not show a difference. As already mentioned, incorporation of particles in the matrix hinders the dislocations movement according to Orowan's mechanism and declines the stress in the matrix by inducing volume changes in the deposit, and prevents propagation of the brittle cracks. In this case, the incorporation values are the most important factors influencing on the residual stress of Ni-P coatings. This is in agreement with EDX data in which incorporated amount of TiO₂ particles was almost two times more than Al₂O₃ or SiC. Meanwhile, adding all types of particles lead to as-deposited Ni-P coatings without crack formation which relates to adsorption of the hydrogen ions around particles in which the amount of adsorption depends on the characteristics of particles like size, concentration and also their zeta potential in the electrolyte.

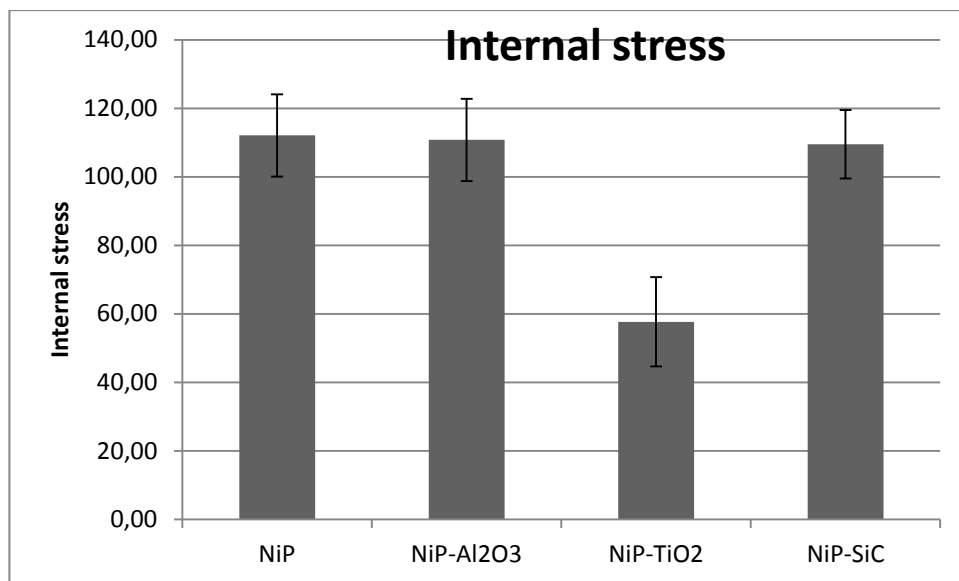


Figure 4.54 Effect of different particle type on the residual stress of Ni-P electrodeposited coating, measured with XRD technique after annealing

Figure 4.55 show the EBSD images of Ni-P composite coatings with different particle type electrodeposited under the same working conditions after annealing. Although the grain boundaries are about to reconstruct due to the annealing, but the quality map does not reveal grain boundaries perfectly. In fact, some grains are lying upon each other thus contributing to mixed TKD patterns. Therefore, the confidence of the pattern indexing is reduced and only single large grains can be detected with a reasonable confidence. Such grains are shown in the Ni orientation map filtered with a confidence index $CI > 0.1$, commonly accepted for cubic structures. As it is observed, none of the three types of coatings show a specific preferred texture. Despite of annealing and recrystallization, the size of incorporated particles is a lot larger than the size of Ni or Ni₃P grains. Therefore, it can be concluded that the dispersion hardening plays almost no role on the strengthening mechanism of Ni-P composite coatings. However, the hardness of ceramic particles itself as a hardening phase can intervene the strengthening of the deposit.

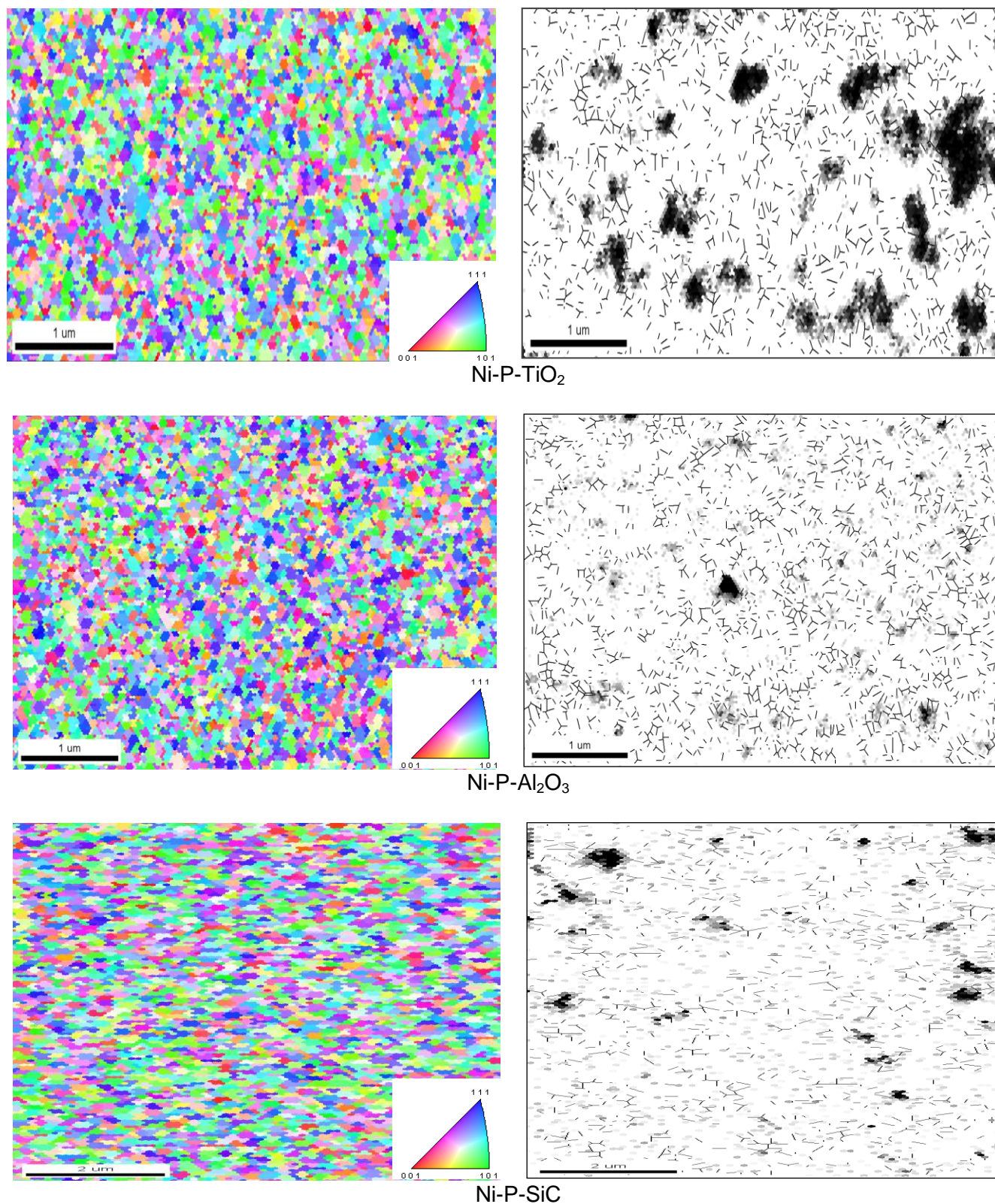


Figure 4.55 EBSD images of Ni-P deposit and Ni-P composite coatings electrodeposited with different particle types under same working conditions

Figure 4.56 shows the results of Martens test for Ni-P and Ni-P composite coatings electrodeposited with SiC, Al₂O₃ and TiO₂ nanoparticles within almost the same particle size of 50nm. As it is seen, when par-

ticles are added into the electrolyte the Martens hardness decreased compared to Ni-P without particles. As already explained, the phosphorous content is the main reason to influence the hardening and softening of the as-plated Ni-P composite which generally involves supersaturated solid solution strengthening and Hall-Petch mechanism. The effect of dispersion hardening due to the incorporation of particles has no significant effect on the hardening of Ni-P matrix, unless the hardening nature of particles itself can improve the hardness of as deposited coating slightly. As mentioned before, adding particles leads to the phosphorous reduction in Ni-P coatings and therefore here in the as-plated coatings with particles the hardness would be less than pure Ni-P without particles. As it is seen in the results for Ni-P-SiC, regardless of the incorporation value a higher value in the Martens results compared to the coatings deposited with TiO_2 or Al_2O_3 is shown, which can relate to the higher hardness of SiC particles compared to Al_2O_3 or TiO_2 .

After annealing, the grain boundaries turn into well-defined high angle boundaries and interior defect density is also decreased significantly. In addition, phosphorus was found to segregate to the boundaries. Therefore, it can be argued that the increase in the hardness and the Hall-Petch slope upon annealing is a consequence of grain boundary relaxation, phosphorus segregation and reduction of interior defects. The strengthening may also result partly from an increase of density owing to the degassing of hydrogen. The addition of phosphorus in Ni has a direct contribution to its strength on increasing the frictional stress, refining grain size and segregation to grain boundaries. Consequently, dispersion and precipitation hardening due to the formation of the Ni_3P phase in the matrix determine the properties of the annealed medium phosphorus composite coatings. This was similarly observed for the Ni-P composite coatings in this study. Figure 4.57 shows the grain size of Ni and Ni_3P phase after annealing by means of XRD. The incorporated particles are still much larger compared to the mean matrix grain size, and therefore their contribution to the dispersion hardening of the composite is limited. Remarkably, the microhardness of the annealed high-phosphorus composite coatings remains high, which is usually not observed in high phosphorus Ni/ Ni_3P coatings. This can be related to the particle incorporation in the matrix, which inhibits the coarsening of the Ni_3P crystals during annealing. Thus, the improved hardness of the high-phosphorus composites is a result of the nano-grained microstructure of the matrix accompanied by the high fraction of reinforcing hard particles.

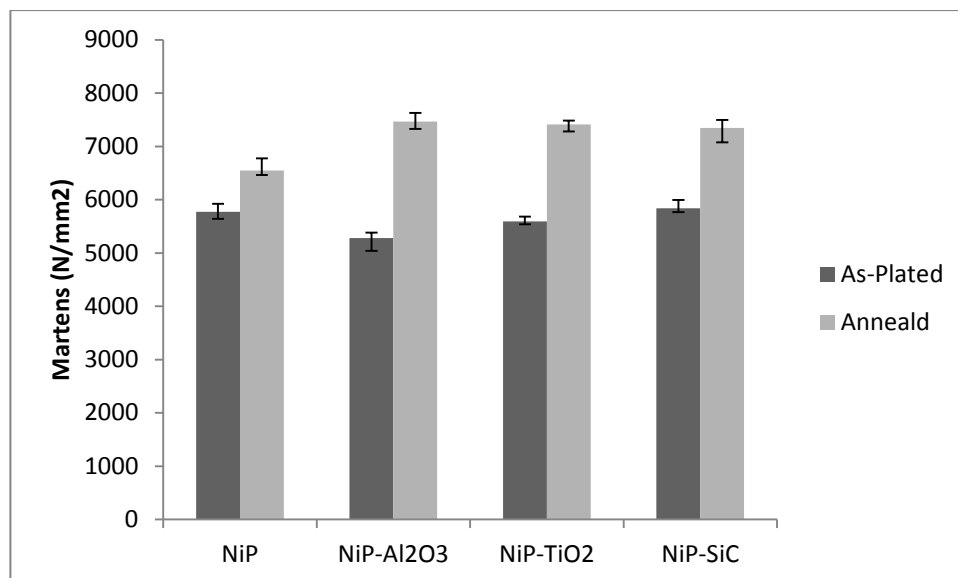


Figure 4.56 Martens test results for Ni-P deposit and Ni-P composite coatings electrodeposited with different particle types under same working conditions

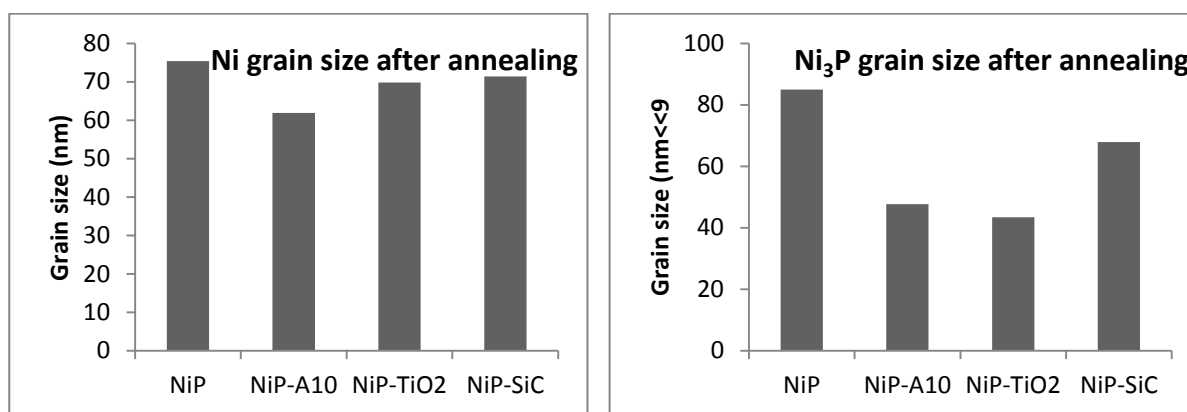


Figure 4.57 Ni and Ni₃P grain size after annealing for Ni-P and Ni-P composite coating electrodeposited with different particle types

4.4.2.3 EIS study of Ni-P composite coatings

Figures 4.58 and 4.59 show the Nyquist plots from electrochemical impedance spectroscopy results during the electrodeposition process for Ni-P and Ni-P-Al₂O₃ with particle nano- and submicron particles and different particle types with the same grain size under the same deposition conditions. The impedance data seems to comprise of a single capacitance loop in high and medium frequencies and also a scattering in low frequencies. As traces of PH₃ and H₂ gas are generated in the Ni-P codeposition process, low frequency scatter occurs.

The effects of particles on the impedance results do not obey a logical trend but it seems that the changes in Nyquist semicircle relates to the change in the phosphorous content of deposits rather than

particles existence. Generally, the coating with less P content shows higher resistance or larger Nyquist semicircle. In fact by adding particles into Ni-P electrolyte, the Ni-P reaction rate at the electrode and the number of nucleation active points on the electrode surface also decreases, leading to an increase in the charge transfer resistance. Moreover, according to the achieved results and also based on the dominating effect of P content on the charge transfer, it is difficult to judge about the exact influence of particle characteristics on the electrodeposition behavior of Ni-P galvanic coatings. In fact, this is the difference in P content by adding particles which changes the impedance charge transfer (as seen Figure 4.59).

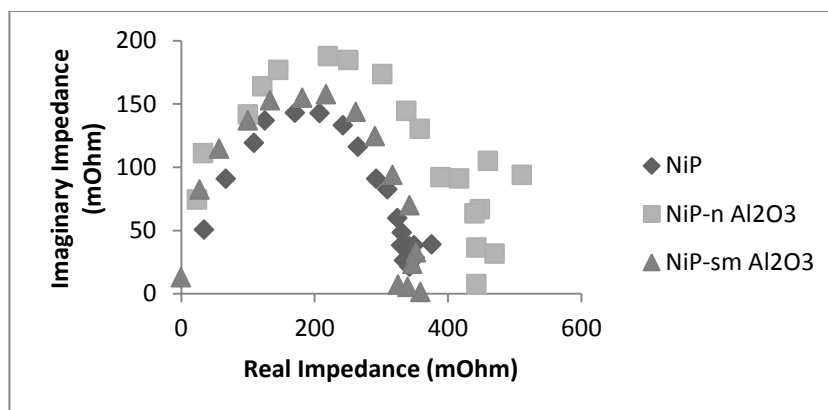


Figure 4.58 Particle size effect on the EIS results of Ni-P electrodeposition

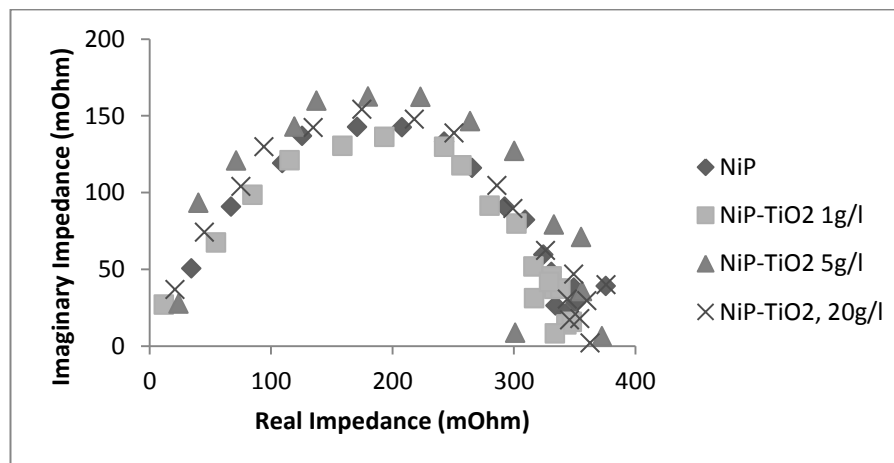
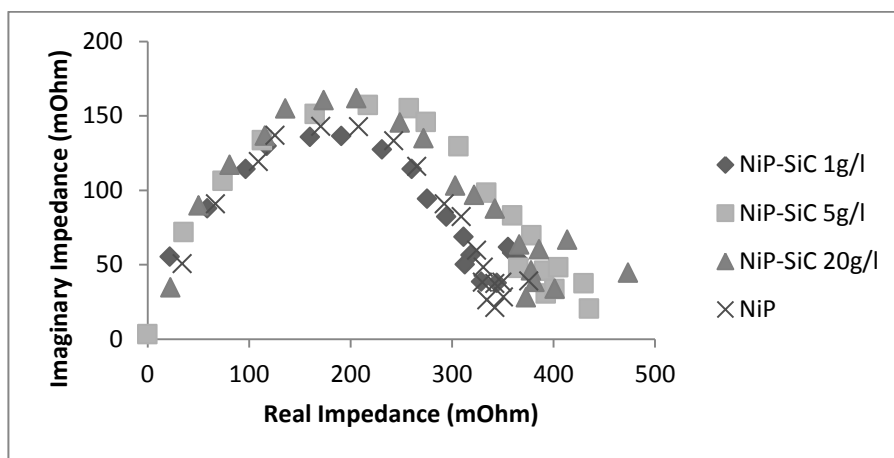
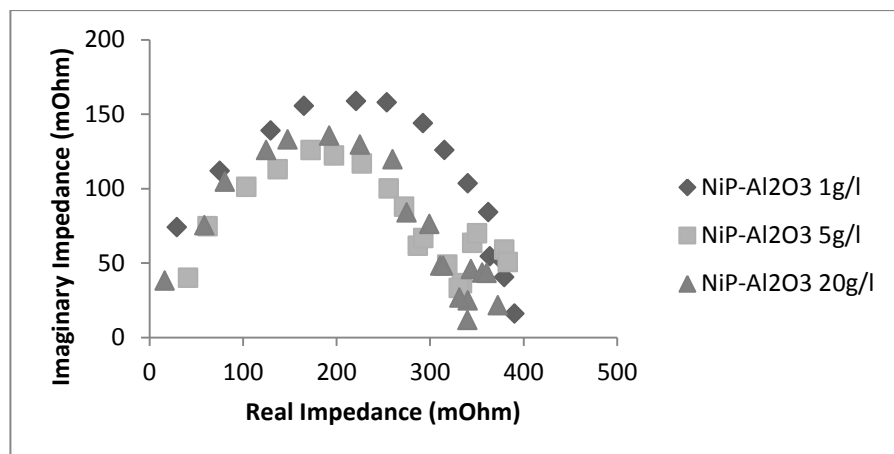


Figure 4.59 Particle type effect on the EIS results of Ni-P electrodeposition

5 Conclusions and Suggested Future Work

5.1 Conclusions

One aim of this work was to substantiate and confirm the past theoretical and semi-empirical suggested models on the electrodeposition mechanism by the help of more empirical results including the characteristics of the layer and in-situ impedance study of the electrocodeposition process. The influence of particle characteristics including type, size and concentration were investigated on the codeposition behavior of Ni-based coatings by the aid of impedance spectroscopy. It was then attempted to correlate the electrochemical behavior (double layer characteristics) with microstructure features and performance of coatings. Finally, the evolution and strengthening mechanisms of electrodeposited Ni-based composite coatings affected by the characteristics of difference reinforcements and matrix was discussed in the results.

In the following section, the key results obtained in this work, which were discussed in detail in the previous sections, will now be summarized. Suggestions for future work are also given at the end of this chapter.

5.1.1 The Electrodeposition of Nickel from Watts electrolyte

The influence of current density on the layer characteristics of Ni electrodeposits including thickness, microstructure, morphology and texture and grain size was investigated. Interestingly, Ni coating electrodeposited at current density of 2 A/dm² showed the higher intensity of (3 1 1) orientation compared to the coatings electrodeposited at 1 and 4 A/dm². Moreover, the coating electrodeposited at this current density showed the lowest grain size among other coatings. The Martens hardness showed an increasing trend with increasing current density from 1 to 2 A/dm². In fact the plating rate rises and therefore nucleation rate of Ni is faster which leads to growth impediment of Ni crystals and finally finer grains and higher strengthening due to the Hall-Petch mechanism [145-147]. By further increase of current density to 4 A/dm², the limited supply of Ni ions to the cathode leads to the formation of a depletion layer of Ni ions near the cathode surface: the so-called mass-transport limitation. Any incoming Ni ions will be captured by outgrowing microstructures, leaving behind pores and gaps in the film. The deposited layer is porous, rough and possesses a tensile residual stress as shown in SEM images from morphology of Ni electrodeposited coatings at different current densities. According to results of impedance investigation, the increase in current density leads to a decline in charge transfer resistance, which behaves reciprocally to the current density. The charge transfer resistance and the cathode double layer are inversely proportional to the current density. These results lead to an interesting prediction concerning the system's behavior under high polarization. In fact, increasing current density leads to an increase in nucleation rate and an increase in current efficiency and rate of cathodic deposition.

5.1.2 The effect of particle size on electrodeposition behavior and features of Ni layer

In order to show the effect of particle size on the electrodeposition behavior of Ni composite coatings, alumina particles with nano- and submicron-size were chosen. Moreover, for the coating electrodeposited with submicron particles, it was obvious that the particles were mainly incorporated within a certain gap from the Ni matrix and growth of nickel around the particle becoming rough. As it was seen in EDX results, under the same conditions, the atomic percentage of Al for submicron particles is higher than the coatings prepared with nanoparticles. In addition, in both cases, the incorporation value of particles rises with increasing the loading of particles in the electrolyte. The reduction in grain size of the Ni crystal by adding particles approves the compactness of the coatings as also confirmed by the results of the morphology. The possibility of transferring Ni ions through the particles was higher at 5 g/l concentration such as the value of the thickness at the given concentration is large, namely around 65 μm . Ni coating exhibited a preferential growth on the crystal face (2 0 0), once nano- Al_2O_3 was codeposited, the growth orientation of the Ni/ Al_2O_3 composite coating was changed from crystal face (2 0 0) to (1 1 1) for nanoparticles and remains (2 0 0) for submicron particles, although the relative intensity of both directions increases by adding more particles into Ni matrix. According to Martens test, it was seen that the addition of nanoparticles leads to a higher Martens hardness at each single concentration in contrast to the addition of submicron particles. The Martens hardness can be controlled by dispersion hardening or the amount of dispersed particles embedded in the layer based on the Orowan mechanism [153]. As it could be seen, by increasing the concentration of particles in the electrolyte, the incorporation value for submicron particles will be higher than that of nanoparticles, but, on the other hand, the number of incorporated particles in the case of applying nanoparticles is higher. This means that the possibility of hindering the dislocations in the coating deposited by nanoparticles is higher. Moreover, as it was already seen, the grain size of the nickel matrix is smaller in the case of nanoparticles. This means that the grain size of the matrix, based on the Hall-Petch effect [154], plays an important role in the hardening mechanism of coatings.

According to impedance results, one possible mechanism to explain the codeposition behavior of particles here is the phenomenon proposed by Guglielmi [1]. At the concentration of 20 g/l, the usage of submicron particles caused higher shrinkage in the semicircle of Nyquist spectrums compared to the addition of nanoparticles to the electrolyte. The value of the charge transfer resistance for submicron particles is lower than that of the nanoparticles, and the double layer capacity for larger particles is moderately higher compared to smaller particle sizes. This means that the thickness of the double layer on the cathodic surface is less than that of nanoparticles in the case of adding submicron particles. The deposition of nickel at the higher concentration of 20 g/l arises faster due to the higher charge transfer and double layer capacity. The reason for the decline in the thickness of coatings or for the reduction of the thickness of deposits at the higher particle concentration of 20 g/l, as it is seen in Figure 4.21 (b), can

be partly related to the blocking of the active surface of the cathode due to the accumulation of particles on the surface.

5.1.3 The effect of particle type on electrodeposition behavior and features of Ni layer

However, with the addition of all three particle types in the electrolytic, the borders of the Ni grains become fuzzy and more compact in comparison to pure Ni with no particle, in the case of adding Al_2O_3 , the morphology seems to be even more compact and homogenous compared to the coatings deposited with SiC and TiO_2 under the same working conditions. Under the same working conditions, the incorporation value for TiO_2 was much higher than Al_2O_3 and SiC for the coatings, especially the incorporation value for SiC despite of 20 g/l particle concentration in the electrolyte seemed to be very dispersed and negligible. SiC particles with conductive nature had better opportunity for Ni crystals to grow rather than on Al_2O_3 or TiO_2 particles with rather inert behavior. The highest incorporation value relates to the coatings electrodeposited with TiO_2 particles. Adding SiC particles showed insignificant changes and also the lowest amount of incorporation value compared to Al_2O_3 and TiO_2 . Moreover, it was found that the coatings deposited with Al_2O_3 particles showed finer microstructure at each single concentration compared to the coatings deposited by SiC and TiO_2 . Meanwhile, the relative intensity of (1 1 1) for the composite coatings decreased almost to half of the value compare to Ni. Moreover, there is an improvement in the direction of (2 2 0) observed by adding Al_2O_3 and TiO_2 particles. The highest relative intensity among these three particle types relates to alumina in (1 0 0) and after that TiO_2 and SiC respectively. Under the same working conditions, adding 20 g/l TiO_2 particles reduces the stress to a minimum of approximately 230 N/mm^2 at 4 A/dm^2 . The grain size of nickel might be smaller with high Al_2O_3 -particle content in the electrolyte, so that residual stress of the first order cannot accumulate as much as with TiO_2 . According to EBSD results, Al_2O_3 influenced more intensely on the refining of Ni grains compared to SiC and TiO_2 . Alumina nanoparticles are predominantly incorporated in the grain boundary zone. The different influence on crystal growth by codeposition of semiconducting particles like silicon carbide compared to non-conductive particles like alumina is striking and should be estimated under the aspect of particle conductivity. Otherwise, the incorporation of SiC particles does not change the columnar growth of nickel.

The mechanism of Orowan and dispersion hardening plays a specific role for the coating with TiO_2 particles according to the number of particles and better distribution. On the other hand, accumulation of SiC particles has a lower effect on the hindrance of dislocations. Moreover, the dominating mechanism of strengthening in Ni- Al_2O_3 composite coatings is mainly due to the Hall-Petch effect and grain refining rather than particles incorporation and Orowan mechanism.

According to EIS results and correlation with layer characterization, two factors of particle type and concentration can influence on the behavior and value of charge transfer resistance.

5.1.4 The electrodeposition behavior of Ni-P electrodeposited from Watts electrolyte containing phosphorous source

Ni-P coatings electrodeposited from the modified Watts Electrolyte contain different concentration of sodium hypophosphate and different current densities. Increasing the phosphorous source and decreasing the current density both caused higher phosphorous content in Ni-P deposits. According to XRD results, only deposits with less than 5 g/l $\text{NaP}_2\text{H}_2\text{O}_2$ are crystalline containing 5.8 wt. % of phosphorus. The deposit without phosphorus presents a preferential orientation of the (2 0 0) plane parallel to the surface, whereas the one with phosphorous favors the plane (1 1 1). The coatings deposited without phosphorus showed pyramidal grains, characteristic of a crystalline structure whereas the deposit elaborated in the presence of $\text{NaP}_2\text{H}_2\text{O}_2$ showed a globular morphology which would return rather to an amorphous structure. By increasing P content, the microstructure of deposits from crystalline inclined towards nanocrystalline and amorphous which can be corresponded to the impedance results. The effect of phosphorous content on the charge transfer Impedance was mostly comparable at lower current density of 1 A/dm^2 . The variations in the potential value as indicated in potential-time in Figure 4.6 can be due to the changes in interfacial pH by time which finally leads to formation of lamellar layers as it was seen in Figure 4.7 a) or 4.8.

5.1.5 The effect of particle size on electrodeposition behavior and features of Ni-P layer

In general, it was found that adding alumina particles in the plating bath electrodeposited under current density of 4 A/dm^2 leads to a reduction in crack phenomenon of Ni-P coatings surface while under the same conditions Ni-P deposit cannot be crack-free. The presence of Al_2O_3 in the Ni-P layer affects heterogeneity of the surface and increases the number of boundaries between Ni and other particles in the matrix. It is observed that particles were dispersed homogeneously in the matrix and adding submicron particles lead to higher value of incorporation compared to nanoparticle, while P content in the coating with submicron particles decline more than the coating electrodeposited with nanoparticles. Therefore, it can be concluded that the presence of Al_2O_3 particles could reduce the P content in the deposit by restriction of phosphine production. Adding particles leads to reduction in P content and the microstructure was shifted to more crystalline phase and there is more possibility for growth of the Ni grains. Therefore, the thickness of layer was larger than the coating with higher P content and rather amorphous structure. According to stress results after annealing, it was seen that adding particles in both cases leads to a decline in internal stress. For submicron particles the internal stress is 5 times smaller than Ni-P without particles. Despite of annealing and recrystallization, the size of incorporated particles is a lot larger than the size of Ni or Ni_3P grains, therefore there is no reliable evidence for crystallinity as confidence index (CI) must be greater than 0.1. It can be concluded that the dispersion hardening plays almost no role on the strengthening mechanism of Ni-P as-deposited coatings. However, the hardness of ceramic particles itself as a hardening phase can intervene the strengthening of the deposit. Remarkably, the microhard-

ness of the annealed composite coatings remains higher than Ni-P without particles but with higher phosphorous content. This can be related to the particle incorporation in the matrix, which inhibits the coarsening of the Ni_3P crystals during annealing. Thus, the improved hardness of the composites is a result of the nano-grained microstructure of the matrix accompanied by the high fraction of reinforcing hard particles.

5.1.6 The effect of particle type on electrodeposition behavior and features of Ni-P layer

Adding each three types of particles – Al_2O_3 , SiC and TiO_2 – into the Ni-P bath also conducted Ni-P composite coatings without cracks. It was seen that Ni-P coating shows a cauliflower-like morphology while embedded particles on the matrix of deposited shows homogeneous finer global structures. The accumulation and incorporation of TiO_2 particles in electrodeposited Ni-P seems to be much higher than Al_2O_3 or SiC particles under the same working condition. Adding all types of particles lead to a rather decline in P content of deposits. The higher value of thickness relates to the Ni-P coating with TiO_2 particles and highest amount of incorporated value compared to Ni-P- Al_2O_3 and Ni-P-SiC with lower amount of codeposited particles. It is seen that adding TiO_2 particles leads to an incredible decline in residual stress of Ni-P coating after annealing, while by adding the same amount of Al_2O_3 or SiC into Ni-P electrolyte, the internal stress did almost show no difference. This is in agreement with EDX data in which the incorporated amount of TiO_2 particles was almost two times more than Al_2O_3 or SiC. In the meantime, adding different particle types lead to Ni-P coatings without crack formation. This relates to adsorption of the hydrogen ions around particles. The confidence of the pattern indexing is reduced and only single large grains can be detected with a reasonable confidence. Such grains are shown in the Ni orientation map filtered with a confidence index $\text{CI} > 0.1$, commonly accepted for cubic structures. As it is observed none of the three types of coatings show a specific preferred texture. Despite of annealing and recrystallization, the size of incorporated particles is a lot larger than the size of Ni or Ni_3P grains. Therefore, it can be concluded that the dispersion hardening plays almost no role the strengthening mechanism of Ni-P composite coatings. However, the hardness of ceramic particles itself as a hardening phase can intervene the strengthening of the deposit. As it is seen when particles are added into the electrolyte the Martens hardness decreased compared to Ni-P without particles. As already explained the phosphorous content is the main influence on the hardening and softening of the as-plated Ni-P composite according to generally involved supersaturated solid solution strengthening and Hall-Petch mechanism. Dispersion and precipitation hardening due to the formation of the Ni_3P phase in the matrix determine the properties of the annealed medium phosphorus composite coatings. Remarkably, the microhardness of the annealed high-phosphorus composite coatings remains high, which is usually not observed in high phosphorus Ni/ Ni_3P coatings. This can be related to the particle incorporation in the matrix, which inhibits the coarsening of the Ni_3P crystals during annealing. Thus, the improved hardness of the high-phosphorus composites is a result of the nano-grained microstructure of the matrix accompanied by the high fraction of reinforcing hard particles. The impedance data for Ni-P composite coatings with different

size and type seems to comprise of a single capacitance loop in high and medium frequencies. It seems that the change in Nyquist semicircle relates to the change in the phosphorous content of deposits rather than particles existence. In other words, coatings with less P content show higher resistance or larger Nyquist semicircles.

5.2 Achievements

The achievement of the work can be summarized as follow:

- It is possible to correlate the effect of current density in Ni electrodeposition from Watts's bath with the layer characterization by the help of impedance spectroscopy.
- The effect of the alumina particle size and concentration on the characteristics of the double layer were determined. A descending trend in the impedance of the charge transfer as well as an ascending trend in the doubled-layer capacity was observed by increasing the Al_2O_3 particle concentration up to 20 g/l. The value of the charge transfer resistance for submicron particles is also lower than that of nanoparticles, and the double layer capacity for larger particles is moderately higher compared to smaller particle sizes.
- For both coatings produced with submicron and nano Al_2O_3 particles, at the middle concentration of 5 g/l, the current efficiency is much higher and both of the coatings show an almost similar strengthening performance, which relates to the simultaneous effect of Hall-Petch and the Orowan mechanisms.
- Despite the low incorporation value of Al_2O_3 nanoparticles compared to submicron particles, the hardness ability of the deposited coating with nanoparticles is higher than of the coatings prepared with submicron particles, which is due to the simultaneous effect of Hall-Petch and the Orowan mechanisms.
- It is observed that the incorporation value of TiO_2 particles with the same particle size as Al_2O_3 and SiC under the same concentration in the electrolyte and same working conditions is much higher. The incorporation value for SiC particles despite of 20 g/l concentration seems to be very dispersed and negligible.
- SiC particles with conductive nature provide better opportunity for Ni crystals to grow rather than on Al_2O_3 or TiO_2 particles with rather inert behavior.
- Despite of higher incorporation value of TiO_2 compared to Al_2O_3 and SiC, under the same working parameters, Al_2O_3 shows smaller Ni grain size in each single concentration compared to TiO_2 and SiC.
- Adding particles into Ni Watts's electrolyte reduces residual stress in the deposited composite coatings, whereas under the same working conditions adding 20 g/l TiO_2 particles reduces the stress, to a minimum of approximately 230 N/mm^2 at 4 A/dm^2 .

- According to EBSD/TKD results, fairly random TiO_2 distribution with particles located near the reconstructed grain boundaries as well as incorporated in nickel crystals. It is seen that Al_2O_3 and SiC are preferentially incorporated in the vicinity of grain boundaries.
- The mechanism of Orowan and dispersion hardening plays a specific role for the coating with TiO_2 particles, while the dominating mechanism of strengthening in Ni- Al_2O_3 and Ni-SiC composite coatings is mainly due to the Hall-Petch effect and grain refining rather than particles incorporation and Orowan mechanism.
- Except the effect of particles concentration on the impedance results, intrinsic particle characteristics for example differences in particle density and surface composition has a determining role on the results.
- Adding $\text{NaP}_2\text{H}_2\text{O}_2$ as phosphorous source into Watts's electrolyte and also declining current density causes an increase in P content in Ni-P coating.
- According to EIS results, there is a correlation between P content in Ni-P deposits and charge transfer resistance. The higher the P content is the lower is the charge transfer resistance.
- The lamellar layers in low and medium P content can be related to the variations of potential during electrodeposition process.
- It is generally possible to reduce crack formation and residual stress in Ni-P electrodeposited coatings by adding particles into the electrolyte. Moreover, adding particles from each type or grain size leads to lowering P content in Ni-P galvanic coatings.
- Under the same working conditions, adding submicron Al_2O_3 leads to higher amount of particle incorporation into Ni-P deposit compared to nanoparticles. Consequently the thickness of deposit with submicron particles is also higher. In general, adding particles increases current efficiency of Ni-P deposits.
- The dominating strengthening mechanism in as-deposited Ni-P composite coatings is mainly solid solution due to the existence of P content and dispersion hardening it has almost no effect on strengthening, while after annealing incorporated particles it could hinder the Ni_3P growth and indirectly affect the strengthening of deposits.
- The accumulation and incorporation of TiO_2 particles in electrodeposited Ni-P seems to be much higher than Al_2O_3 or SiC particles under the same working condition.
- It is seen that adding TiO_2 particles leads to incredible decline in residual stress of Ni-P coating after annealing, while by adding the same amount of Al_2O_3 or SiC into Ni-P electrolyte, the internal stress did almost show no difference.
- Adding each type of particle type leads to a decrease in hardening of Ni-P deposit due to the decline in P content and, on the other hand, the hardening after annealing for the deposits with all three types of particles were higher than Ni-P without particles.

- The change in Nyquist semicircle is influenced strongly under the change of phosphorous content in the deposits rather than the existence of particles.

5.3 Suggested future works

The electrodeposition mechanism of Ni-based electrodeposited composite coatings can be described by EIS investigations. The effect of particle characteristics such as particle size and type of the behavior of charge transfer and double-layer were indicated as influential parameters. It is believed that there would be also a relationship between zeta-potential of particles in the electroplating bath with the results of impedance during electrocodeposition in order to get a better insight about the mechanism of electrodeposition in composite coatings.

One of the most critical aspects of using nanoparticles in plating baths with high ionic strengths is the difficulty to keep them in suspension and to prevent the agglomeration, despite of using surfactant and ultrasound. A surface treatment of the particles by grafting of polymer brushes can enable a combined electrostatic and steric stabilization of the colloidal dispersion.

Another influential surface property of the nanoparticles is their hydrophilicity, i.e. the tendency of getting solvated by water. Due to the formation of a hydration layer around the particles, they remain separated from the electrode by a small gap which substantially affects the particle embedding by the growing metal matrix. The degree of hydration, i.e. the thickness of the hydration layer, can be influenced by a proper selection of the operating conditions such as particle characteristics and electrolyte composition. Aqueous electrolytes are most commonly used for galvanic applications. A partial or complete substitution of the water by organic solvents (e.g. methanol, ethanol, etc.) can affect the state of hydration and therefore influence the interaction between particle and electrode. Finally, the particle incorporation behavior might change which can substantially alter the film properties.

Another suggested idea is to investigate the fatigue behavior of layers by performing tensile test with dog-bone samples from deposited layers. Fatigue resistance plays a significant factor especially for micro-engines produced from Ni and especially Ni-P deposits by LIGA process.

Due to the nanoparticle incorporation, the structure and properties of the metal matrix was found to change considerably. With reference to an industrial application a detailed characterization of the chemical, electrical, and mechanical film properties is required. Particularly, the effect of functional nanoparticles, e.g. microcapsules, on the strengthening and corrosion mechanism of the metal matrix has to be clarified in view of an optimization of the film properties.

For the purpose of scaling-up or industrialization of the ECD process, the use of experimental setups with a practical orientation combined with bigger and complex shaped substrates is mandatory. Additionally, a plan of procedures for electrolyte monitoring, with special regard to a possible aging of the electrolyte dispersions, should be developed.

References

1. Guglielmi, N., (1972), Kinetics of the deposition of inert particles from electrolytic baths, *J. Electrochem. Soc.*, 119 (8), 1009-1012.
2. Roos, J. R., Celis, J. P. & Helsen, J. A., (1977), *Tran. of the Inst. of Metal Finishing*, 55, 113.
3. Low, C. T. J., Wills, R. G. A. & Walsh, F. C., (2006), Electrodeposition of composite coatings containing nanoparticles in a metal deposit, *Surface & Coatings Technology*, 201, 371–383.
4. Davis, J. R., (2000), *ASM Specialty Handbook: Nickel, cobalt and their alloys*, ASM International.
5. Stoye, D. & Freitag, W., (1998), *Paints, coatings and solvents*, 2nd edition, Wiley-VCH Verlag GmbH, Weinheim.
6. Brock, T., Groteklaes, M. & Mischke, P., (2000), *European coatings handbook*, Vincentz Network GmbH & Co KG, Hannover.
7. Li, Z., Sun, X., Zheng, Y. & Zhang, H., (2013), Microstructure and magnetic properties of micro NiFe alloy arrays for MEMS application, *J. Micromech. Microeng.*, 23.
8. Namburi, L., (2001), *ELECTRODEPOSITION OF NiW ALLOYS INTO DEEP RECESSES*, Master thesis, The Department of Chemical Engineering, Louisiana State University.
- 9.
10. Jian, L., Desta, Y. M., Goettert, J., Bednarzik, M., Loechel, B., Jin, Y., Aigeldinger, G., Singh, V., Ahrens, G., Gruetzner, G., Ruhmann, R. & Degen, R., (2003), SU-8 based deep x-ray lithography/LIGA, *Proc. SPIE 4979*, Micromachining and Microfabrication Process Technology VIII, 394 doi: 10.1117/12.478246
11. Duch, M., (2002), Electrodeposited Co-Ni alloys for MEMS, *J. Micromech. Microeng.*, 12, 400–405.
12. Hormes, J., Gottert, J., Lian, K., Desta, Y. & Jian, L., (2003), Materials for LiGA and LiGA-based Microsystems, *Nuclear Instruments and Methods in Physics Research, B* 199, 332–341.
13. Panda, A. & Podlaha, E. J., (2003), Nanoparticles to Improve Mass Transport Inside Deep Recesses, *Electrochem. Solid-State Lett.*, 6 (11), C149- C152.
14. Park, D.-Y., Myung, N. Y., Schwartz, M. & Nobe, K., (2002), Nanostructured magnetic CoNiP electrodeposits: Structure—Property relationships, *Electrochimica Acta*, 47, 2893- 2900.
15. Lee, C.-Y., Hsu, C.-H. & Wu, M.-W., (2010), The HER property of electrodeposited Ni-P electrode with micro-patterned structure, *International Conference on Optics, Photonics and Energy Engineering*. doi: 10.1109/opee.2010.5508183
16. Jiang, K., (2010), Electrochemical Co-Deposition of Metal-Nanoparticle Composites for Microsystem Applications, From: *Cutting edge nanotechnology*, InTech.

17. Furukawa, S. & Mehregany, M., (1996), Electroless plating of nickel on silicon for fabrication of high-aspect-ratio microstructures, *Sensors and Actuators A: Physical*, 56, 261-266.
18. Chou, M.-C., Ger, M.-D., Ke, S.-T., Huang, Y.-R. & Wu, S.-T., (2005), The Ni-P-SiC composite produced by electro-codeposition, *Materials Chemistry and Physics*, 92, 146–151.
19. Zangari, G., (2010), Microelectromechanical systems, From: *Electrodeposition of metals and alloys for MEMS*.
20. Winkler, F. & Guttman, M., (2005), Galvanisch-Nickel-Phosphoralternatives Material zur Beschichtung von Bauteilen oder zum Einsatz in der Mikrosystemtechnik, *Galvanotechnik*, 8.
21. Myung, N. V., Park, D.-Y., Yoo, B.-Y. & Sumodjo, P. T. A., (2003), Development of electroplated magnetic materials for MEMS, *Journal of Magnetism and Magnetic Materials*, 265, 189–198.
22. Hu, C. C. & Cheu, C.-H., (2000), *Electrodeposition of Nickel-Phosphorus Deposits with a Variable Magnetic Property*, from: www3.electrochem.org/dl/ma/198/pdfs/0636 [15.08.2015].
23. Kobayashi, S., Kamata, A. & Watanabe, T., (2010), Surface crack nucleation and propagation in electrodeposited nanocrystalline Ni-P alloy during high cycle fatigue, *Journal of Physics: Conference Series*, 240, 012053.
24. Teh, K. S., Chen, Y. T. & Lin, L. W., (2005), MEMS Fabrication Based on Nickel-Nanocomposite: Film Deposition and Characterization, *J. Micromech. Microeng.*, 15, 2205-2215.
25. Wronkowska, A. A. & Wronkowski, A., (1992), Optical properties of polycrystalline and amorphous $\text{Ni}_{1-x}\text{P}_x$ layers by ellipsometry, *J. Mater. Sci.*, 27, 1842-1848.
26. Ke, S.-T., Lee, J.-L., Yeh, Y.-M., Lee, S.-J. & Ger, M.-D., (2008), A Study of the Microstructure and Properties of Electroformed Ni-P Model Insert., *Key Engineering Materials*, 364-366, 232 -236.
27. Boylan, K., Ostrander, D., Erb, U., Paulumbo, G. & Aust, K T., (1991), An In Situ TEM Study of the Thermal Stability of Nanocrystalline Ni-P, *Scripta Metall. Mater.*, 25, 2711-2716.
28. Marshall, G. W., Lewis, D. B. & Dodds, B. E., (1992), Electroless Deposition of Ni-P Alloys with and without the Use of Superimposed Pulsed Current, *Surf Coat. Technol.*, 53, 223-730.
29. Lashmore, D. S. & Weinroth, J. F., (1982), Pulsed Electrodeposition of Nickel-Phosphorus Metallic Glass Alloys, *Plat. Surf Finish.*, 69, 72-76.
30. Jeong, D. H., Erb, U., Aust, K. T. & Palumbo, G., (2003), The relationship between hardness and abrasive wear resistance of electrodeposited nanocrystalline Ni-P coatings, *Scripta Mater.*, 48, 1067-1072.
31. Dini, J. W., Donaldson, R. R., Syn, C. K. & Sugg, D. J., (1990), Diamond Tool Wear of Electrodeposited Nickel-Phosphorous Alloy, *SUR/EIN '90: 77th American Electroplaters and Surface Finishers Society (AESE) Annual Technical Conference*, Boston.

32. Crousier, J., Hanane, Z. & Crousier, J. P., (1993), A Cyclic Voltammetry Study of the Ni-P Electrodeposition, *Electrochim. Acta.*, 38 (2/3), 261-266.
33. Bredael, E., Celis, J. P. & Roos, J. R., (1993), NiP Electrodeposition on a Rotating-Disc Electrode and in a Jet Cell: Relationship Between Plating Parameters and Structural Characteristic, *Surf. Coat. Technol.*, 58, 63-71.
34. Shervedani, R. K. & Lasia, A. J., (1997), Studies of the hydrogen evolution reaction on Ni-P electrodes, *J. Electrochem. Soc.*, 144 (2), 511-519.
35. Budniok, A. & Serek, A., (2002), New Electrode Materials Containing Titanium Powder in an Amorphous Matrix of Ni-P, *Key Eng. Mater.*, 239-232 213-217
36. Kobayashi, S. & Kashikura, Y., (2003), Grain Growth and Mechanical Properties of Electrodeposited Nanocrystalline Nickel-4.4 mass% Phosphorous Alloy, *Miner. Sei. Eng., A.358*, 76-83.
37. Bredael, F., Blanpain, B., Celis, J. P. & Roos, J.R., (1994), On the Amorphous and Crystalline State of Electrodeposited Nickel-Phosphorous Coatings, *J. Electrochem. Soc.*, 141 (1), 294-299.
38. Ng, P. K., Snyder, D. D. & LaSala, J., (1988), Structure and Crystallization Of Nickel-Phosphorous Alloys Prepared by High-Raft Electrodeposition, *J. Electrochem. Soc.*, 135 (6), 1376-131.
39. Daly, B. P. & Barry, F. J., (2003), Electrochemical Nickel-Phosphorous Alloy Formation, *Int. Mater. Rev.*, 48 (5), 326-338.
40. Mc Mohan, G. & Erb, U., (1989), Structural Transitions in Electroplated Ni-P Alloys, *J. Mater. Sci. Lett.*, 8, 865-868.
41. Toth-Kadar, E., Bakonyi, I., Solyom, A., Hering, J. & Konczos, G., (1987), Preparation and Characterization of Electrodeposited Amorphous Ni-P Alloys, *Surf. Coat. Technol.*, 31, 31-43.
42. Lin, C. S., Lee, C. Y., Chen, F. J. & Li, W., (2005), Structural Evolution and Internal Stress of Nickel-Phosphorous Electrodeposits, *J. Electrochem. Soc.*, 152 (6), 370-375.
43. Yang, H. & Kang, S.-W., (2000), Improvement of thickness uniformity in nickel electroforming for the LIGA process, *International Journal of Machine Tools & Manufacture*, 40, 1065–1072.
44. Loechel, B., (2000), Thick-layer resists for surface micromachining, *J. Micromech. Microeng.*, 10, 108–115.
45. Narayan, R. & Mungole, M. N., (1985), Electrodeposition of Ni-P alloy coatings. *Surface Technology*, 24 (3), 233-239.
46. GALVANOTECHNIK, (2006) Einsatz von Galvanisch Nickel-Phosphor, Jahrgang 60.
47. Brenner, A., Couch, D. E. & Williams, E. K., (1950), Electrodeposition of Alloys of Phosphorus with Nickel or Cobalt, *Research Paper RP2061*, 44.

48. Zhaoeng, F. (1997), Electrodeposition of Amorphous Ni-P Alloy Coatings, *Trans.nonferrous Met.Soc.China*, Vol.7, N.3, from: <http://www.ysxbcn.com/down/upfile/soft/2010626/1997-3-31.pdf>
49. Lin, C. S., Lee, C. Y., Chen, F. J., Chien, C. T., Lin, P. L. & Chung, W. C., (2006), Electrodeposition of Nickel. Phosphorus Alloy from Sulfamate Baths with Improved Current Efficiency. *Journal of The Electrochemical Society*, 153 (6), C387-C392.
50. Djokić, S. S., (2013), Electrodeposition and Electroless Deposition of NiWP Alloys, *ECS Trans*, 53 (11), 15-25.
51. Chang, L, Chen, C.-H. & Fang, H., (2008), Electrodeposition of Ni-P Alloys From a Sulfamate Electrolyte: Relationship Between Bath pH and Structural Characteristics, *Journal of The Electrochemical Society*, 155 (1), D57-D61.
52. Ordine, A. P., Díaz, S. L., Margarit, I. C. P. & Barcia, O. E., (2006), Electrochemical study on Ni-P electrodeposition, *Electrochimica Acta*, 51, 1480–1486.
53. Chang, L., Kuo, P. W. & Chen, C. H. (2007), Strengthening mechanisms in electrodeposited Ni-P alloys with nanocrystalline grains, *Scripta Materialia*, 56, 713–716.
54. Popczyk, M., Budniok, A., Scholl, H. & Blaszczyk, T., (2006), Structure and Electrochemical Characterization of Electrolytic Ni-Co-P and Ni-W-P Layers, *Materials Science Forum*, Vols. 514-516, 460-464.
55. Spearing, S. M., (2000), Materials Issues in Microelectromechanical Systems (MEMS), *Acta materialia*, 48,179-196.
56. Chen, F. J., Pan, Y. N., Lee, C. Y. & Lin, C. S., (2010), Internal Stress Control of Nickel–Phosphorus Electrodeposits Using Pulse Currents, *Journal of The Electrochemical Society*, 157 (3), 154-158.
57. Allameh, S. M., Lou, J., Kavshe, F., Buchheit, T. & Soboyajo, W. O., (2004), An investigation of fatigue in LIGA Ni MEMS thin films, *Materials Science and Engineering, A* 371, 256–266.
58. Dzedzina, R. & Hagarová, M., (2013), Effect of Additive on the Internal Stress in Galvanic Coatings, *Int. J. Electrochem. Sci.*, 8, 8291 - 8298.
59. Celis, J. P. & Roos, J. R., (1982), Electrolytic and Electroless Composite Coatings, *Reviews in Coatings and Corrosion*, 5(1-4), p.1
60. Morana, R., (2006). The influence of particle type and Conditions on composite electrodeposition, *Doctoral thesis*, Loughborough University.
61. Gyftou, P., Pavlatou, E. A. & Spyrellis, N., (2008), Effect of Pulse Electrodeposition Parameters on the Properties of Ni/Nano-SiC Composites, *Appl. Surf. Sci.*, 25, 5910 - 5916.
62. Singh, D. K. & Singh, V. B., (2012), Electrodeposition and characterization of Ni–TiC composite using N-methylformamide, *Mater. Sci. Eng. A*, 532, 493- 499.

63. Lampke, T., Wielage, B., Dietrich, D. & Leopold, A., (2006), Details of crystalline growth in codeposited electroplated nickel films with hard (nano)particles, *Appl. Surf. Sci.*, 253, 2399 - 2408.
64. Ebrahimi, F., Bourne, G. R., Kelly, M. S. & Matthews, T. E., (1999), Mechanical properties of nanocrystalline nickel produced by electrodeposition, *Nanost. Mater.*, 11, 343 - 350.
65. Ferkel, H., Müller, B. & Reihemann, W., (1997), Electrodeposition of Particle Strengthened Nickel-Films, *Mater. Sci. Eng. A*, 234, 474 - 476.
66. Fawzy, M. H., Ashour, M. M. & Abd El-Halim, A. M., (1996), Effect of Some Operating Variables on the Characteristics of Electrodeposited Ni- α -Al₂O₃ and Ni-TiO₂ Composites, *Trans. Inst. Met. Finish.*, 74, 72 - 77.
67. Xiaowei, Z., Yifu, S., Yingying, Z. & Huiming, J., (2011), Mechanism and microstructure of nickel-ceria composite coatings prepared by pulse current deposition under the ultrasonic field, *J. Rare Earths*, 29, 883 - 887.
68. Wang, W., Hou, F. Y., Wang, H. & Guo, H. T., (2005), Fabrication and characterization of Ni-ZrO₂ composite nanocoatings by pulse electrodeposition, *Scripta Mater*, 53, 613 - 618.
69. Haq, I. & Khan, T. I., (2011), Tribological behavior of electrodeposited Bi-SnO₂ composite coatings on steel, *Surf. Coat. Technol.*, 205, 2871.
70. Kumar, K., Chandramohan, R. & Kalyanaraman, D., (2004), Effect of heat treatment on cobalt and nickel electroplated surfaces with Cr₂O₃ dispersions, *Appl. Surf. Sci.*, 277, 383 - 386.
71. Stroumbouli, M., Gyftou, P., Pavlatou, E. A. & Spyrellis, N., (2005), , Codeposition of ultrafine WC particles in Ni matrix composite electrocoating, *Surf. Coat. Technol.*, 195, 325 - 332.
72. Wang, S. C. & Wei, W. C. J., (2003), Kinetics of electroplating process of nano-sized ceramic particle/Ni composite, *Mater. Chem. Phys.*, 78, 574 - 580.
73. Nowak, P., Socha, R. P., Kaisheva, M., Fransaer, J., Celis, J. P. & Stoinov, Z., (2000), Electrochemical Investigation of the Codeposition of SiC and SiO₂ Particles with Nickel, *J. Appl. Electrochem.*, 30, 429 - 437.
74. Maurin, G. & Lavanant, A., (1995), Electrodeposition of nickel/silicon carbide composite coatings on a rotating disc electrode, *J. Appl. Electrochem.*, 25, 1113 - 1121.
75. Gyftou, P., Pavlatou, E. A., Spyrellis, N. & Hatzilyberis, K. S., (2000), Nickel matrix composite coatings: Application in textile machinery and evaluation on cotton products quality, *Trans. Inst. Met. Finish.*, 78 (6), 223.
76. Gyftou, P., Stroumbouli, M., Pavlatou, E. A. & Spyrellis, N., (2002), Electrodeposition of Ni/SiC Composites by Pulse Electrolysis, *Trans. Inst. Met. Finish.*, 80 (3), 88 - 91.
77. Khazrayie, M. A. & Aghdam, A. R. S., (2010), Si₃N₄/Ni nanocomposite formed by electroplating: effect of average size of nanoparticulates. *Trans. Nonferrous Met. Soc. China (English Edition)*, 20, 1017.

78. Praveen Kumar, C. M. & Venkatesha, T. V., (2012), Ni - Si₃N₄ composite electrodeposition, characterization and corrosion behavior, *Phys. Scr.*, **86**, 015804.
79. Pompei, E., Magagnin, L., Lecis, N. & Cavallotti, P. L., (2009), Electrodeposition of nickel-BN composite coatings, *Electrochim. Acta*, **54**, 2571- 2574.
80. Chen, X. H., Cheng, F. Q., Li, S. L., Zhou, L. P. & Li, D. Y., (2002), Electrodeposited nickel composites containing carbon nanotubes, *Surf. Coat. Technol.*, **155**, 274- 278.
81. Zimmerman, A. F., Palumbo, G., Aust, K. T. & Erb, U., (2002), Mechanical Properties of nickel silicon carbide nanocomposites, *Materials Science and Engineering A*, **328**, 137–146.
82. Shen, G.-R., Cheng, Y.-T. & Tsai, L.-N., (2005), Synthesis and Characterization of Ni-P-CNT's Nanocomposite Film for MEMS Applications, *IEEE TRANSACTIONS ON NANO-TECHNOLOGY*, **4** (5), 539- 547.
83. Malfatti, C. F., Ferreira, J. Z., Santos, C. B., Souza, B. V., Fallavena, E. P., Vaillant, S. & Bonino, J. P., (2005), Ni-P-SiC composite coatings: the effects of particles on the electrochemical behaviour, *Corrosion Science*, **47**, 567–580.
84. Hou, K.-H., Hwub, W.-H., Ke, S.-T. & Ger, M.-D., (2006), Ni-P-SiC composite produced by pulse and direct current plating, *Materials Chemistry and Physics*, **100**, 54–59.
85. Berkh, O., Eskin, S. & Zahavi, J., (1996), Properties of Electrodeposited Ni-P-SiC Composite Coatings, *Metal Finishing*, **94** (3), 35-40.
86. Zoikis-Karathanasis, A., Pavlatou, E. A. & Spyrellis, N., (2010), Pulse electrodeposition of Ni-P matrix composite coatings reinforced by SiC particles, *Journal of Alloys and Compounds*, **494**, 396–403.
87. Urm, K. W., Lee, S. H., Kim, W. S., Cho, C. Y. & Lee, J. H., (2007), Pulse Electroplating of Ni-P-Nano TiO₂ and ZrO₂ for Steam Generator Tube Repair, *Advanced Materials Research*, **26-28**, 1067-1070.
88. Aslanyan, I. R., Celis, J.-P. & Shuster, L. Sh., (2011), The Effect of SiC Additives on Fretting Wear of Electroplated Ni-P Coatings, *Journal of Friction and Wear*, **32** (2), 74–78.
89. Shi, Y. L., Yang, Z., Xu, H., Li, m. K. & Li, H. L., (2004), Preparation of electroplated Ni-P-ultrafine diamond, Ni-P-carbon nanotubes composite coatings and their corrosion properties, *Journal of Materials Science*, **39**, 5809 – 5815.
90. Papavasiliopoulou, P., Zoikis- Karathanasis, A., Pavlatou, E. A. & Spyrellis, N., (2008), Effect of plating parameters in NiP-SiC Electrodeposition, in: *Proceedings of the 7th International Conference "The Coatings in Manufacturing Engineering"*, Kalithea Chalkidiki, Greece, 417-425.
91. Hou, K. H., Jeng, M. C., Shen, Y. K. & Ger, M. D., (2007), The Wear Behavior of Pulse Current Electroforming Ni-P-SiC Composite Coatings, *Key Engineering Materials*, **364-366**, 358-363.

92. Aslanyan, I. R., Bonino, J.-P. & Celis, J.-P., (2006), Effect of reinforcing submicron SiC particles on the wear of electrolytic Ni-P coatings. Part 1. Uni-directional sliding, *Surface & Coatings Technology*, 200, 2909– 2916.
93. Berkh, O., Bodnevas, A. & Zahavi, J., (1995), Electrodeposited Ni- P-Sic Composite Coatings, *Plating and Surface Finishing*, 82 (11), 62-66.
94. Rabizadeh, T. & Yeganeh, M., (2011), Influence of TiC nanoparticles on microstructures and properties of electrodeposited Ni–P coatings, *IET Micro & Nano Letters*, 6 (9), 790-793.
95. Marshall, G., Lewis, D. B., Clayton, D., Blake, K. & Dodds, B., (1997), The electrodeposition of Ni-P-Al₂O₃ deposits, *Surface and coating technology*, 96, 353-358.
96. Huang, H. C., Chung, S.-T., Pan, S.-J., Tsai, W.-T & Lin, C.-S., (2010), Microstructure evolution and hardening mechanisms of Ni–P electrodeposits, *Surface & Coatings Technology*, 205, 2097–2103.
97. Greco, V. P. & Baldauf, W., (1968), Electrodeposition of Ni-Al₂O₃, Ni-TiO₂ and Cr-TiO₂ Dispersion Hardened Alloys, *Plating*, 55, 250
98. Ehrhardt, J., (1985), Composite Electroplating Using the Brush Technique, *Industrial and Engineering Chemistry - Product Research and Development*, 24 (4), 575.
99. Bazzard, R. & Boden, P. J., (1972), Nickel-Chromium Alloys by Co-deposition: Part 1- Co-deposition of Chromium Particles in a Nickel Matrix, *Transactions of the Institute of Metal Finishing*, 50, 63.
100. Foster, J. & Cameron, B., (1976), The Effect of Current Density and Agitation on the Formation of Electrodeposited Composite Coatings, *Transactions of the Institute of Metal Finishing*, 54, 178.
101. Zahavi, J. & Kerbel, H., (1982), Properties of Electrodeposited Composite Coatings, *Plating and Surface Finishing*, 69 (1), 76.
102. Stankovic, V. D. & Gojo, M., (1996), Electrodeposited Composite Coatings of Copper with Inert, Semiconductive and Conductive Particles, *Surface and Coatings Technology*, 81(2-3), 225.
103. Sova, V., (1987), Electrodeposited Composite Coatings for Protection from High Temperature Corrosion, *Transactions of the Institute of Metal Finishing*, 65, 21.
104. Chen, E. S., Lakshminarayanan, G. R. & Sautter, F. K., (1971), The Codeposition of Alumina and Titania with Copper, *Metallurgical Transactions*, 2, 937.
105. Stojak, J. L., & Talbot, J. B., (1999), Investigation of Electrocodeposition Using a Rotating Cylinder Electrode, *Journal of the Electrochemical Society*, 146 (12), 4504.
106. Stojak, J. L. & Talbot, J. B., (2001), Effect of Particles on Polarization During Electrocodeposition Using a Rotating Cylinder Electrode, *Journal of Applied Electrochemistry*, 31, 559.

107. Benea, L., Bonora, P. L., Borello, A., Martelli, S., Wenger, F., Pointhiaux, P. & Galland, J., (2001), Composite Electrodeposition to Obtain Nanostructured Coatings, *Journal of the Electrochemical Society*, 148 (7), C461 – C465.
108. Masalki, J., Szczygiel, B., & Gluzek, J., (2002), EIS Study of the Codeposition of SiC Powder with Nickel in a Watts Bath, *Transactions of the Institute of Metal Finishing*, 80 (3), 101.
109. Greco, V. P., (1989), A Review of Fabrication and Properties of Electrocomposites, *Plating and Surface Finishing*, 76(10), 68.
110. Suzuki, Y. & Asai, O., (1987), Adsorption Co-deposition Process of Al₂O₃ Particles onto Ag-Al₂O₃ Dispersion Films, *Journal of the Electrochemical Society*, 134 (8), 1905.
111. Verelest, M., Bonino, J. P. & Rousset, A., (1991), Electroforming of Metal Matrix Composite: Dispersoid Grain Size Dependence of Thermostructural and Mechanical Properties, *Materials Science and Engineering*, A135, 51.
112. Stojak, J. L., Fransaer, J. & Talbot, J. B. (2002), *Review of Electrocodeposition*, in: Alkire, R. C. & Kolb, D.M. (Eds.), *Adv. Electrochem. Sci. Eng.*, Wiley-VCH Verlag, Weinheim.
113. Hovestad, A. & Janssen, L. J. J., (1995), Electrochemical codeposition of inert particles in a metallic matrix, *J. Appl. Electrochem.*, 25 (6), 519 -527.
114. Musiani, M., (2000), Electrodeposition in Composites: An Expanding Subject in Electrochemical Materials Science, *Electrochim. Acta*, 45, 3397 – 3402.
115. Helle, K. & Walsh, F., (1997), Electrodeposition of composite layers consisting of inert inclusion in a metal matrix, *Trans. Inst. Met. Finish.*, 75, 53- 58.
116. Talbot, J. B., (2004), Electrocodeposition of Nanocomposite Films, *Plat. Surf. Finish.*, 91, 60-65.
117. Varaksin, A. Y., Kurosaki, Y. & Satoh, I., (1995), An analytical investigation of turbulence reduction by small solid particles. In: *International Symposium on Heat Transfer Enhancement in Power Machinery*, Abstracts of Papers, Moscow, Part 1, 34.
118. Princeton Applied Research Application note AC1, (2009) *Basics of Electrochemical Impedance Spectroscopy*, from <http://www.princetonappliedresearch.com/download.asbx?AttributeFileId=8406b254-b6d4-4341-9f48-87a04ce7ee3d> [21.04.2013].
119. Gabrielli, C., (1984), Identification of Electrochemical Processes by Frequency Response Analysis, *Schlumberger Technologies Technical Report Number 004/83*.
120. Song, M. K., (2011), Synthesis and Characterization of Nanostructured, Mixed-Valent Compounds for Electrochemical Energy Storage Devices, *PhD dissertation*, Georgia Institute of Technology.
121. Gomez, E., Pollina, R. & Valles, E., (1995), Nickel electrodeposition on different metallic substrates, *J. Electroanal. Chem.*, 386, 45- 56.

122. Epelboin, I. & Wiart, R., (1971), Mechanism of the Electrocrystallization of Nickel and Cobalt in Acidic Solution, *J. Electrochem. Soc.*, 118 (10), 1577- 1582.
123. Epelboin, I., Jousselein, M. & Wiart, R., (1981), Impedance measurements for nickel deposition in sulfate and chloride electrolytes, *Journal of Electroanalytical Chemistry and Interfacial Electrochemistry*, 119 (1), 61- 71.
124. Chassaing, E., Jousselein, M. & Wiart, R., (1983), The Kinetics of Nickel Electrodeposition: Inhibition by Adsorbed Hydrogen and Anions, *J. Electroanal. Chem.*, 157, 75- 88.
125. Wiart, R., (1990), Elementary steps of electrodeposition analysed by means of impedance spectroscopy, *Electrochim. Acta*, 35, 1587.
126. Proud, W. G. & Muller, C., (1993), The Electrodeposition of Nickel on Vitreous Carbon- Impedance Studies, *Electrochim. Acta*, 38, 405- 413.
127. Grande, W. C. & Talbot, J. B., (1993), Electrodeposition of thin films of nickel- iron. 1. Experimental, *J. Electrochem. Soc.*, 140 (3), 669- 674.
128. Bockris, J. O'M. & Reddy, A. K. N., (1970), *Modern Electrochemistry*, Vol. 2, London and Plenum Press, New York.
129. Vazquez-Arenas, J. & Pritzker, M., (2010), EIS Study of Nickel Deposition in Borate–Sulfate Solutions, *J. Electrochem. Soc.*, 157 (5), D283- D294.
130. Yeh, S. H. & Wan, C. C., (1994), Codeposition of SiC powders with nickel in a Watts bath, *J. Appl. Electrochem.*, 24 (10), 993-1000.
131. Watson, S. W., (1993), Electrochemical study of SiC particle occlusion during nickel electrodeposition, *J. Electrochem. Soc.*, 140 (8), 2235- 2238.
132. Sohrabi, A. & Dolati, A., (2012), A study on the mechanism of electrodeposition of Ni/SiC composite coatings using impedance technique, *ECS Trans.*, 41 (44), 47-57.
133. Hu, F. & Chan, K. C., (2005), Deposition behaviour and morphology of Ni–SiC electrocomposites under triangular waveform, *Applied Surface Science*, 243 (1), 251–258.
134. Hu, F., Chan, K. C. & Qu, N. S., (2007), Effect of magnetic field on electrocodeposition behavior of Ni-SiC composites, *J. Solid State Electrochem*, 11 (2), 267–272.
135. Benea, L., Bonora, P. L., Borello, A., Martelli, S., Wenger, F., Ponthiaux, P. & Galland, J., (2002), Preparation and investigation of nanostructured SiC-nickel layers by electrodeposition, *Solid State Ionics*, 151 (1-4), 89– 95.
136. Socha, R. P., Nowak, P., Laajalehto, K. & Väyrynen, J., (2004), Particle-electrode surface interaction during nickel electrodeposition from suspensions containing SiC and SiO₂ particles, *Colloids and Surfaces A: Physicochem. Eng. Aspects*, 235, 45–55.
137. Wei, H., Tan, C.-Y., Cui, H., Liu, Y. & Zheng, Z.-Q., (2010), Kinetics analysis of Ni-TiO₂ composite system during initial stages of electro-crystallization, *J. Cent. South Univ. Technol.*, 17, 460-466.

138. Benea, L., (2009), Electrodeposition and tribocorrosion behaviour of ZrO_2 -Ni composite coatings, *J. Appl. Electrochem.*, 39, 1671–1681.
139. Shi, L., Sun, C., Gao, P., Zhou, F. & Liu, W., (2006), Mechanical properties and wear and corrosion resistance of electrodeposited Ni-Co/SiC nanocomposite coating, *Appl. Surf. Sci.*, 252, 3591.
140. Wu, G., Ning, L., Dian, L. W., De, R. Z., Bo, Q. X. & Kurachi, M., (2004), Effect of $\alpha\text{-Al}_2\text{O}_3$ particles on the electrochemical codeposition of Co-Ni alloys from sulfamate electrolytes, *Materials Chemistry and Physics*, 87 (1-2), 411–419.
141. Watson, S. W. & Walters, P. R., (1991), The effect of chromium particles on nickel electrodeposition, *Journal of Electrochemical Society*, 138(12), 3633-3637.
142. Hovestad, A. & Janssen, L. J. J., (2005), Electroplating of Metal Matrix Composites by Codeposition of Suspended Particles, In: Conway, B. E., Vayenas, C. G., White, R. E. & Gamba-Adelco, M. E., (2005), *Modern Aspects of Electrochemistry*, Vol. 38, Kluwer Academic/Plenum Publishers, New York.
143. Hu, F. & Chan, K. C., (2006), Effect of pulse frequency on electrodeposition behaviour of Ni-SiC composites, *Int. J. Surf. Engin. and Coat.*, 84 (5), 252-255.
144. Bicelli, L. P., Bozzini, B., Mele, C. & D'Urzo, L., (2008), A Review of Nanostructural Aspects of Metal Electrodeposition, *Int. J. Electrochem. Sci.*, 3, 356 – 408.
145. Watson, S. A., (2008), *Ni Development Institute Tech. Series Reports 10047–10055*.
146. Hadian, S. E. & Gaba, D. R., (1999), Residual Stresses in Electrodeposits of Nickel and Nickel-Iron Alloys, *Surf. Coat. Technol.*, 122, 118- 135.
147. Sadak, J. C. & Sautter, F. K., (1974), Composition, mechanical properties, and structure of electrodeposited cobalt-iron alloys, *J. Vac. Sci. Technol.*, 11, 771.
148. Stephens, L. S., Kelly, K. W., Simhadri, S., McCandless, A. B. & Meletis, E. I., (2001), Mechanical property evaluation and failure analysis of cantilevered LIGA nickel microposts, *J. Microelectromechanical Systems*, 3, 347.
149. Scharf, I., Sieber, M & Lampke, T., (2014), Calculation approach for current-potential behaviour during pulse electrodeposition based on double-layer characteristics, *Transactions of the Institute of Metal Finishing*, 92 (6), 325-335.
150. Kondo, K., Ohgishi, A. & Tanaka, Z., (2000), Electrodeposition of Zinc-SiO₂ Composite, *Journal of the Electrochemical Society*, 147 (7), 261.
151. Bozzini, B. & Fanigliulo, A., (2002), Raman Spectroscopy of Organic Species Incorporated into Electrodeposited Gold Layer, *Transactions of the Institute of Metal Finishing*, 80(1), 25.
152. Surviliene, S., Orlovskaja, L., Bikulcius, G. & Bialozor, S., (2001), Effect of MoO₂ and TiO₂ on Electrodeposition and Properties of Chromium Coating, *Surface and Coating Technology*, 137, 230.

153. Garcia, I., Conde, A., Langeelan, G., Fransaer, J. & Celis, J. P., (2003), Improved Corrosion Resistance Through Microstructural Modifications Induced by SiC-Particles with Electrolytic Nickel, *Corrosion Science*, 45, 1173.
154. Zhu, T. T., Bushby, A. J. & Dunstan, D. J., (2008), Materials mechanical size effects: a review, *Materials Technology*, 23 (4), 193- 209.
155. Chia, K., Jung, K. & Conrad, H., (2005), Dislocation density model for the effect of grain size on the flow stress of a Ti-15.2 at.% Mo b-alloy at 4.2-650K, *Mater. Sci. Eng. A*, 409, 32–38.
156. Han, B. Q. & Lavernia, E. J., (2005), Deformation mechanisms of nanostructured alloys, *Adv. Eng. Mater.*, 7, 457.
157. Scattergood, R. O., Koch, C. C., Murty, K. L. & Brenner, D., (2008), Strengthening mechanisms in nanocrystalline alloys, *Mater. Sci. Eng. A*, 493, 3- 11.
158. Schuh, C. A., Nieh, T. G. & Iwasaki, H., (2003), The effect of solid solution W additions on the mechanical properties of nanocrystalline Ni, *Acta Mater*, 51, 431- 443.
159. Detor A. J. & Schuh, C. A., (2007), Tailoring and patterning the grain size of nanocrystalline alloys, *Acta Mater*, 55, 371- 379.
160. Liu, F., & Kirchheim, R., (2004), Nano-scale grain growth inhibited by reducing grain boundary energy through solute segregation, *J Cryst Growth*, 264, 385.
161. Krill, C. E., Klein, R., Janes, S. & Birringer, R., (1995), Thermodynamic stabilization of grain boundaries in nanocrystalline alloys, *Mater. Sci. Forum*, 179- 181, 443- 448.
162. Li, H. Q. & Ebrahimi, F., A-Struct Mater Prop Microstruct Process, *Mater. Sci. Eng.*, 347, 93.
163. Cheng, S., Spencer, J. A. & Milligan, W. W., (2003), Strength and tension/ compression asymmetry in nanostructured and ultrafine-grain metals, *Acta Mater*, 51 (15), 4505- 4518.
164. Erler, F., Jakob, C., Romanus, H., Spiess, L., Wielage, B., Lampke, T. & Steinhauser, S.,(2003) Interface behaviour in nickel composite coatings with nanoparticles of oxidic ceramic, *Electrochim. Acta*, 48, 3063–3070.
165. Chang, L. M., An, M. Z., Guo, H. F. & Shi, S. Y., (2006), Microstructure and properties of Ni–Co/nano- Al_2O_3 composite coatings by pulse reversal current electrodeposition, *Appl. Surf. Sci.*, 253, 2132–2137.
166. Dietrich, D., Sadeghi, A., Sendzik, A., Schulze, A., Mehner, T., Podlesak, H., Nickel, D., Scharf, I. & Lampke, T., (2013), A new insight into the phosphorus distribution of nanocrystalline Ni-Ni₃P-diamond composites, *Journal for Electrochemistry and Plating Technology*, 1645.
167. Peeters, P., Hoorn, G. v. d., Daenen, T., Kurowski, A. & Staikov, G., Properties of electroless and electroplated Ni–P and its application in microgalvanics, *Electrochim. Acta*, 47, 161–169.
168. Mizushima, I., Tang, P. T., Hansen, N. H. & Somers, M. A. J., (2005), Development of a new electroplating process for Ni-W alloy deposits, *Electrochim. Acta*, 51, 888-896.

169. Grosjean, A., Rezrazi, M., Takadoum, J. & Berçot, P., (2001), Hardness, friction and wear characteristics of nickel- SiC electroless composite deposits, *Surf. Coat. Technol.*, 137, 92–96.
170. Celis, J. P., Roos, J. R., Buelens, C. & Fransaer, J., (1991), Mechanism of electrolyte composite plating: survey and trends, *Trans. Inst. Metal Finish.*, 69 (4), 133–139.
171. Lin, C. S. & Huang, K. C., (2004), Codeposition and Microstructure of Nickel-SiC Composite Coating Electrodeposited from Sulphamate Bath, *J. Appl. Electrochem.*, 34, 1013- 1019.
172. Sombatsompop, N., Sukeemith, K., Markpin, T. & Tareelap, N., (2004), A new experimental apparatus of electro-codeposited system for ni-WC composite coatings, *Mater. Sci. Eng. A*, 381, 175- 188.
173. Pavlatou, E. A., Stroumbouli, M., Gyftou, P. & Spyrellis, N., (2006), Hardening effect induced by incorporation of SiC particles in nickel electrodeposits, *J. Appl. Electrochem.*, 36, 385–394.
174. Szczygiel, B., (1995), Adsorption of Ni(II)-Ions on the Surface of SiC Powder in the Formation of Dispersion Coating, *Trans. Inst. Met. Finish.*, 73 (4), 142–146.
175. Sergueeva, A. V., Stolyarov, V. V., Valiev, R. Z. & Mukherjee, A. K., (2001), Advanced Mechanical Properties of Pure Titanium with Ultrafine Grained Structure, *Scripta Mater.*, 45, 747-752.
176. Wang, Y. M., Cheng, S., Wei, Q. M., Ma, E., Nieh, T. G. & Hamza, A., (2004), Effects of annealing and impurities on tensile properties of electrodeposited nanocrystalline Ni, *Scripta Mater.*, 51, 1023- 1028.
177. MSE 2090: *Introduction to Materials Science*, Chapter 7, Dislocations and strengthening mechanisms. From: people.virginia.edu/~lz2n/mse209/Chapter7.pdf [11.10.2014]
178. Abbaschian, R., Abbaschian, L. & Reed-Hill, R. E., (2008), *Physical Metallurgy Principles*, 4th edition, Cengage Learning.

Publications

Journals

1. Sadeghi, A., Hoseinnejad, H., Sieber, M., Scharf, I. & Lampke, T., (2016), Correlating the Layer Properties of Ni-alumina Composite Coatings and the Mechanism of Codeposition, *International Journal of Chemistry*, 8, 2.
2. Sadeghi, A., Sieber, M., Scharf, I. & Lampke, T., (2015), Co-deposition Behavior of Alumina Nanoparticles and Properties of Ni-Al₂O₃ Nanocomposite Coatings, *Coating and Interface Analysis*, 47 (6), 738-744
3. Dietrich, D., Sadeghi, A., Senzdik, A., Schultze, A., Mehner, T., Podelsak, H., Nickel, D., Scharf, I. & Lampke, T., (2013), A new insight into the phosphorous distribution of nanocrystalline Ni-Ni₃P-Diamond composites, *Journal of Electrochemistry and Plating Technology*.
4. Sadeghi, A., Dietrich, D., Mehner, T., Scharf, I., Nickel, D. & Lampke, T., (2014), Phosphorus Distribution in Electrodeposited Ni-P-Diamond Composites Influencing Structure and Mechanical Properties, *Advanced Materials Research*, 829, 105-109.
5. Lampke, T., Dietrich, D. & Sadeghi, A., (2016), TEM Imaging and TKD mapping: Interaction of nanoparticles incorporating in Ni matrix, *under Publishing*

International Conference

Sadeghi, A., Dietrich, D., Scharf, I., Mehner, T., Nickel, D. & Lampke, T., (2013), Phosphorus distribution in electrodeposited Ni-P-diamond composites influencing structure and mechanical properties, *Materials Science and Engineering*, UFGNSM 2013, Tehran,.

Poster

Sadeghi, A., Dietrich, D., Scharf, I. & Lampke, T., (2013), Correlation between mechanical properties and microstructure in Ni and Ni/P-diamond electrodeposited coatings, *WTK colloquium*, Chemnitz.